Effects of Design Details on Stress Concentrations in Welded Rectangular Hollow Section Connections

by
Sara Daneshvar
M. Sc., Iran University of Science and Technology, 2015

B. SC., Iran University of Science and Technology, 2013

A Dissertation Submitted in Partial Fulfillment of the
Requirements of the Degree of

DOCTOR OF PHILOSOPHY

in the Department of Civil Engineering

Supervisory Committee

Effects of Design Details on Stress Concentrations in Welded Rectangular Hollow Section Connections

by
Sara Daneshvar
M. Sc., Iran University of Science and Technology, 2015
B. SC., Iran University of Science and Technology, 2013

Supervisory Committee

Dr. Min Sun, Supervisor

Department of Civil Engineering

Dr. Cheng Lin, Departmental Member

Department of Civil Engineering

Dr. Kian Karimi, Outside member

British Columbia Institute of Technology

Abstract

For fatigue design of welded hollow structural sections connections, the "hot spot stress method" in CIDECT Design Guide 8 is widely used. This method forms the basis of various national and international design standards. This thesis sought to address some contemporary design issues where the existing approaches cannot be directly applied. Modified design approaches were proposed for various practical design details.

For galvanizing of welded tubular steel trusses, sufficiently large holes to allow for quick filling, venting and drainage must be specified. These holes, quite often specified at the hot spot stress locations, will inevitably affect connection fatigue behaviour. In Chapter 1, six rectangular hollow section (RHS) connections were tested under branch axial loading. The stress concentration factors (SCFs) obtained from the experimental investigation were compared with those calculated using the formulae in CIDECT Design Guide 8. It was shown that the predictions based on the current formulae were unsafe. Hence, finite element (FE) models were developed and validated by comparison with the experimental data. A subsequent parametric study was conducted, including 192 FE models with different hole locations and non-dimensional parameters [branch-to-chord width (β), branch-to-chord thickness (τ), and chord slenderness (2γ) ratios]. SCF formulae for RHS connections with vent/drain holes at different locations were established based on the experimental and FE data. In Chapter 2, by modifying the 192 parametric models in Chapter 1, FE analysis was performed to examine the existing SCF formulae in CIDECT Design Guide 8 for RHS T-connections under branch in-plane bending. The parametric study showed that the existing SCF formulae can lead to unsafe predictions. Critical hot spot stress locations were thus identified. The effects of both branch in-plane bending and chord loading were studied. New design formulae that take the vent and drain holes into account were proposed.

The design rules in CIDECT Design Guide 8 assumes sufficient chord continuity on both sides of connection. Therefore, the existing formulae cannot be directly applied to RHS-to-RHS connections situated near a truss/girder end. Chapter 3 sought to develop new approach for calculation of SCFs in such connections. 256 FE models of RHS-to-RHS X-connections, with varied chord end distance-to-width (e/b_0) and non-dimensional parameters were modelled and analyzed. The analysis was performed under quasi-static axial compression force(s) applied to the branch(es) and validated by comparison of strain concentration factors (SNCFs) to SNCFs obtained from full-sized connection tests. For all 256 connections, SCFs were determined at five critical hot spots on the side of the connection near the open chord end. The SCFs were found to vary as a function of e/b_0, 2γ and β. Existing formulae in CIDECT Design Guide 8 to predict SCFs in directly welded RHS-to-RHS axially loaded X-connections were shown to be conservative when applied to a connection near an open chord end. SCF reduction factors (ψ), and a parametric formula to estimate ψ based on e/b_0, 2γ and β, were derived. For RHS-to-RHS connections situated near a truss/girder end, reinforcement using a chord-end cap plate is common; however, for fatigue design, formulae in current design guidelines [for calculation of SCFs] cater to: (i) unreinforced connections, with (ii) sufficient chord continuity beyond the connection on both sides. Chapter 4 sought to develop definitive design guidelines for such connections. The parametric models in Chapter 3 were modified to simulate such connections. Existing SCF formulae in CIDECT Design Guide 8 were shown to be inaccurate if applied to cap plate-reinforced end connections. SCF correction factors (ψ), and parametric formulae to estimate ψ based on e/b_0, β, τ and 2γ, were derived. The same methodology was used in Chapter 5 to study the SCFs in square bird-beak (SBB) and diamond bird-beak

(DBB) tubular steel X-connections situated at the end of a truss or girder. A comprehensive parametric study, including 256 SBB and 256 DBB connection models, covering wide ranges of chord end distance-to-width (e/b_0) and non-dimensional parameters, was performed. Two sets of correction factor (ψ) formulae for consideration of the chord end distance effect were derived, for SBB and DBB X-connections, respectively.

Table of Contents

List of Figures

List of Tables

Glossary

Abbreviation or symbol	Definition
a, b, c, d, e, f, g, h	Coefficients for proposed design equations
b_0	Overall width of chord member
b_1	Overall width of branch member
COV	Coefficient of variation
h_0	Overall depth of chord member
h_1	Overall depth of branch member
SCF	Stress concentration factor
SCF_{FE}	Stress concentration factor obtained from finite element analysis
SCF_{FOR}	Stress concentration factor obtained using proposed formulae
SNCF	Strain concentration factor
t_0	Wall thickness of chord member
t_1	Wall thickness of branch member
$\varepsilon_{\parallel}$	Strain parallel to weld toe
$\varepsilon_{\perp}$	Strain perpendicular to weld toe
ν	Poisson's ratio
A_0	Cross-sectional area of chord member
L_1	Branch member length
P_0	Force at chord end
P_1	Force at branch end
$S_{n,b}$	Branch nominal stress
$S_{n,ch}$	Chord nominal stress
S_{rhs}	Hot spot stress
$SCF_{chord\text{-}loading}$	Stress concentration factor for chord loading
$SCF_{ipb\text{-}in\text{-}branch}$	Stress concentration factor for branch in-plane bending
W_1	Elastic section modulus of branch member
E	Young's modulus
$L_{r,max}$	distance from weld toe to end point of extrapolation zone
$L_{r,min}$	distance from weld toe to starting point of extrapolation zone
SCF_A	branch SCF at hot spot A
SCF_B	chord SCF at hot spot B
SCF_C	chord SCF at hot spot C
SCF_D	chord SCF at hot spot D
SCF_E	branch SCF at hot spot E
$SCF_{b\_crown,ax}$	branch SCF at the crown point
$SCF_{b\_saddle,ax}$	branch SCF at the saddle point
$SCF_{ch\_crown,ax}$	chord SCF at the crown point
$SCF_{ch\_saddle,ax}$	chord SCF at the saddle point
$SCF_{end,i}$	SCF at hot spot *i* in an RHS-to-RHS axially loaded X-connection near an open chord end
SCF_i	SCF at hot spot *i* in an RHS-to-RHS axially loaded X-connection
b_p	branch plate width
F_2	reduction factor to account for "end effects" in CIDECT DG8
$X_{1\text{-}4}$	SCF parameter for CHS-to-CHS X-connections
d_0	chord diameter
d_1	branch diameter
e	end distance = distance from the heel/toe of the closest branch to the chord end

e_{min}	minimum required end distance
h_0	chord height
h_1	branch height
i	parameter used to designate a critical (hot spot) location (i = A, B, C, D or E)
l_0	chord length
r_i	inner corner radius
r_o	outer corner radius
α	chord length parameter (= $2l_0/b_0$ or $2l_0/d_0$)
β	branch-to-chord width ratio (= b_1/b_0); branch-to-chord diameter ratio (= d_1/b_0)
γ	half chord width-to-thickness ratio (= $b_0/2t_0$); half chord diameter-to-thickness ratio (= $d_0/2t_0$)
τ	branch-to-chord thickness ratio (= t_1/t_0)
ϑ	acute angle between the branch and chord (in degrees)
ψ	reduction factor for end connection
$SCF_{end\ connection}$	SCF in end-connection model
$SCF_{control\ model}$	SCF in control model (connection with sufficient chord continuity)

Acknowledgments

First and foremost, I would like to express my special appreciation and thanks to my advisor Dr. Min Sun, who has been a tremendous mentor for me. I appreciate all his contributes of time, ideas, support and patience to make my PhD experience productive and stimulating. I would like to thank him for encouraging my research and for allowing me to grow as a research scientist. His advice on both research as well as on my career have been invaluable. The joy and enthusiasm of his, for research was contagious and motivational for me, even during tough times in the PhD pursuit. In addition to our academic collaboration, I greatly value the close personal rapport that Dr. Sun and I have forged over the years. I quite simply cannot imagine a better advisor.

For this dissertation, I would like to thank my reading committee members: Dr. Cheng Lin, Dr. Kian Karimi for their time, interest, and constructive comments. I also want to thank you for letting my defense be an enjoyable moment, and for your brilliant comments and suggestions. Among many other things, I am thankful to both technician and administrative teams in Civil engineering department for their supports in providing any demand for the laboratory experimental work.

My time at UVic was made enjoyable in large part due to the many friends and groups that became a part of my life. I would like to thank all individuals in my research group especially Kamran Tayyebi and Prakriti Sharma for their support throughout my degree. I would also like to thank Amirali Ahmadian for sharing knowledge and experience in the finite element software, Abaqus/CAE, Issac Ma for sharing his experience for the experimental work of my research and Alexis Lafferriere for proofreading my dissertation. I am grateful for their help and for many other people and memories.

I am deeply thankful to my family, words cannot express how grateful I am for their love, encouragement, raising me with love of science and supporting me in all pursuits. Dedicated to my parents who taught me love and perseverance, and my brothers that have always been reliable supporters during tough times, standing by me with compassion and selflessness without whom the completion of this dissertation would have never been possible.

Chapter 1

1. RHS X-Connections with Vent and Drain Holes under Branch Axial Loading

1.1. Introduction

Corrosion protection is of paramount importance to exposed steel structures such as bridges, industrial plants, transmission towers and coastal structures. Among different techniques, hot-dip galvanizing is one of the most cost-effective measures since galvanized steel structures are often maintenance-free (i.e. the service life of the zinc coating generally exceeds the design life of the structure it protects) [1]. To support the sustainable development agenda, the popularity of galvanized tubular steel structures has expanded significantly over the years [2-5] (see Figure 1.1 for examples).

(a) Roof truss at T Rowe Price Parking Garage Baltimore, MD, United States

(b) Arthur Ray Teague Parkway Pedestrian Bridge Bossier City, LA, United States

Figure 1.1. Examples of galvanized tubular steel structures

(Photos courtesy of the American Galvanizers Association)

To fully appreciate the longevity of galvanized steel structures, recent research efforts [6-12] have been made to study the effects of galvanizing and fabrication details on structural performances, especially for structures subject to fatigue loadings. In particular, research has been performed on the effects of general galvanizing practice and geometric configuration on thermally-induced stress and strain demands on structural components [5, 13-18]. For hot-dip galvanizing of welded tubular steel trusses, sufficiently large holes to allow for quick filling, venting and drainage are essential. The dimensions and locations of the holes need to be carefully specified by the fabricators to ensure that the tubular trusses are coated inside and out. One reason to specify sufficiently large holes is to allow for a quick flow of molten zinc to overcome buoyant force, and to shorten the total immersion time. Excessively thick zinc coating on the

base steel will be developed due to a long immersion time. Such coating is not economic and can be brittle due to the overreaction between the zinc bath and the base steel [4]. Adequate sizing of holes also minimizes differential thermal stresses experienced by the structure upon galvanizing [19]. In addition, any pickling acid or rinse water trapped in the connection during surface preparation can be converted to superheated steam during galvanizing which may damage the structure. It is also a potential hazard to personnel and equipment (see Figure 1.2 for an example). AISC Design Guide 24 [20] recommends vent holes with a minimum diameter of 13 mm and drain holes with a minimum diameter of 25 mm. All branch members shall have two holes at each end. Depending on the truss configuration and the dipping angle during galvanizing, holes may be specified at different locations around the perimeter of the welded joint.

Figure 1.2. Hazard to personnel and equipment caused by insufficient venting and drainage

(Photo courtesy of Wedge Group Galvanizing)

For fatigue design of welded connections made of hollow structural sections (HSS), the “hot spot stress method” in CIDECT Design Guide 8 [21] considers the uneven stress distribution around the perimeter of the welded joint. It determines the permissible number of load cycles for a given hot spot stress range at a specific joint location from a fatigue strength curve. This method forms the basis of various national and international design standards. However, the design rules in CIDECT Design Guide 8 cannot be directly used in the design of galvanized HSS connections since vent and drain holes are quite often specified at the locations where hot spot stresses occur (see Figure 1.3. for examples). Hence, the existing formulae and charts for the determination of Stress Concentration Factors (SCFs) are not applicable.

(a) Galvanized tubular truss with holes Ford Pedestrian Bridge in Chicago, IL, United States

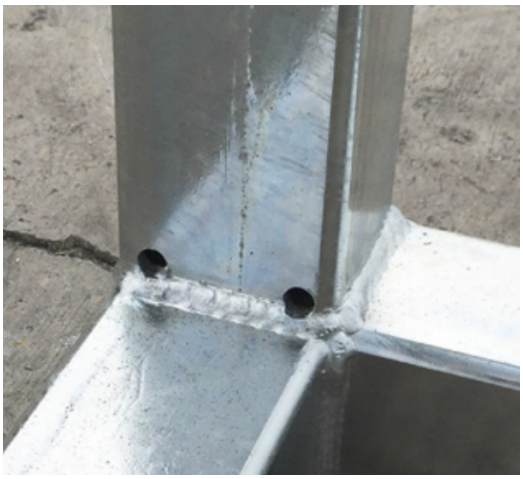

(b) Holes near weld at corner regions of a RHS connection

Figure 1.3. Vent and drain holes in galvanized RHS connections

Recent reports [4,9,11] on premature cracking and early decommission of some galvanized steel structures have attracted a lot of attention in both industry and academia. However, research in this field is still insufficient. In particular, very limited information is available for fatigue design of galvanized HSS connections. The research presented in this chapter focuses on the effects of vent and drain holes on the fatigue behaviours of galvanized RHS connections. Formulae for calculation of SCFs in such connections under branch axial loading were developed.

1.2. Identification of Hot Spot Stress Locations

The "hot spot stress method" recommended in CIDECT Design Guide 8 [21] is widely used for the design of welded HSS connections under fatigue loading. The design procedures are as follows:

Step 1: Determine the nominal stress ranges in the connecting members due to member loads;

Step 2: Determine the SCFs, which are the ratios between the hot spot stresses at the joint and the nominal stresses in the connecting members;

Step 3: Determine the hot spot stress ranges at the joint, based on the results from Steps 1 and 2;

Step 4: Determine the fatigue life of the welded joint using the hot spot stress-versus-fatigue life curves (S-N curves), based on the results from Step 3.

For determination of hot spot stresses in uniplanar RHS T- and X-connections, the design guide recommends calculation of SCFs at five locations (i.e. locations A to E in Figure 1.4). The SCFs for multiplanar RHS connections can be determined using the SCFs for uniplanar RHS connections with a correction factor.

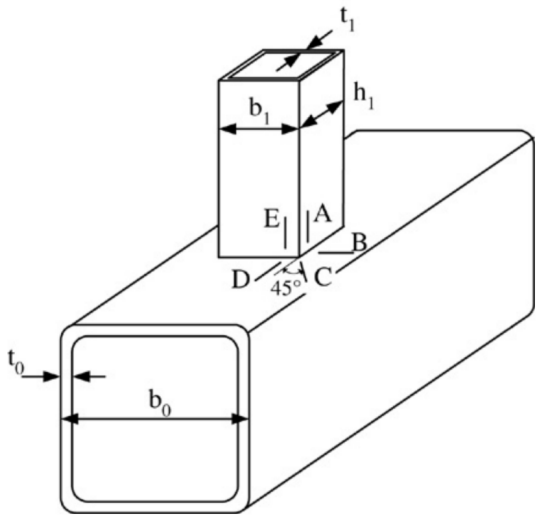

Figure 1.4. Locations of hot spot stresses in uniplanar T- or X-connections (adapted from [21])

In general, for galvanizing vent holes shall be specified at the highest point and drain holes at the lowest point. Hence, depending on the truss configuration and the dipping angle during galvanizing, holes may be specified at different locations around the perimeter of the welded joint (e.g. flat face or corner, side wall or transverse wall of an RHS branch). Figure 1.3 shows the possible hole locations in practice. Since a 25-mm diameter hole can be relatively large for branch members of commonly specified cross-sectional sizes, the hole can redistribute the stress around the welded joint, and the SCFs for such connections will be influenced. This section identifies the hot spot stress locations for connections with holes via a preliminary finite element (FE) analysis. Chain strain gauges are installed at these locations for experimental determination of hot spot stresses (see Section 1.3). The experimental data forms the basis of the finite element study in this paper (see Sections 1.4 and 1.6).

Three RHS-to-RHS X-connections under branch axial loading were modelled using the general purpose FE software ABAQUS [22]. The nominal dimensions of the chord and branch members are the same for the three connections (chord: 178×178×13 mm; branch: 89×89×9.5 mm). The only difference among the three connections is the specification of vent/drain holes (see Figure 1.5). The details of a typical FE model are shown in Figure 1.6. The profile suggested by [23,24], shown in Figure 1.7, was used to model the weld. Due to the symmetry of the connection geometry and loading condition, one half of each connection was modelled. The connections are fixed at the bottom. The top branch end and the chord end are free. Symmetry boundary conditions were applied along the cut face. All modelling details conform to the recommendations in CIDECT Design Guide 8 [21]. Linear elastic properties were applied to both the steel and weld materials in the FE models, where Young's modulus (E) = 200 GPa, and Poisson's ratio (ν) = 0.3.

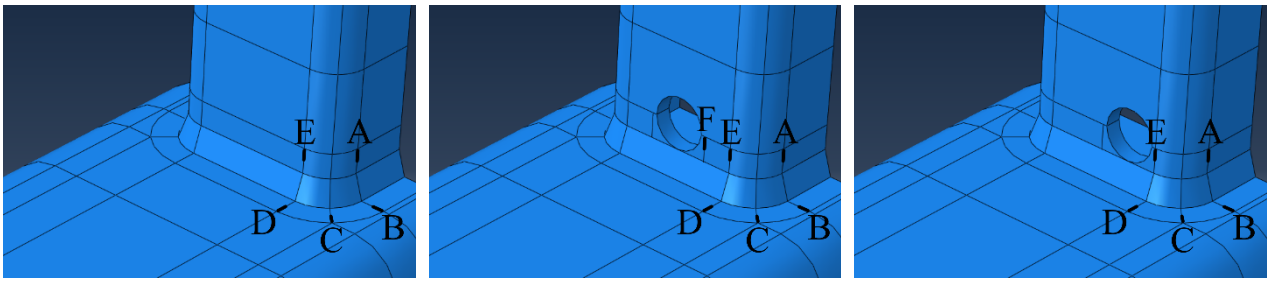

(a) Connection with no hole (b) Connection with hole on flat face (c) Connection with hole at corner region

Figure 1.5. Connection models in preliminary FE analysis and lines of interest

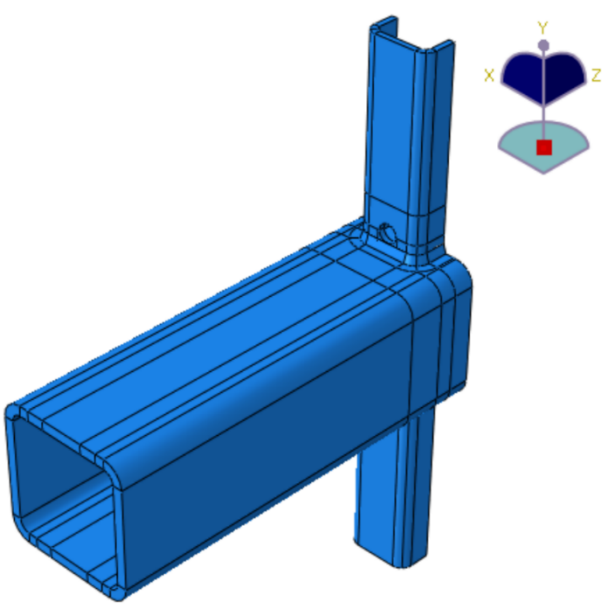

(a) Typical connection model

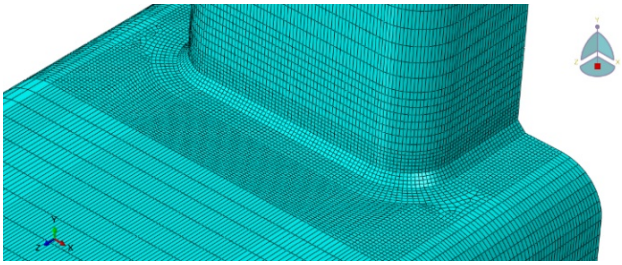

(b) Typical mesh pattern for connection without vent and drain holes

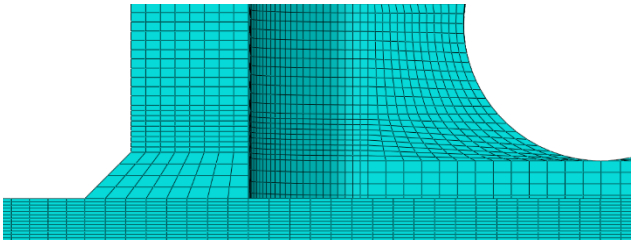

(c) Typical mesh pattern at weld and hole locations

Figure 1.6. Example FE RHS-to-RHS connection geometry, mesh layout and hole location

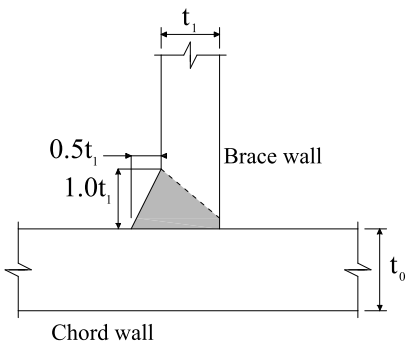

Figure 1.7. Weld simulation using profile suggested by [23,24]

The fatigue phenomenon is a progressive degradation of material strength under repeatedly applied loading. Failure of a connection starts from the appearance of visible cracks and the subsequent crack growth, which eventually leads to member fracture. The allowable fatigue load is typically much lower than the allowable load from static design [21]. Hence, for all FE analyses in this research, static branch axial load of an appropriate magnitude was applied to ensure that all hot spot stresses remained in the linear elastic region. For all three models in the preliminary FE analysis, a 60 kN compression load was applied. Using the approach recommended in CIDECT Design Guide 8 [21], the nominal stress was calculated by dividing the applied load by the branch cross-sectional area. The calculated value agrees well with the stress readings in the FE models.

The stresses at the weld toe (on both branch and chord sides) around the entire perimeter of the welded joint of each preliminary FE model were carefully monitored. A comparison of the three connection models with and without holes under the same load level is shown in Figure 1.8. As can be seen, the stresses at the weld toe near the hole are in general higher than those at the same location in the reference model (i.e. the model with no hole). Hence, different from the connection with no hole, where CIDECT Design Guide 8 [21] suggests that the calculation be performed along the five recommended lines of interest (i.e. Lines A to E in Figure 1.5(a)), for the connections with holes at the center of branch flat faces (i.e. branch transverse walls), it was deemed necessary to monitor the stresses along another potential Line F (see Figure 1.5(b)) adjacent to the hole in the experimental program. On the other hand, for the connections with corner holes, the lines of interest are the same as those in their counterparts with no hole (see Figure 1.5(c)). Further discussion is included in Section 1.3.4.

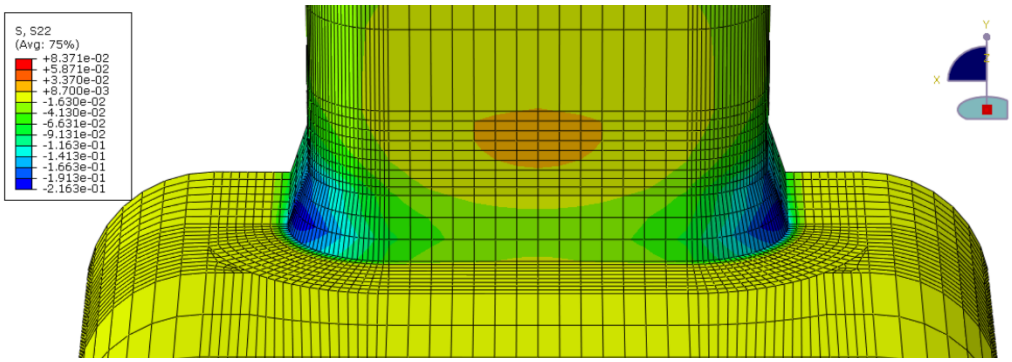

(a) Connection with no hole

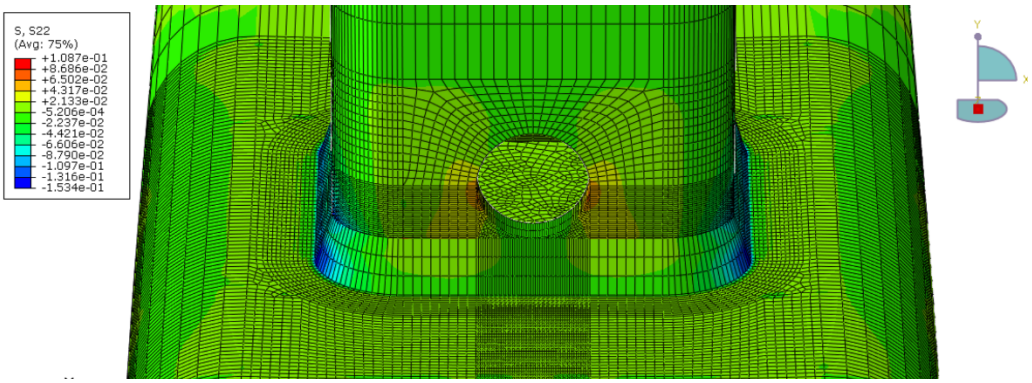

(b) Connection with holes at flat faces

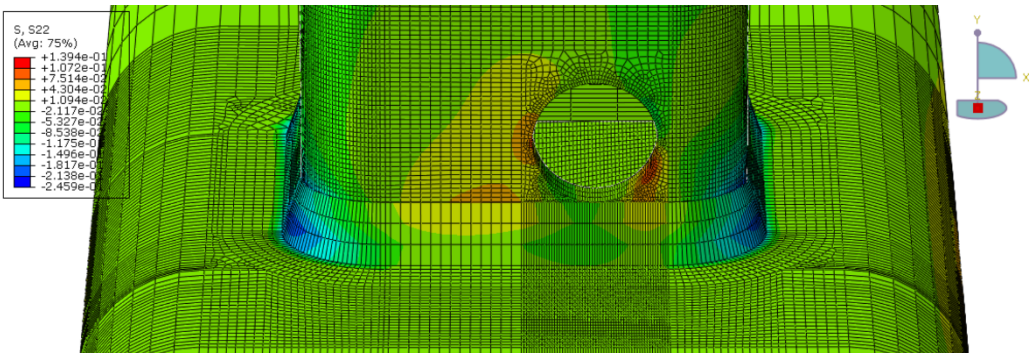

(c) Connection with holes at corner regions

Figure 1.8. Stress contours of FE models

1.3. Experimental Program

1.3.1. Connection specimens

Six connection specimens were tested in this research. The RHS used to fabricate the connection specimens were produced to Grade 350W Class C according to CSA G40.20/G40.21 [25]. The material has a nominal yield strength of 350 MPa, and a nominal tensile strength of 450 MPa. The drawing for a typical connection is shown in Figure 1.9. The dimensions of the six connection specimens are listed in Table 1.1. Each specimen ID in Table 1.1 includes two components. The first component distinguishes the specimen by its configuration, where X = X connection with no hole; XF = X connection with holes at flat faces; and XC = X connection with holes at corners. The second component is the branch-to-chord width ratio of the connection specimen.

Based on the St. Venant's principle, the chord and branch members should be sufficiently long to minimize the influence of end constrains on stress distribution. Following the suggestions by Tong et al. [24] and Feng and Young [26], in this research the branch lengths are $3b_1$, and the chord length are $6b_0$. The branch and chord members were joined by partial joint penetration welds, using a flux cored arc welding process [27]. The connection specimens were selected in such a way that the most interesting parameters are covered, including holes at different locations and the branch-to-chord width ratio (β). The effects of the chord width-to-thickness ratio (2γ) and the branch-to-chord thickness ratio (τ) are investigated via a parametric study in Section 1.6, and hence are kept constants in the experimental study. As can be seen in Table 1.1, the non-dimensional parameters (β, 2γ and τ) are within the ranges of validity of the relevant design provisions in CIDECT Design Guide 8 [21], where $0.35 \leq \beta \leq 1.0$, $12.5 \leq 2\gamma \leq 25.0$ and $0.25 \leq \tau \leq 1.0$.

Table 1.1. Nominal geometry of test specimens

Specimen ID	Chord ($b_0 \times h_0 \times t_0$) (mm)	Branch ($b_1 \times h_1 \times t_1$) (mm)	$\beta = b_1/b_0$	$2\gamma = b_0/t_0$	$\tau = t_1/t_0$
X-0.5	178×178×13	89×89×9.5			
XF-0.5	178×178×13	89×89×9.5	0.5	14	0.622
XC-0.5	178×178×13	89×89×9.5			
X-0.7	178×178×13	127×127×9.5			
XF-0.7	178×178×13	127×127×9.5	0.714	14	0.622
XC-0.7	178×178×13	127×127×9.5			

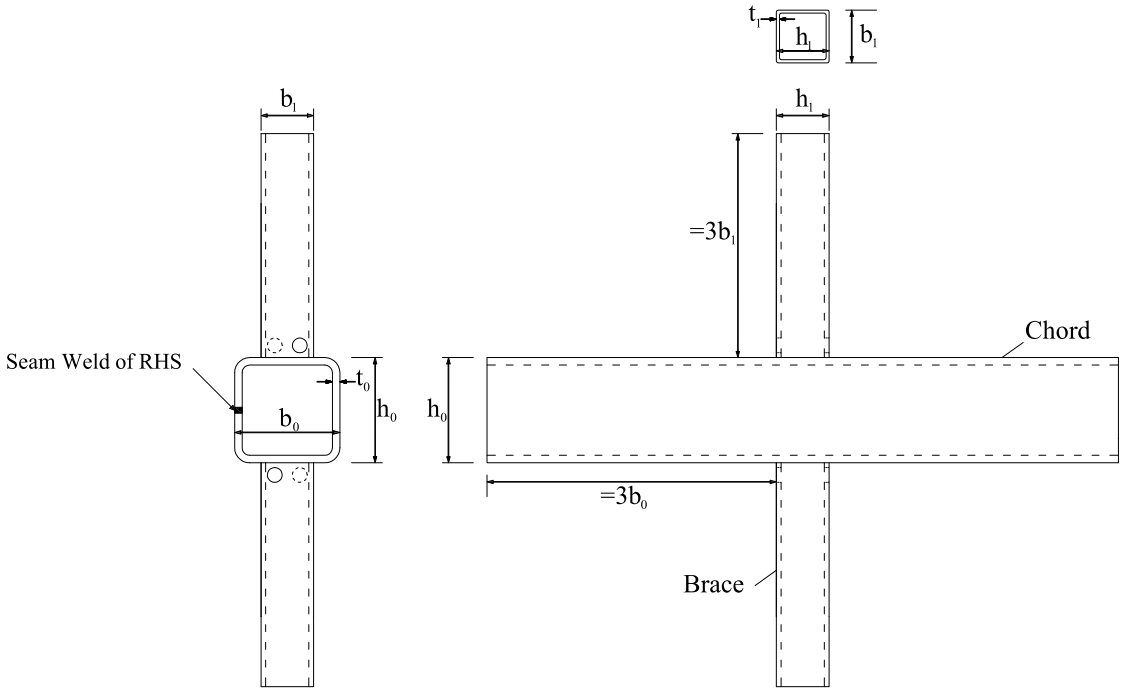

Figure 1.9. Typical connection specimen and symbol definitions

1.3.2. Instrumentations

Similar to the concept of SCF, CIDECT Design Guide 8 [21] defines the Strain Concentration Factor (SNCF) as the ratio of the hot spot strain at the joint and the nominal strain in the member due to a basic member load which causes this hot spot strain (i.e. SNCF = hot spot strain / nominal strain). Since strain gauges measure only strains, SNCFs are typically determined in experimental research. The values can then be converted to SCFs using the relationship between SNCFs and SCFs (see Section 1.4.3).

Chain strain gauges, specially designed for experimental research on stress concentrations (see Figure 1.10), were used. Each gauge is composed of five uniaxial strain gauges on a 12 mm backing. It allows the measurements of five strain values at 2 mm intervals. For the connection specimen dimensions in Table 1.1, the chain strain gauge configuration allows measurements of strains within the extrapolation zones recommended by CIDECT Design Guide 8 (see Figure 1.11) [21]. The chain strain gauges are installed on the branch and chord member surfaces along the lines of interest identified by the preliminary FE analysis (see Figure 1.12). Two sets of chain strain gauges were installed on two sides of the connection so that average SNCF-values can be obtained. For connection specimens X-0.5, XC-0.5, X-0.7 and XC-0.7, 10 chain strain gauges (A1 to E1 on one side, and A2 to E2 on the other side) were installed. For connection specimens XF-0.5 and XF-0.7, 12 chain strain gauges (A1 to F1, and A2 to F2) were installed. Following the recommendations in CIDECT Design Guide 8 [21], $L_{r,min}$ in Figure 1.11 was taken to be the greater value between 0.4 times the RHS branch or chord member wall thickness (t_0 or t_1) and 4 mm. $L_{r,max}$ equals $L_{r,min}$ plus the RHS branch or chord member wall thickness. Hence, for each line

of interest on the branch or chord, four strain readings were obtained from the first four uniaxial strain gauge elements of a chain at locations 6 mm, 8 mm, 10 mm and 12 mm away from the weld toe. Other than the chain strain gauges, four linear strain gauges were installed on the four sides and at the mid-length of the branch member to measure the nominal strain due to the applied loads. The SNCF values were later calculated by dividing the hot spot strains by the nominal strains. The measured nominal strains also ensured that a pure branch axial load was applied (i.e. without any bending moment). Close up views of the strain gauges and the data acquisition device are shown in Figure 1.13.

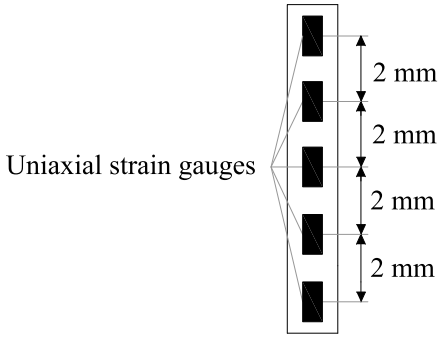

Figure 1.10. Schematic diagram of chain strain gauges

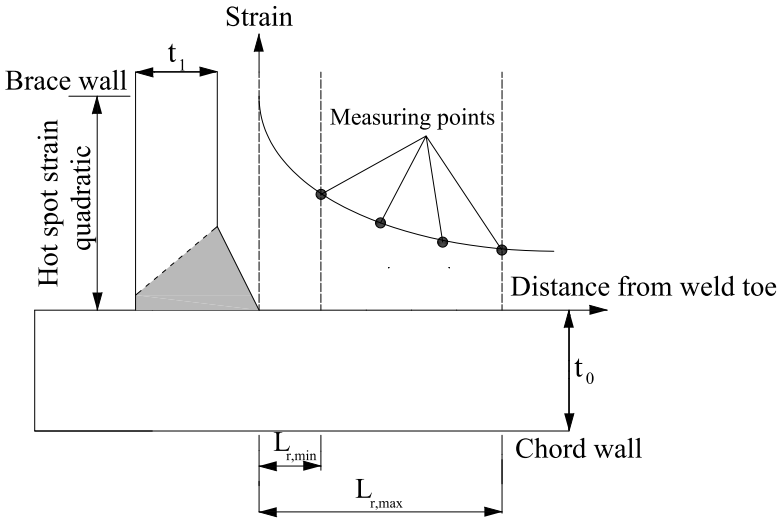

Figure 1.11. Determination of hot spot strain using quadratic extrapolation (adapted from [21])

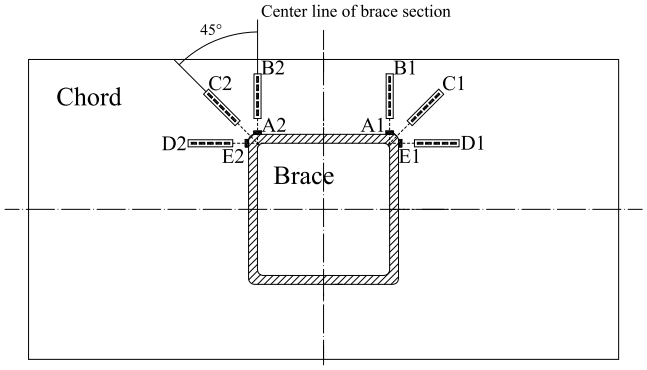

(a) Connection specimens with no hole (X-0.5 and X-0.7)

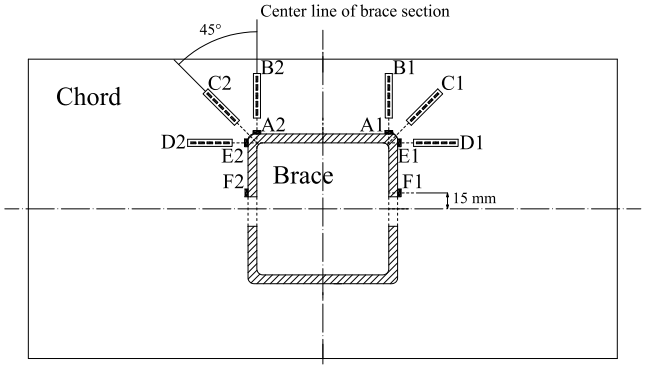

(b) Connection specimens with holes on flat faces (XF-0.5 and XF-0.7)

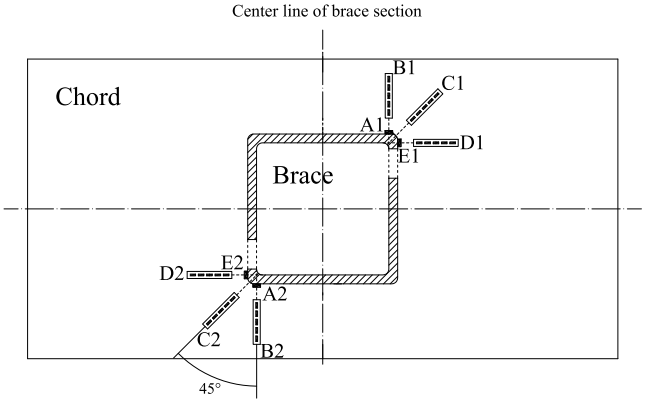

(c) Connection specimens with holes at corner regions (XC-0.5 and XC-0.7)

Figure 1.12. Location of chain strain gauges on chord and branch members

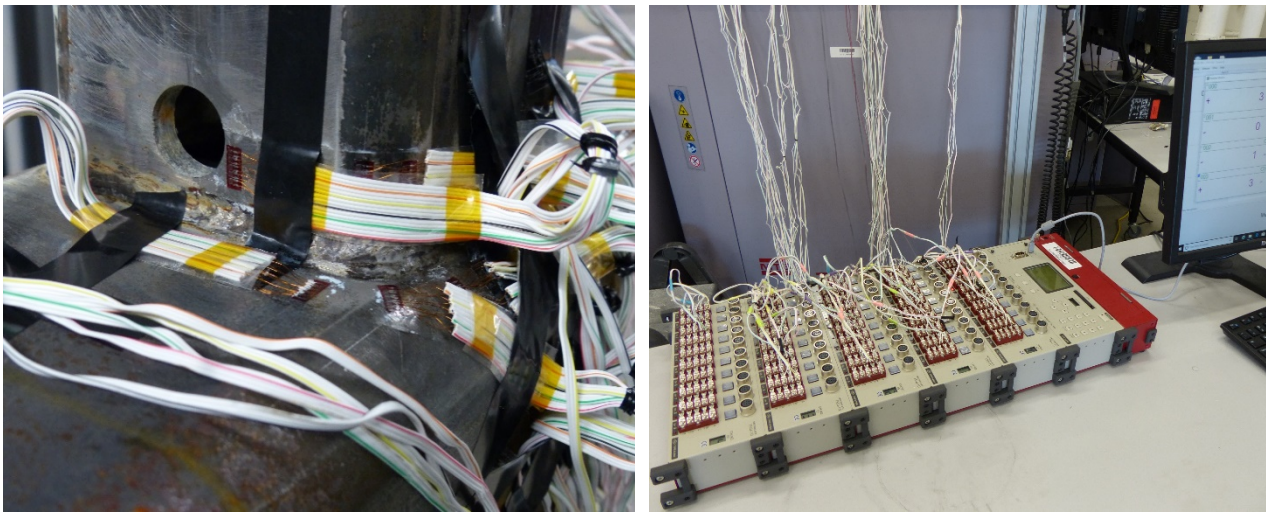

Figure 1.13. Data acquisition

1.3.3. Testing procedures

For unfilled HSS connections, the difference between SNCFs respectively caused by branch axial tension and compression is in general negligible [24,26]. Hence, the same formulae were adopted in CIDECT Design Guide 8 [21] for the unfilled connections under branch tension and compression. In this study, a universal testing machine was used to apply quasistatic branch axial compression loads to the connection specimens. The load magnitudes were determined based on the preliminary FE analysis in Section 1.2, so that the stress levels were always kept in the linear elastic range. For fatigue design, engineers first calculate stress concentration factors (SCFs) in connections. Using the calculated SCFs and codified S-N curves, the connection fatigue resistance can be determined. For research, SCFs are typically determined by testing connections under quasi-static loading. On the other hand, development of S-N curves requires fatigue testing of connections. The research focuses only on the former.

The test setup is shown in Figure 1.14. Force control was used to drive the hydraulic actuator (at a speed of 10 kN/min) to apply the branch axial loading. For all six connection specimens, the load was applied at four stages (30, 40, 50 and 60 kN). At the end of each stage, the strain gauge readings were recorded after pausing the applied load for 2 minutes, which is recommended by Feng and Young [26]. The objective is to allow stress relaxation and to consider the time lag between the testing machine and the data acquisition device. For each stage, the hot spot strains at all locations of interest were recorded and checked to ensure linear elastic response. Using the quadratic extrapolation approach, the average SNCF-values at each hot spot locations were calculated by averaging all values (including the data from the two sets of gauges on both sides of the connection specimen) at all predetermined load levels.

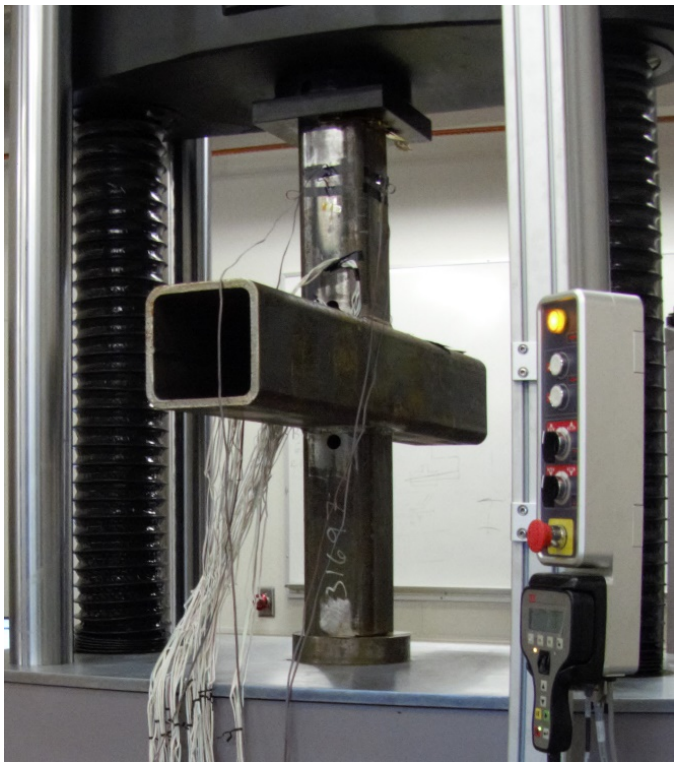

Figure 1.14. Test setup

1.3.4. Test results and discussion

Based on the strain gauge readings, strain (or stress) concentration in the adjacent area of the hole was observed, which was consistent with the preliminary FE analysis results. In both experimental testing and preliminary FE analysis, branch axial compression loads were applied to the connections. According to the strain gauge readings and the numerical simulation results, maximum compressive stresses were observed in the two branch side walls at the welded joint location. On the other hand, tensile stresses were observed near the center of the two branch transverse walls. The same was observed by [28-30] during connection testing under small branch axial compression loads, due to geometric compatibility of the connection. The mechanism is illustrated in Figure 1.15. As shown, the deformation of the chord cross section is restrained by the branch. In other words, the branch member, through the weld, pulls up the chord face. Therefore, tensile stresses are developed at the center of the branch transverse walls. The SNCFs calculated using the experimental data of the six connection specimens are shown in Figure 1.16(a) and (b). It should be noted that, although the stresses on line F were tensile, following the suggestions by [24,26], positive SNCF-values are shown in the figures for connection specimens XF-0.5 and XF-0.7 for simplification.

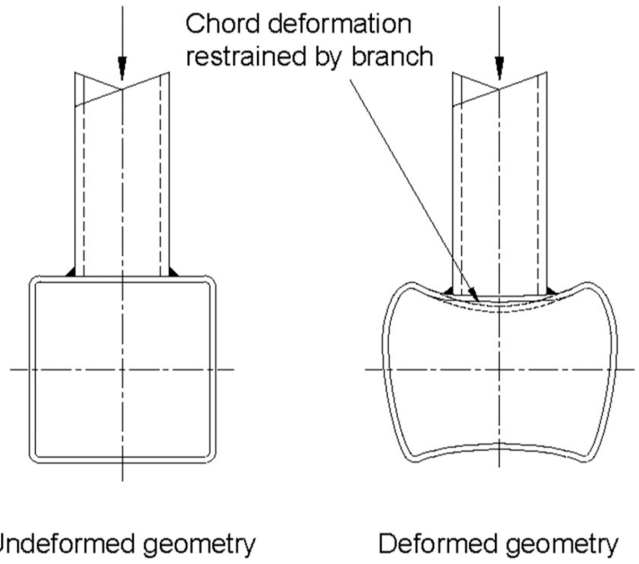

Figure 1.15. Geometric compatibility for RHS-to-RHS connection (adapted from [30])

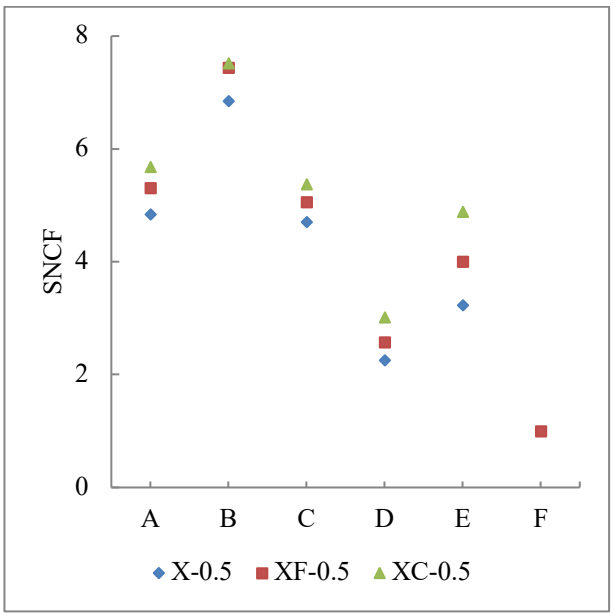

(a) Connection specimens with β=0.5

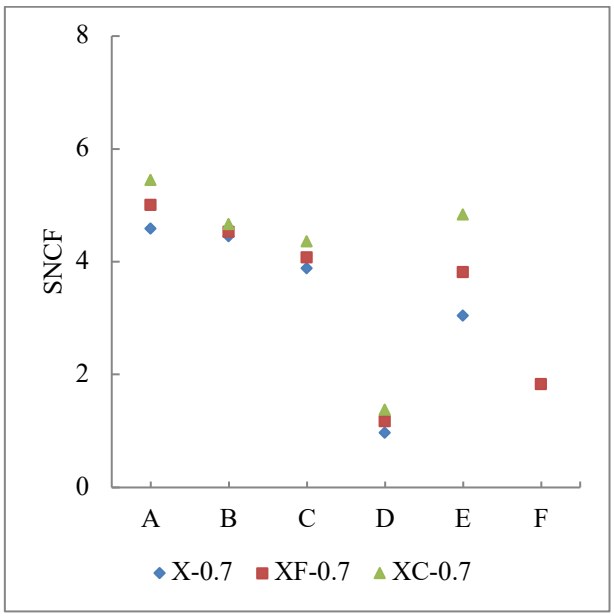

(b) Connection specimens with β=0.7

Figure 1.16. Experimentally obtained SNCFs

It can be seen from Figs. 16(a) and (b) that:

1) For the six RHS-to-RHS connection specimens with the selected β-ratios (0.5 and 0.7), high SNCFs occurred at Lines A, B, C and E, when subject to branch axial loading.

2) The SNCFs for the three connections with a medium β-ratio ($\beta = 0.5$) are in general higher than their counterparts with a higher β-ratio ($\beta = 0.7$).

3) The above observations are consistent with the trends in the design charts from CIDECT Design Guide 8 [21].

4) The SNCFs at Line F were low. However, the Line F-value was higher than the corresponding Line D-value for the connection specimen with a β-ratio of 0.7. Hence, whether Line F can be a potentially critical hot spot stress location remains unknown. Therefore, it was deemed necessary to include Line F in the parametric study in Section 1.6.

5) The SNCFs for connection specimen with vent and drain holes, especially for those with corner holes, can sometimes be significantly larger than those from their counterparts with no holes (by up to 59%). It is possible that such difference can be even larger for connections with other non-dimensional parameters, which are not covered in the testing program. In addition, the effects of 2γ and τ are not included in Figure 1.16. Hence, a parametric study is highly desirable.

1.4. Finite Element Analysis

1.4.1. Finite element modelling and verification

To evaluate the effect of vent and drain holes over a wider range of connection geometric parameters, the experimental results in Section 1.3 were extended using FE modelling. For initial validation of the FE models, the measured geometric properties of the six connection specimens in Table 1.1 were used to develop replicate FE models in ABAQUS [22]. Same as the preliminary FE analysis discussed in Section 1.2, linear elastic material properties were applied to both the steel and weld materials. One half of each connection was modelled to simplify the problem. The profile suggested by Tong et al. [24] was used to model the weld (see Figure 1.7). Load application, boundary conditions and other modelling details are the same as those for the preliminary FE analyses in Section 1.2, all of which are consistent with the recommendations given by CIDECT Design Guide 8 [21]. A sensitivity analysis was carried out to determine the appropriate mesh size and pattern. In order to capture the effects of the geometric discontinuity due to the existence of the hole, the length of all sizes of any solid element at the joint location were forced to be no larger than 0.5 mm. Away from the joint, larger elements were used, with a biased mesh pattern ensuring a smooth transition between the areas of fine and coarse mesh (as shown in Figure 1.6). All finite element analyses were performed in a linear elastic manner so that the SNCF- and SCF-values are not affected by different load levels.

1.4.2. Evaluation against experimental results

For validation of the modelling approach used herein, quadratic extrapolation following the recommendations in CIDECT Design Guide 8 [21] was performed to determine the SNCFs at the same locations where the chain strain gauges were installed on the chord and branch members. For FE validation, the models have the same chord, branch and weld sizes as the connection specimens. The mesh sizes are compatible with the chain strain gauges sizes. Strains in the FE models at the exact locations where the stains were measured were compared to the experimental data. The FE values are compared to the experimentally obtained SNCFs in Figure 1.17. As shown, the SNCFs values obtained from the experiments and the FE analyses agree well according to the means and coefficients of variation of the calculated test result-over-FE result ratios. In general, the FE values are larger than the test results, which is favourable for fatigue assessment since a higher SNCF gives a conservative estimate of fatigue life. Hence, further credence was given to the modelling approach.

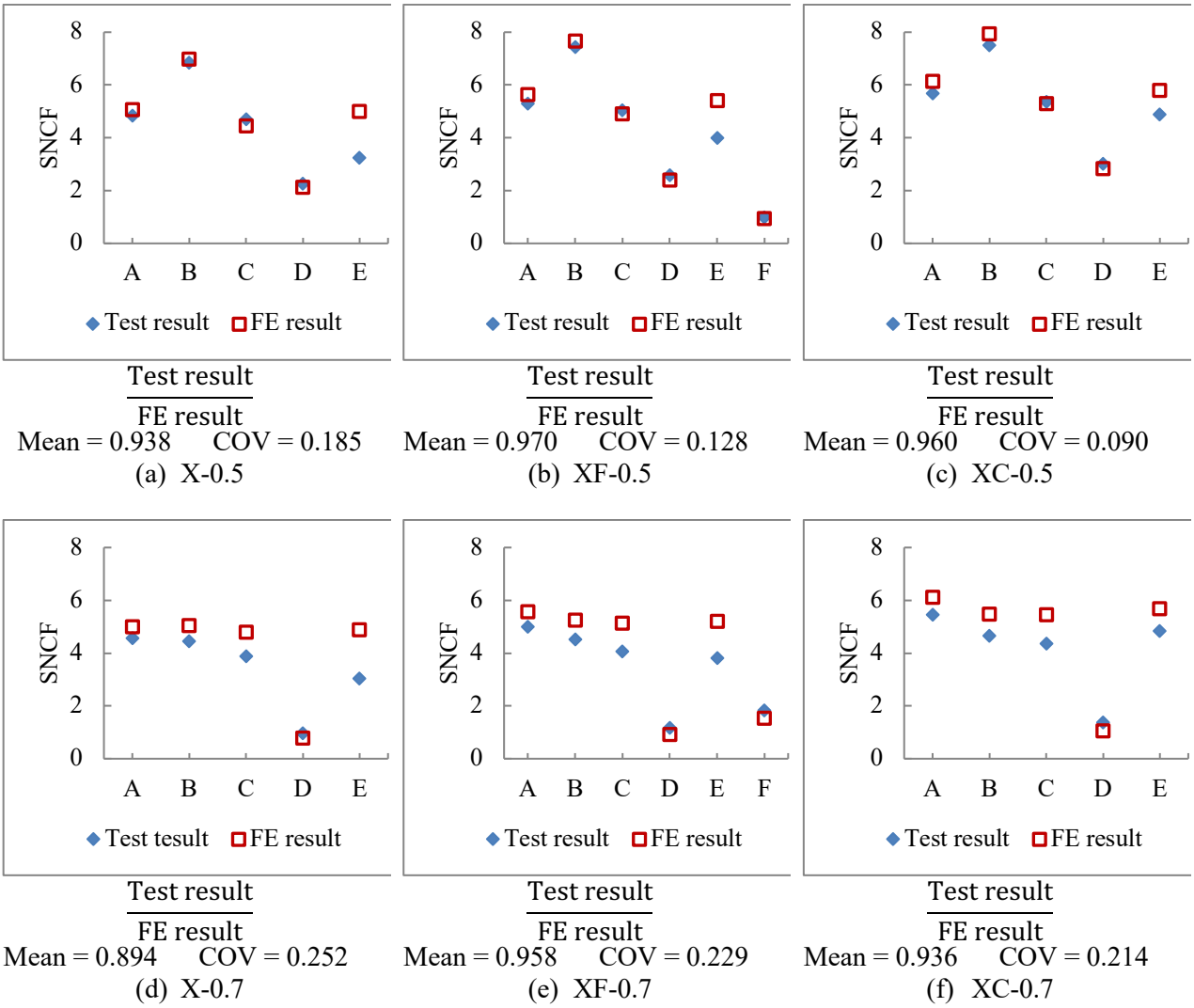

Figure 1.17. Comparison of SNCFs values obtained from experiments and FE analyses

1.4.3. Relationship between SNCF and SCF

As previously mentioned, for fatigue research, it is common to measure experimentally and extrapolate hot spot strains so that SNCFs can be calculated [24,26]. The relationships between SNCF and SCF, recommended by CIDECT Design Guide 8 [21], for rectangular and circular hollow section connections are shown here as Equation 1.1 and Equation 1.2. The two equations were developed assuming a plane stress condition [24,26] (see Equation 1.3), using the available experimental and FE data on strains perpendicular and parallel to the weld toe. As can be seen, the relationships between SNCF and SCF are different for connections of different configurations. Hence, whether Equation 1.1 can be directly applied to RHS connections with vent and drain holes needs to be confirmed.

For joints in rectangular hollow section connections:

$$\mathrm{SCF} = 1.1\mathrm{SNCF} \qquad \text{Equation 1.1}$$

For joints in circular hollow section connections:

$$\mathrm{SCF} = 1.2\mathrm{SNCF} \qquad \text{Equation 1.2}$$

$$\mathrm{SCF} = \frac{1 + \nu\frac{\varepsilon_{\parallel}}{\varepsilon_{\perp}}}{1 - \nu^2}\mathrm{SNCF} \qquad \text{Equation 1.3}$$

where ν = Poisson's ratio;

$\varepsilon_{\parallel}$ = strain parallel to the weld toe; and

$\varepsilon_{\perp}$ = strain perpendicular to the weld toe.

In this research, the results from the FE analyses were used to determine the relationship between SCF and SNCF, using the approach suggested by Tong et al. [23,24]. The strains and stresses perpendicular to the weld toe along the lines of interest were used to determine the SCF- and SNCF-values. The values were plotted in Figure 1.18, which shows a high correlation between the values, and proves the applicability of Equation 1.1. This is because, among the stress components, only the one perpendicular to the weld toe is significantly enlarged by the stress concentration effect due to the geometric discontinuity [26]. Hence, in this research the relationship recommended by CIDECT Design Guide 8 [21] for RHS connections (i.e. Equation 1.1) was used to convert the experimentally obtained SNCFs to SCFs. The relationship was proven to be accurate in the parametric study as well (Section 1.6), since the strains parallel to the weld toe are in general much smaller than the strain perpendicular to the weld toe, hence they have minor effects in Equation 1.3. In particular, the average SCF/SNCF-value is 1.09 and 1.14 for Lines A and E adjacent to the hole at the branch corner region. Similarly, the average SCF/SNCF-value is 1.15 for Line F adjacent to the hole at the center of branch transverse wall.

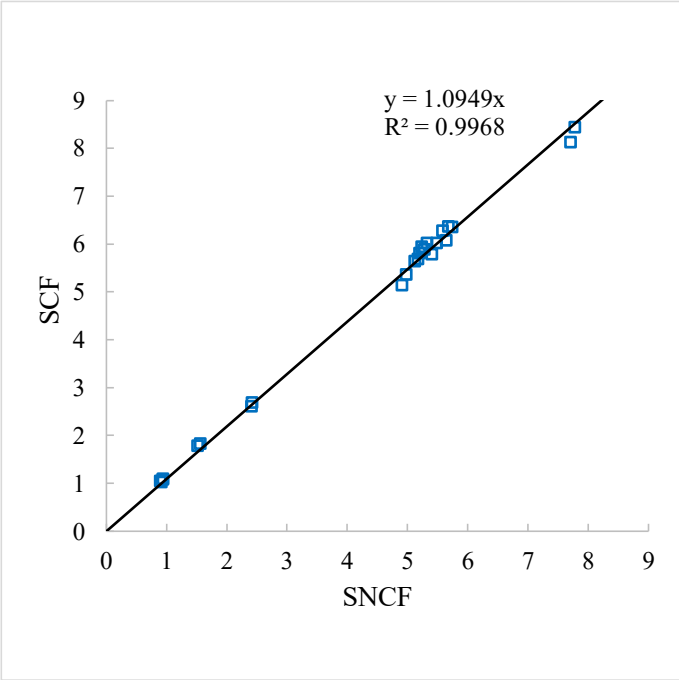

(a) XF-0.5 and XF-0.7

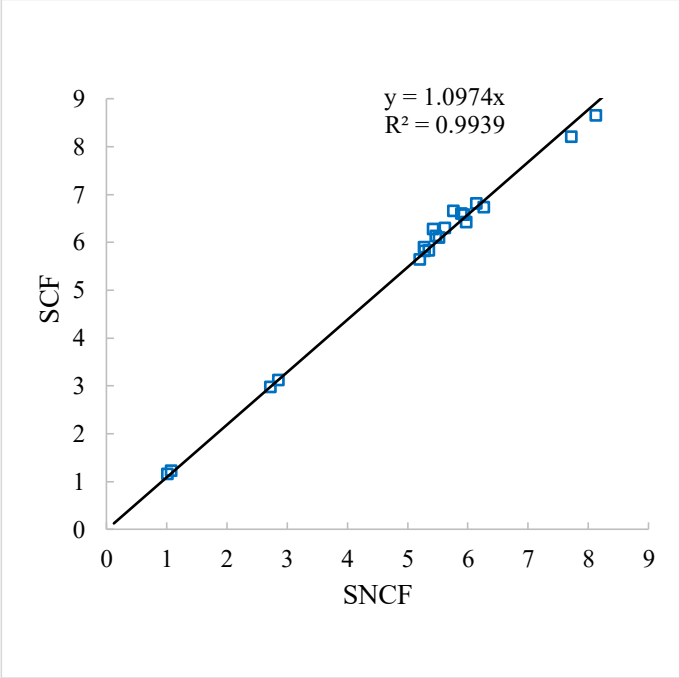

(b) XC-0.5 and XC-0.7

Figure 1.18. Relationship between SNCF and SCF

1.5. Comparison with Test Results Using Relevant Design Formulae

The SCF formulae for uniplanar RHS T- and X-connections adopted by CIDECT Design Guide 8 [21] are listed here as Equation 1.4 to Equation 1.7.

For branch member (lines A and E):

$$SCF_{A \text{ and } E} = (0.013 + 0.693\beta - 0.278\beta^2)(2\gamma)^{(0.790+1.898\beta-2.109\beta^2)} \quad \text{Equation 1.4}$$

For joints with fillet welds:
Multiply branch $SCF_{A \text{ and } E}$ by 1.4
For chord member (lines B, C and D):

$$SCF_B = (0.143 - 0.204\beta + 0.064\beta^2)(2\gamma)^{(1.377+1.715\beta-1.103\beta^2)}\tau^{0.75} \quad \text{Equation 1.5}$$

$$SCF_C = (0.077 - 0.129\beta + 0.061\beta^2 - 0.0006\gamma)(2\gamma)^{(1.565+1.874\beta-1.028\beta^2)}\tau^{0.75} \quad \text{Equation 1.6}$$

$$SCF_D = (0.208 - 0.387\beta + 0.209\beta^2)(2\gamma)^{(0.925+2.389\beta-1.881\beta^2)}\tau^{0.75} \quad \text{Equation 1.7}$$

For X-joints with $\beta = 1.0$:
Multiply SCF_C by a factor of 0.65
Multiply SCF_D by a factor of 0.50
The range of validity for Equation 1.4 to Equation 1.7 are as follows:
$0.35 \leq \beta \leq 1.0$
$12.5 \leq 2\gamma \leq 25.0$
$0.25 \leq \tau \leq 1.0$
A minimum SCF of 2.0 is recommended for all locations.

Using the experimentally obtained SNCFs, and the relationship in Section 1.4.3, SCFs were calculated at all locations of interest for the six connections specimens. The values are compared to the predicted values using the above calculation rules in Figure 1.19. As shown in Figure 1.19(a) and (d), adequate safety margins are inherent in the correlations between the predictions using [21] and the test results of the connection specimens without vent and drain holes. However, such safety margins are smaller for the connection specimens with holes, especially for those with holes at the branch corner regions (i.e. XC-0.5 and XC-0.7). Whether the CIDECT formulae give conservative predictions for connections with holes and other non-dimensional parameters needs to be confirmed by a parametric study. In fact, according to the parametric study in Section 1.6, it was found that the predictions using [21] can be unsafe. Hence, new parametric formulae for better prediction of SCFs in galvanized RHS connections with vent and drain holes need to be developed.

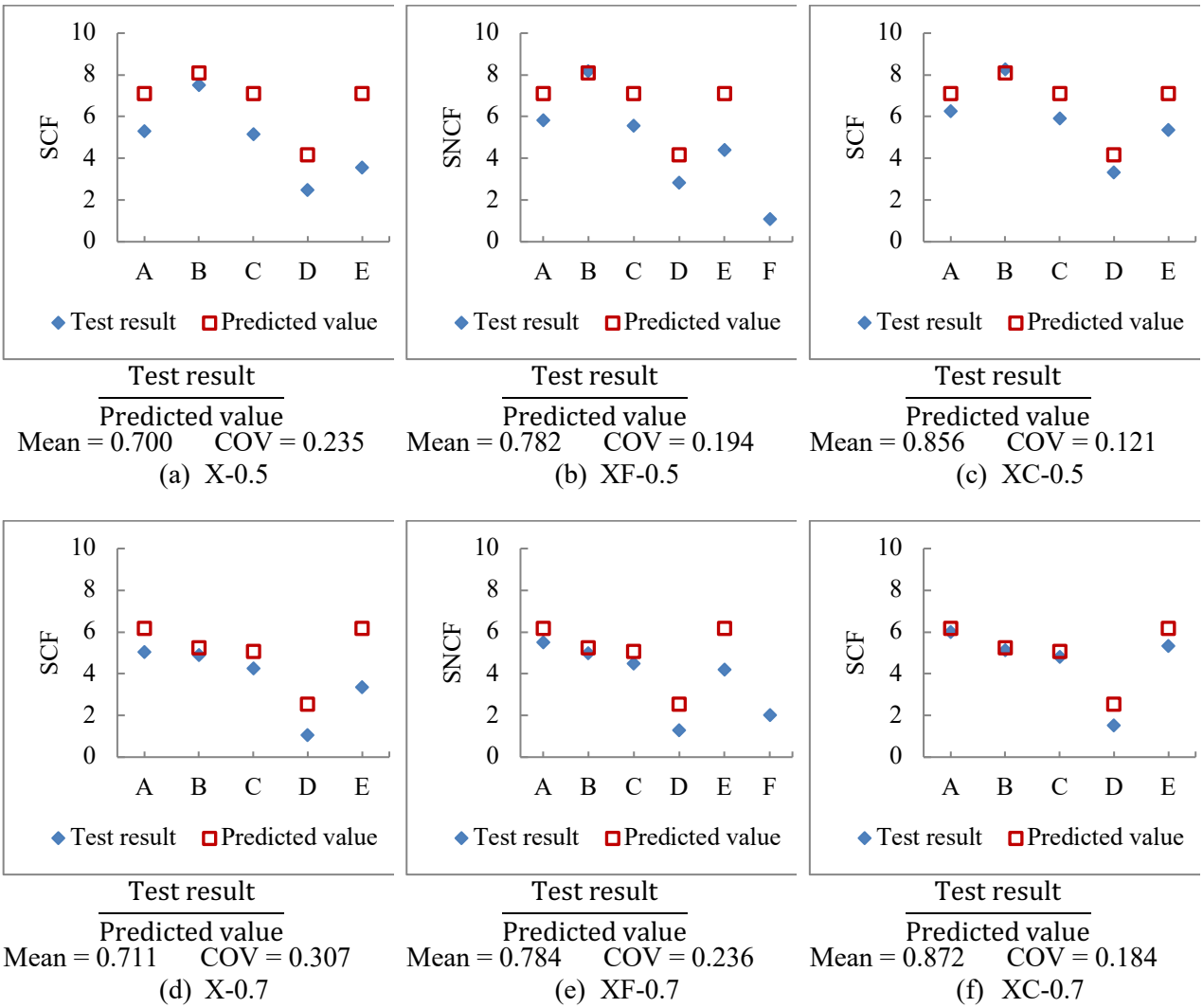

Figure 1.19. Comparison of experimental SCFs with predictions using formulae in CIDECT Design Guide 8 [21]

1.6. Parametric Study

A range of non-dimensional key parameters was chosen to create all possible θ = 90° square RHS-to-RHS X-connections under branch axial loading for the parametric study. For connections without holes, the parameters varied were: $\beta = b_1/b_0 = 0.35, 0.50, 0.65$ and 0.80; $2\gamma = b_0/t_0 = 12.5, 16.0, 20.0$ and 25.0; and $\tau = t_1/t_0 = 0.25, 0.50, 0.75$ and 1.0. A total of 64 permutations exist for the values given. The same non-dimensional parameters were used to develop the connections with holes on the branch flat face and corner region. A 25 mm-hole diameter was used. Hence, a total of 192 parametric models were developed and analysed. Similar to the preliminary FE analysis, linear elastic properties were applied to both the steel and weld materials in the FE models, where Young's modulus (E) = 200 GPa, and Poisson's ratio (ν) = 0.3.

The chord member of all parametric models had a constant width of b_0 = 200 mm, and had a length of at least $6b_0$, to ensure that the connection was sufficiently far away from the support to mitigate the effects of end constraints on the stress distribution at the joint. Similarly, all branches were longer than $3b_1$ to avoid "end effects" [24,26]. The remaining model dimensions were calculated from the β, 2γ and τ values for each specific model, and a weld profile shown in Figure 1.7 was used for all connection models. Within the selection of parametric models, the branch width ranged from 70 mm to 160 mm. The chord wall thickness ranged from 8 mm to 16 mm. The branch wall thickness ranged from 2 mm to 16 mm. The sizes are in general within the range of practical applications. Selected results from the parametric study are shown in Figure 1.20 to Figure 1.22 to show the influences of the non-dimensional parameters. In general, the highest SCFs are found for medium β-ratios. The lower the 2γ-ratio, the lower is the SCF. The lower the τ-ratio, the lower is the SCF in the chord, but it has less effect on the branch. For the connections without vent and drain holes, high SCFs often occur in the chord at locations B and C. On the other hand, for the connections with vent and drain holes, high SCFs can often occur at other locations as well, such as locations D and E. In general, the trends in these figures agree well with the design charts in [21]. Comparisons of selected FE results and predicted values by CIDECT Design Guide 8 [21] are shown in Figure 1.23. Based on the results from the 192 parametric models, it was found that:

(1) For the 64 connections with holes on the branch transverse walls, the SCFs at location F never governed. Hence, it can be concluded that Line F is not a line of interest.

(2) For the 64 connections with no hole, the SCFs in the branch and chord are on average 77% and 83% of the predicted values calculated using the CIDECT formulae [21]. For the 64 connections with holes on the branch transverse wall, the SCFs in the branch and chord are on average 4% and 20% higher than the predicted values. For the 64 connections with holes at the branch corner regions, the SCFs in the branch and chord are on average 12% and 44% higher than the predicted values. Hence, it is unsafe to use the existing formulae, and new formulae that take vent and drain holes into account need to be proposed.

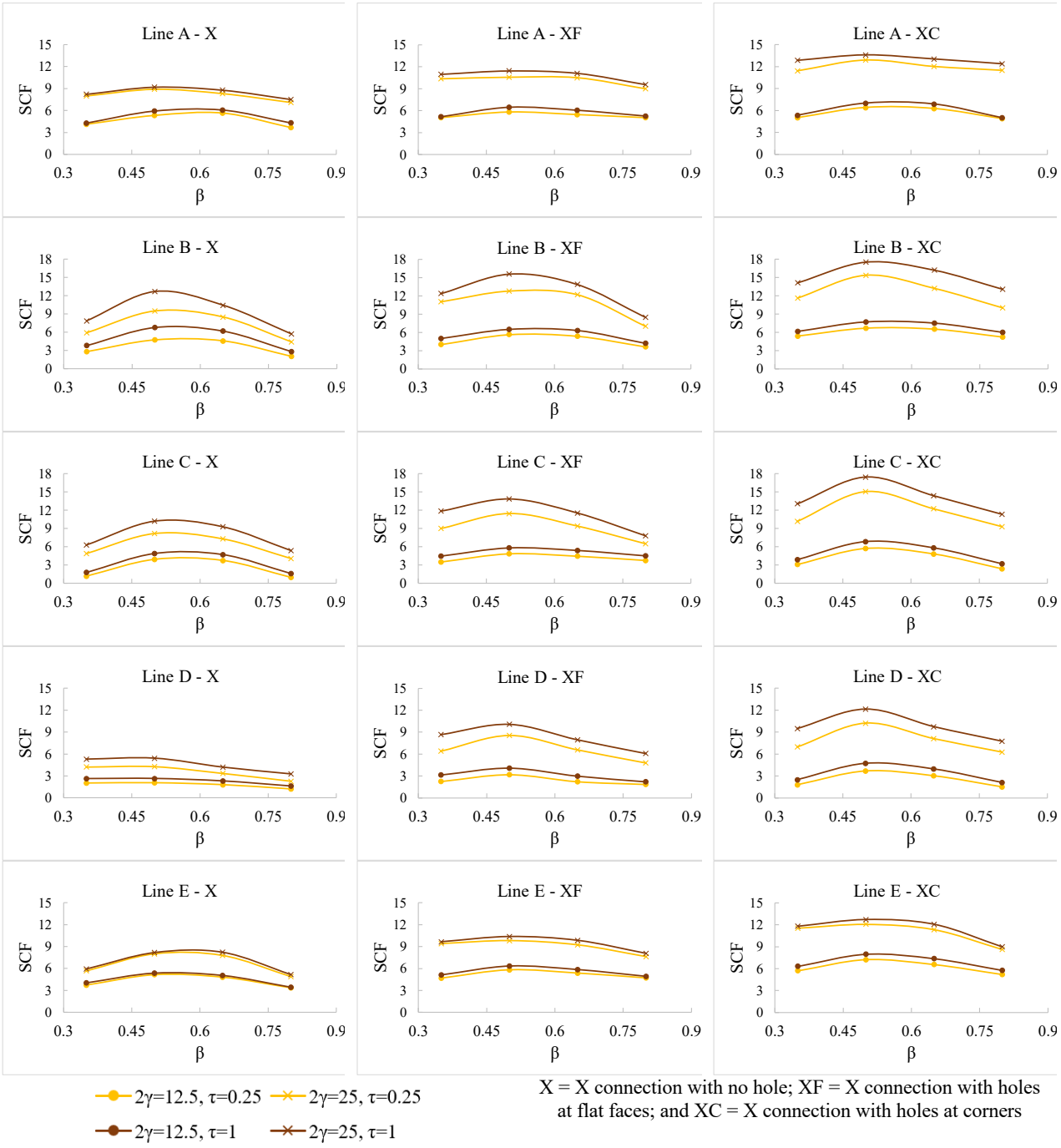

Figure 1.20. Influence of β on SCFs in RHS connections with and without holes under branch axial loading

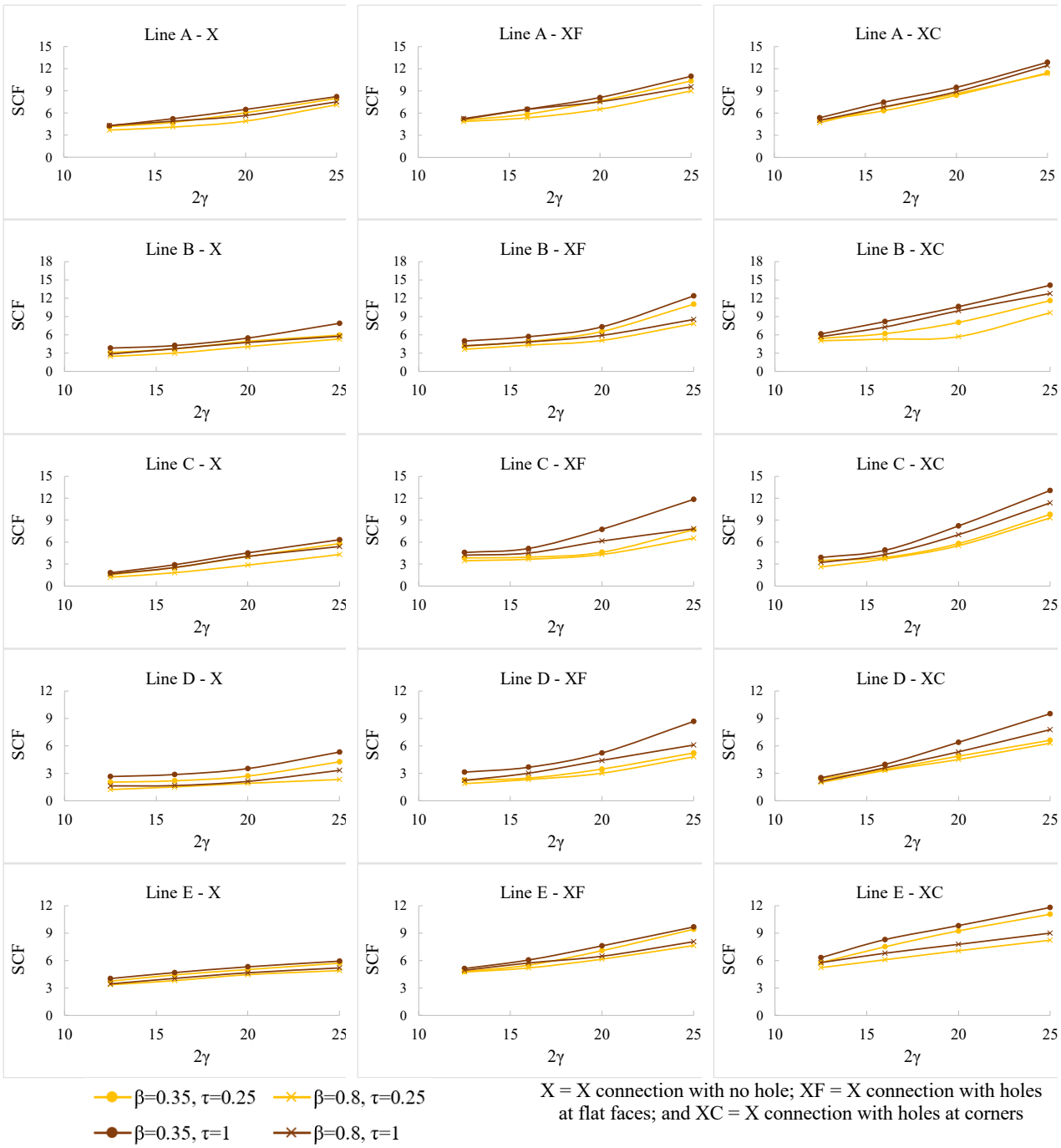

Figure 1.21. Influence of *2γ* on SCFs in RHS connections with and without holes under branch axial loading

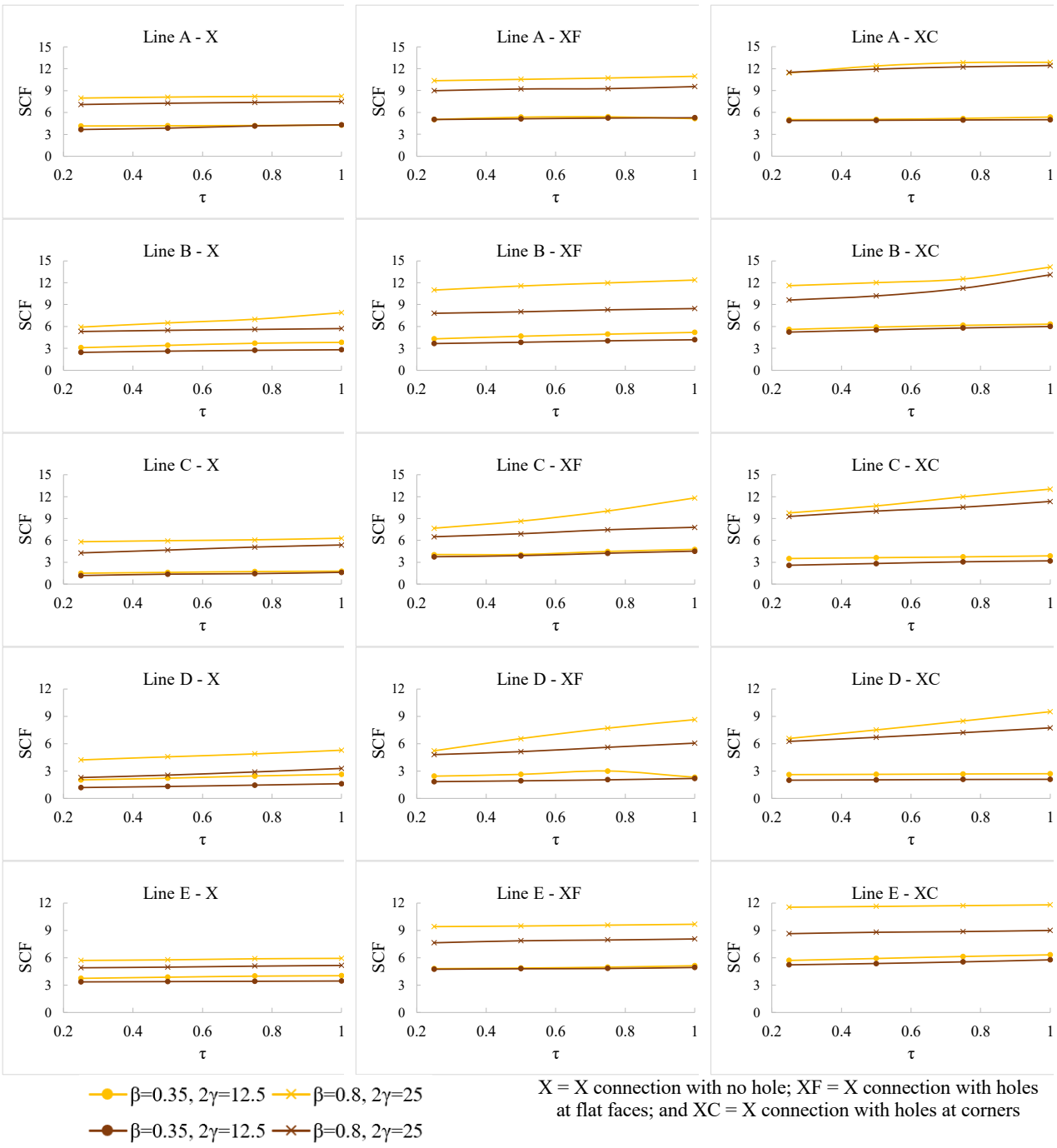

Figure 1.22. Influence of τ on SCFs in RHS connections with and without holes under branch axial loading

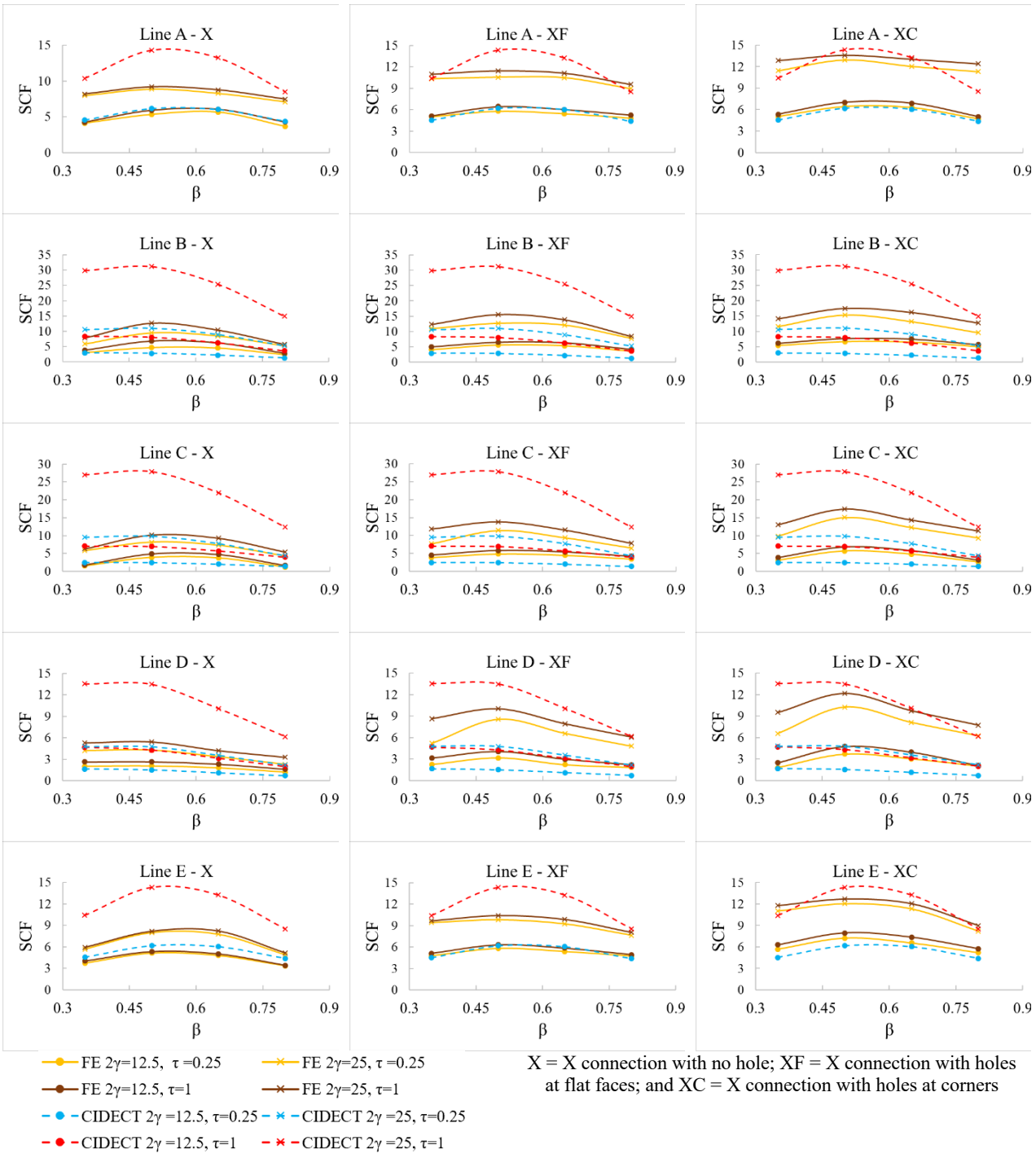

Figure 1.23. Comparison of selected FE results with predicted values by CIDECT Design Guide 8 [21]

1.7. Proposed SCF formulae and verification

Using the data from the parametric study, multiple regression analysis following the procedures adopted by [24,26] were performed to develop the SCF formulae for RHS T- and X-connections with vent and drain holes at different locations. Equation 1.8 suggested by [24,26] was used in this study as the general format.

$$SCF = (a + b \cdot \beta + c \cdot \beta^2 + d \cdot 2\gamma) \cdot (2\gamma)^{(e+f \cdot \beta + g \cdot \beta^2)} \cdot (\tau)^h \quad \text{Equation 1.8}$$

where the constants a to h will be determined by multiple regression analysis. It is true that analytical solutions can be developed. However, the thesis aims to develop revised approaches based on the existing ones in current design standards. Since the existing formulae are based on regression. The thesis used the same approach.

The proposed equations are for calculation of stress concentration factors (SCFs). In design, hot spot stresses are calculated by multiplying the SCFs with nominal stress. Nominal stress (linear elastic) in member is affected by loading magnitude, member section property and material property. The SCFs are essentially magnifying factors which are not influenced by material property.

The thesis used the conventional regression approach to develop the stress concentration factors (SCFs) formulae. The "safety margin" is included in the other steps of the existing design approach. Thus, , the SCF data points were not enveloped.

Based on the parametric study, the SCF formulae for uniplanar RHS T- and X-connections *with vent and drain holes on the branch transverse walls* are listed here as Equation 1.9 to Equation 1.13.

For branch member (lines A and E):

$$SCF_A = (0.188 + 2.100\beta + 0.657\beta^2 + 0.076\gamma)(2\gamma)^{(0.348 - 0.797\beta - 1.050\beta^2)}\tau^{0.045} \quad \text{Equation 1.9}$$

$$SCF_E = (-0.123 + 2.106\beta + 4.215\beta^2 + 0.182\gamma)(2\gamma)^{(0.184 + 0.744\beta - 1.183\beta^2)}\tau^{0.026} \quad \text{Equation 1.10}$$

For joints with fillet welds:
Multiply branch $SCF_{A \text{ and } E}$ by 1.4
For chord member (lines B, C and D):

$$SCF_B = (-0.228 + 1.71\beta - 2.446\beta^2 + 0.232\gamma)(2\gamma)^{(-0.157 + 2.340\beta - 2.458\beta^2)}\tau^{0.068} \quad \text{Equation 1.11}$$

$$SCF_C = (-0.408 + 1.870\beta + 2.446\beta^2 + 0.232\gamma)(2\gamma)^{(-0.157 + 2.340\beta - 2.458\beta^2)}\tau^{0.068} \quad \text{Equation 1.12}$$

$$SCF_D = (0.634 - 1.361\beta + 0.782\beta^2 - 0.002\gamma)(2\gamma)^{(0.374 + 2.380\beta - 0.831\beta^2)}\tau^{0.074} \quad \text{Equation 1.13}$$

For X-joints with $\beta = 1.0$:
Multiply SCF_C by a factor of 0.65
Multiply SCF_D by a factor of 0.50
The range of validity for Equation 1.9 to Equation 1.13 are as follows:
$0.35 \leq \beta \leq 1.0$
$12.5 \leq 2\gamma \leq 25.0$
$0.25 \leq \tau \leq 1.0$
A minimum SCF of 2.0 is recommended for all locations.

Based on the parametric study, the SCF formulae for uniplanar RHS T- and X-connections *with vent and drain holes at the branch corner regions* are listed here as Equation 1.14 to Equation 1.18.

For branch member (lines A and E):

$$SCF_A = (-0.101 + 2.097\beta + 2.251\beta^2 + 0.134\gamma)(2\gamma)^{(0.385 + 0.491\beta - 0.777\beta^2)}\tau^{0.051} \quad \text{Equation 1.14}$$

$SCF_E = (1.074 - 1.784 + 0.945\beta^2 - 0.012\gamma)(2\gamma)^{(0.416+2.179\beta-1.227\beta^2)}\tau^{0.037}$ Equation 1.15

For joints with fillet welds:

Multiply branch $SCF_{A\ and\ E}$ by 1.4

For chord member (lines B, C and D):

$SCF_B = (-0.213 + 1.698\beta + 1.999\beta^2 + 0.112\gamma)(2\gamma)^{(0.196+1.914\beta-2.198\beta^2)}\tau^{0.070}$ Equation 1.16

$SCF_C = (-0.466 + 1.902\beta + 1.806\beta^2 + 0.152\gamma)(2\gamma)^{(0.109+2.027\beta-2.335\beta^2)}\tau^{0.067}$ Equation 1.17

$SCF_D = (0.668 - 1.587\beta + 0.983\beta^2 - 0.016\gamma)(2\gamma)^{(0.391+2.395\beta-0.447\beta^2)}\tau^{0.082}$ Equation 1.18

For X-joints with $\beta = 1.0$:

Multiply SCF_C by a factor of 0.65

Multiply SCF_D by a factor of 0.50

The range of validity for Equation 1.14 to Equation 1.18 are as follows:

$0.35 \leq \beta \leq 1.0$

$12.5 \leq 2\gamma \leq 25.0$

$0.25 \leq \tau \leq 1.0$

A minimum SCF of 2.0 is recommended for all locations.

The SCFs obtained from the FE analyses (SCF_{FE}) and those determined using the proposed formulae (SCF_{FOR}) are compared in Figure 1.24. As shown, the values agree well, indicating a good accuracy of the multiple regression analysis.

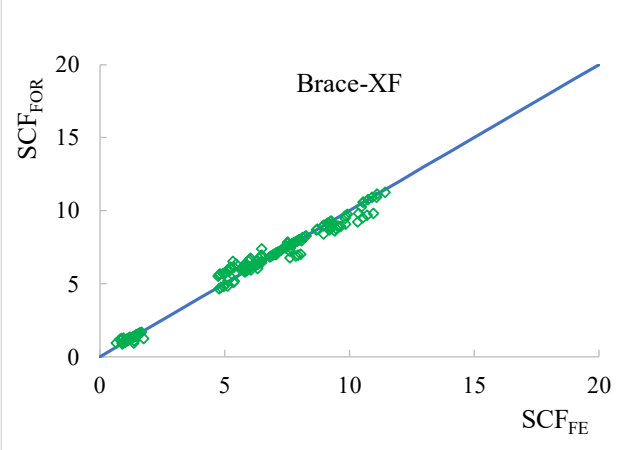

$SCF_{FOR/FE}$	Line A	Line E
Mean	1.014	1.000
COV	0.066	0.067

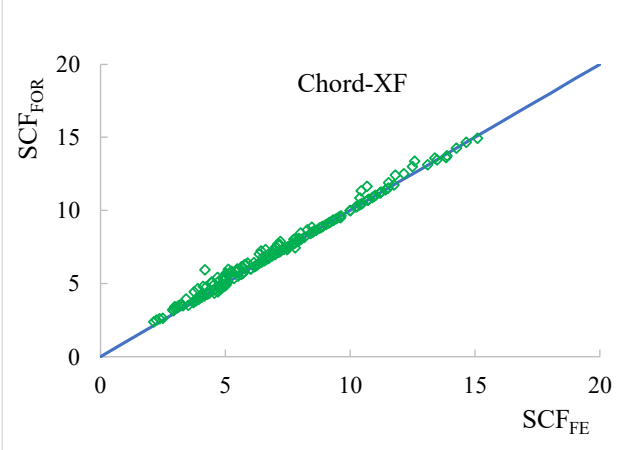

$SCF_{FOR/FE}$	Line B	Line C	Line D
Mean	1.029	1.049	0.985
COV	0.063	0.051	0.109

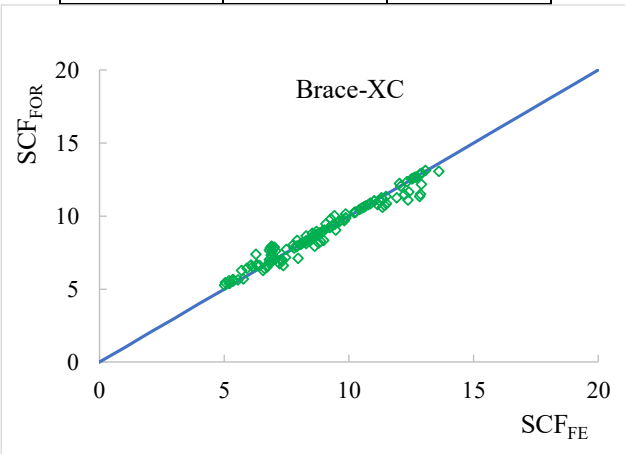

$SCF_{FOR/FE}$	Line A	Line E
Mean	1.013	0.994
COV	0.057	0.043

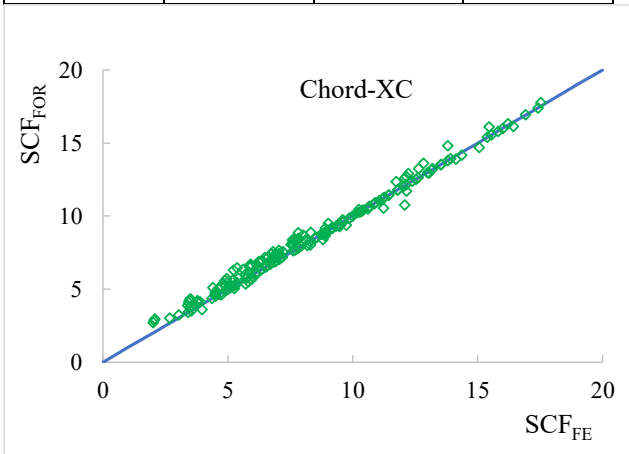

$SCF_{FOR/FE}$	Line B	Line C	Line D
Mean	1.021	1.033	1.056
COV	0.042	0.050	0.098

XF = X connection with holes at flat faces; and XC = X connection with holes at corners

Figure 1.24. Comparison of SCF values determined by proposed formulae and FE analyses

1.8. Conclusions

In this chapter, stress concentration factors (SCFs) in galvanized RHS-to-RHS X-connections with vent and drain holes under branch axial loading have been investigated. By analysing the data from six experimental tests and 192 finite element connection models, it was found that the design values calculated using the formulae in CIDECT Design Guide 8 can be unsafe, since vent and drain holes are in practice often specified near the recommended hot spot stress locations. Based on a subsequent parametric study covering varied hole location, branch-to-chord width ratio, chord width-to-thickness ratio, and branch-to-chord thickness ratio, modified formulae were proposed to provide accurate

predictions of SCFs in such connections. The proposed formulae also apply to RHS-to-RHS T-connections with vent and drain holes at different locations under branch axial loading.

Chapter 2

2. RHS T-Connections with Vent and Drain Holes under Branch In-Plane Bending

2.1. Introduction

Hot-dip galvanizing is a cost-effective approach for protection of steel structures against corrosion. The metallurgical reaction between steel and molten zinc forms a tightly-bounded alloy coating, providing maintenance-free longevity of steel structures [20]. Hot-dip galvanized steel can withstand harsh environmental or operational conditions to fulfill the intended design life [1]. In particular, to support the sustainable development agenda, the popularity of galvanized tubular steel structures has expanded significantly over the years, since both zinc and steel are recyclable materials. Permanent or temporary building solutions are available for a wide range of sectors including aviation, industrial, marine, offshore, oil and gas, as well as sports. However, the effects of galvanizing and the associated fabrication process on the performance of tubular steel components, especially connections under fatigue loadings, has been a point of debate to date [3]. In particular, for hot-dip galvanizing, holes to allow for filling, venting and drainage must be specified at the welded joint location of the tubular steel connections. Adequate sizing of the galvanizing holes also minimizes the differential thermal stresses experienced by the structure during the hot-dipping process. One can speculate that the galvanizing holes at the welded joint locations will inevitably influence the stress concentrations of the connections, and in turn the fatigue behaviour of the galvanized tubular steel structures (e.g. bridges, mobile crane and communication tower). However, there is no definitive published guidance on this topic from structural steel associations.

For fatigue design of welded tubular steel connections, the hot spot stress method recommended by the CIDECT Design Guide 8 [21] is widely used, which forms the basis of various national and international steel design standards for various applications (see Section 2.3 for details). However, the provisions cannot be directly used in the design of galvanized tubular steel connections since the formulae for calculation of Stress Concentration Factors (SCFs) do not consider the effects of galvanizing holes. Hence, new formulae need to be proposed. Recent research has been performed on the effects of general galvanizing practice and structural details on: (1) the possible changes in material properties, and (2) the thermally-induced stress and strain demands on structural components [7-19]. However, these investigations do not explicitly address the above fatigue design issue on galvanized tubular steel structures. This study focused on welded rectangular hollow section (RHS) moment T-connections. Finite element (FE) modelling was performed to study the combined effects of: (1) vent and drain holes at different locations; (2) branch in-plane bending; and (3) chord loading. A parametric study including 192 FE models with varied non-dimensional parameters was performed. Critical hot spot stress locations were identified. Formulae for calculation of (SCFs) in such connections were developed.

2.2. Specification of vent and drain holes

According to AISC Design Guide 24 [20], sufficiently large holes to allow for quick filling, venting and drainage must be specified at the joint locations prior to galvanizing welded tubular steel trusses. The aim is to:

(1) Ensure that the tubular structures are completely coated inside and out. Any air trapped in pockets will prevent the preparation chemicals from adequately cleaning the surface, and in turn will prevent the molten zinc bath from reacting with the steel;

(2) Allow a quick flow of molten zinc to control the total immersion time. If the holes are not sufficiently large, the molten zinc will not be able to enter quickly and the item may become buoyant, causing it to float off the jig or be subject to erratic immersion. Excessively long immersion time in general results in overreaction between steel and molten zinc. Excessively thick zinc coating on the base steel will be developed in this case. Such coating is not economic and can be brittle due to the overreaction [3]; and

(3) More importantly, adequate sizing of holes minimizes differential thermal stresses experienced by the structure upon galvanizing [23]. Since the molten zinc bath is typically maintained at 450ºC, the hot-dipping process can convert any pickling acid or rinse water trapped in the connection during surface preparation to superheated steam. The steam pressure can result in significant deformation or even sudden cracking of the structure. The latter is a potential hazard to personnel and equipment. Figure 2.1 shows an example of what can happen to a galvanizing bath when a tubular steel component has not been properly vented. As shown, at galvanizing temperature, the superheated steam and the resultant pressure quickly expanded, and teared the steel component with an explosive force. This force has caused damage of the steel component and the molten zinc to be spilled over the facility. The galvanizing personnel and equipment are at great risk in this case.

Figure 2.1. Hazard to personnel and equipment caused by insufficient venting in steel component

(Photo courtesy of Wedge Group Galvanizing)

(a) Galvanized tubular truss with holes
Ford Bridge in Chicago, IL, United States

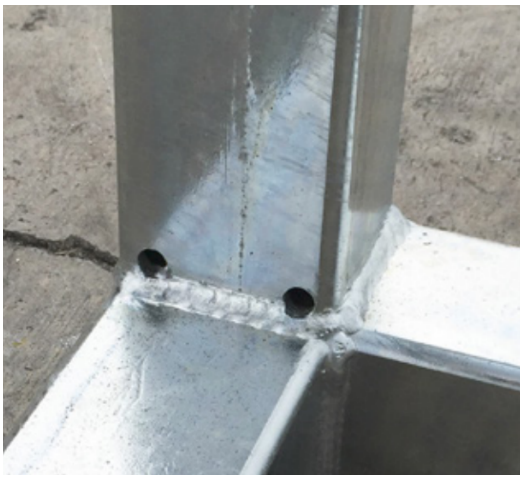

(b) Holes near the weld at the corner regions of an RHS connection

Figure 2.2. Vent and drain holes in galvanized RHS connections

2.3. Current fatigue design approach for RHS moment T- and X-connections

Fatigue life is commonly related to the stress concentrations at the welded joint locations [21]. Extensive research on the behaviour and design of tubular structures has been conducted in the field of fatigue strengths of connections. Based on a large amount of research data, design procedures have been developed and implemented in various guidelines for fatigue design of both onshore and offshore structures, including: API RP2A-LRFD [24], AWS D1.1 [33], CIDECT Design Guide 8 [21], DNV RP-C203 [42], and ISO 14347 [35]. For applications in onshore structures in particular, the provisions in CIDECT Design Guide 8 [21] and ISO 14347 [35] are similar since both documents evolved from the recommendations by the International Institute of Welding Subcommission XV-E [36] for design of welded tubular joints under fatigue loading. Since this research focuses on onshore structures, the relevant provisions in CIDECT Design Guide 8 [21] were used for comparison purposes. For fatigue design of welded connections made of hollow structural sections (HSS), the "hot spot stress method" in CIDECT Design Guide 8 [21] considers the uneven stress distribution around the perimeter of the welded joint. It determines the permissible number of load cycles for a given hot spot stress range at a specific joint location from a fatigue strength curve. It should be noted that the provisions in CIDECT Design Guide 8 [21] has formed the basis of various national and international steel design standards for various applications. For example, for the design of pedestrian bridges where galvanized tubular steel trusses are often specified, the AASHTO design guide [37] suggests that for square and rectangular HSS components and details, the nominal fatigue resistance should be taken from the provisions in CIDECT Design Guide 8 [21].

For analysis undertaken using a sophisticated three dimensional finite element modelling approach, the hot spot stress ranges can be directly obtained from the analysis for each load combination. It should be noted that such approach is in general not feasible for structural designers. In a design office setting, simplified structural analysis using frame analysis is typically conducted to determine the member forces

and moments, which can be used to calculate the nominal stress ranges. SCFs can then be determined using the simplified parametric formulae or charts in CIDECT Design Guide 8 [21]. The hot spot stress range at one location of interest under one load case is the product of the nominal stress range and the corresponding SCF. Superposition of the hot spot stress ranges at the same location can be used for combined load cases.

A typical planar RHS T-connection is shown in Figure 2.3 where the geometric parameters and the locations of interests (lines of measurement A to E) are defined. For planar RHS T- and X-connections under in-plane bending on the branch, CIDECT Design Guide 8 [21] adopted the following equations for calculation of SCFs for the branch nominal stress ($S_{n,b}$) at the locations of interests:

For branch member (lines A and E):

$$SCF_{A,ipb} = SCF_{E,ipb} = (0.390 - 1.054\beta + 1.115\beta^2)(2\gamma)^{(-0.154+4.555\beta-3.809\beta^2)} \quad \text{Equation 2.1}$$

For joints with fillet welds, multiply branch SCF_A and SCF_E by 1.4.

For chord member (lines B, C and D):

$$SCF_{B,ipb} = (-0.011 + 0.085\beta - 0.073\beta^2)(2\gamma)^{(1.722+1.151\beta-0.697\beta^2)}\tau^{0.75} \quad \text{Equation 2.2}$$

$$SCF_{C,ipb} = (0.952 - 3.062\beta + 2.382\beta^2 - 0.0228 \cdot 2\gamma)(2\gamma)^{(-0.690+5.817\beta-4.685\beta^2)}\tau^{0.75} \quad \text{Equation 2.3}$$

$$SCF_{D,ipb} = (-0.054 + 0.332\beta - 0.285\beta^2)(2\gamma)^{(2.084-1.062\beta+0.527\beta^2)}\tau^{0.75} \quad \text{Equation 2.4}$$

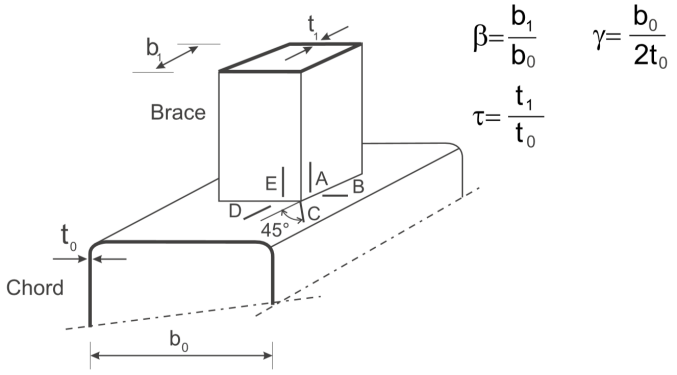

Figure 2.3. Geometric parameters and locations of interests for fatigue design of RHS T-connection (adapted from [21])

Since the isolated connection (especially those in experimental testing or numerical simulation) has to be in equilibrium, for T-connection in particular, chord loading will be developed due to: (1) branch axial force or branch in-plane bending; and (2) support reactions at the pin and roller supports at the chord ends. CIDECT Design Guide 8 [21] adopted the following formulae for calculation of the additional hot spot stresses due to the chord nominal stress under chord axial force and chord in-plane bending at the locations of interest:

For branch member (lines A and E):

$SCF_{A,ch} = SCF_{E,ch} = 0$ (negligible) Equation 2.5

For chord member (lines B, C and D):

$SCF_{B,ch} = 0$ (negligible) Equation 2.6

$SCF_{C,ch} = 0.725(2\gamma)^{0.248\beta}\tau^{0.19}$ Equation 2.7

$SCF_{D,ch} = 1.373(2\gamma)^{0.205\beta}\tau^{0.24}$ Equation 2.8

A minimum SCF of 2.0 is recommended for all locations and all load conditions (i.e. Equation 2.1 to Equation 2.4, Equation 2.7 and Equation 2.8). The ranges of validity of the above equations are as follows:

$0.35 \leq \beta \leq 1.0 \qquad 12.5 \leq 2\gamma \leq 25 \qquad 0.25 \leq \tau \leq 1.0$

It can be seen from Equation 2.1 to Equation 2.8 that the branch hot spot stresses (Lines A and E) and the chord hot spot stress at Line B are functions of only the branch loading. On the other hand, the chord hot spot stresses at Lines C and D are the superposition of those from both the branch and chord loadings [21]. For a given hot spot stress range at a specific joint location, the S-N curves in the design guide can then be used to determine the permissible number of load cycles for a given hot spot stress range at a specific joint location. However, as can be seen in Figure 2.3, large vent and drain holes are quite often specified at the locations recommended by the design guide for calculation of hot spot stresses. Hence, new formulae and charts need to be developed.

2.4. Summary of experimental data

Daneshvar and Sun [38] investigated the effects of vent and drain holes on the SCFs in RHS-to-RHS X-connections under branch axial loading. Ideally T-shaped moment connections should be tested. However, since (1) testing of full-scale connection is expensive and (2) the FEA in this study is purely linear elastic, the experimental data from X-connections (under branch axial loading) was used for FE validation for T-shaped moment connections and was deemed sufficient. The testing program included six RHS-to-RHS X-connections with and without holes. The six connection specimens were fabricated using RHS produced to Grade 350W Class C according to CSA G40.20/G40.21 [27] (nominal yield strength = 350 MPa, nominal tensile strength = 450 MPa), and partial joint penetration welds, using the flux cored arc welding process [40]. The connection specimen IDs in Table 2.1 include two components. The first distinguishes the specimen by its configuration, where X = X connection with no hole; XF = X connection with holes at the center of branch flat faces, XC = X connection with holes at corners. The second component is the branch-to-chord width ratio of the connection specimen. Figure 2.4 shows a drawing for a typical connection with holes specified at the branch corner regions. The connection specimens were selected in such a way that the most interesting parameters are covered, including holes at different locations and the branch-to-chord width ratio (β).

Table 2.1. Nominal geometry of test specimens

Specimen ID	Chord ($b_0 \times h_0 \times t_0$) (mm)	Branch ($b_1 \times h_1 \times t_1$) (mm)	$\beta = b_1/b_0$	$2\gamma = b_0/t_0$	$\tau = t_1/t_0$
X-0.5	178×178×12.7	89×89×9.53			
XF-0.5	178×178×12.7	89×89×9.53	0.5	14	0.75
XC-0.5	178×178×12.7	89×89×9.53			
X-0.7	178×178×12.7	127×127×9.53			
XF-0.7	178×178×12.7	127×127×9.53	0.7	14	0.75
XC-0.7	178×178×12.7	127×127×9.53			

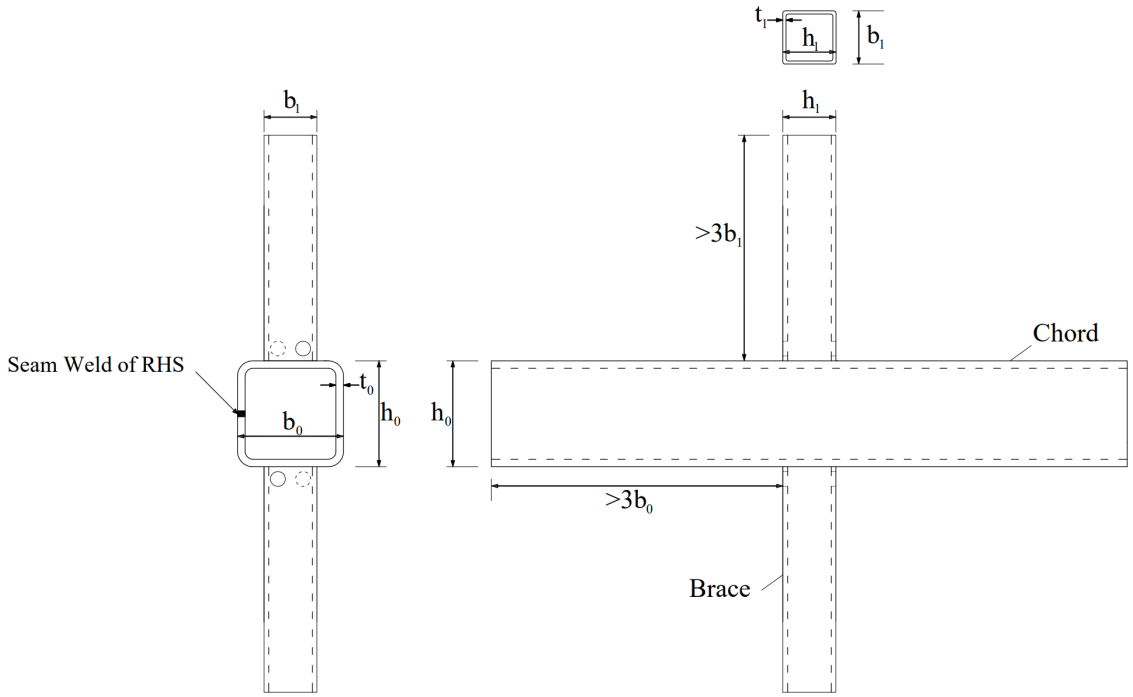

Figure 2.4. Typical connection specimen and symbol definitions

For determination of SCFs using the experimental approach, the Strain Concentration Factors (SNCFs) are determined first since only strains can be directly measured using strain gauges [29-32]. Specialized chain strain gauges were installed on the connection specimens at the critical hot spot stress locations identified by a preliminary FE analysis. As shown in Figure 2.5, the locations include those recommended by the CIDECT Design Guide 8 [21] and those near the galvanizing holes to consider the local stress concentrations. The details of the FE analysis can be found in Daneshvar and Sun [38]. During testing, a branch axial compression load was applied following a predetermined multi-stage loading scheme based on the preliminary FE analysis to ensure a linear elastic behaviour. At each loading stage, the hot spot strains were calculated using the quadratic extrapolation method recommended by the CIDECT Design Guide 8 [21], the average SNCF-values at each hot spot locations were calculated by averaging all values (including the data from the two sets of gauges on both sides of the connection specimen) at all predetermined load levels. The average SNCFs for the six connection specimens are shown in Figure 2.6.

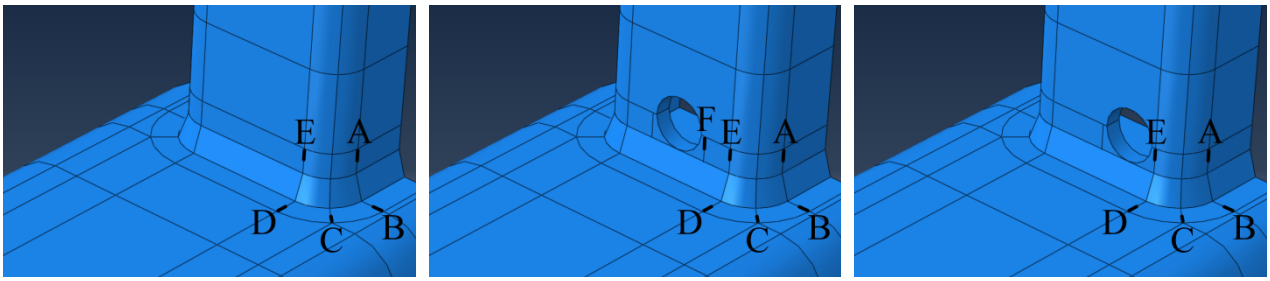

(a) Connection with no hole (b) Connection with hole on flat face (c) Connection with hole at corner region

Figure 2.5. Typical connection models and lines of interest

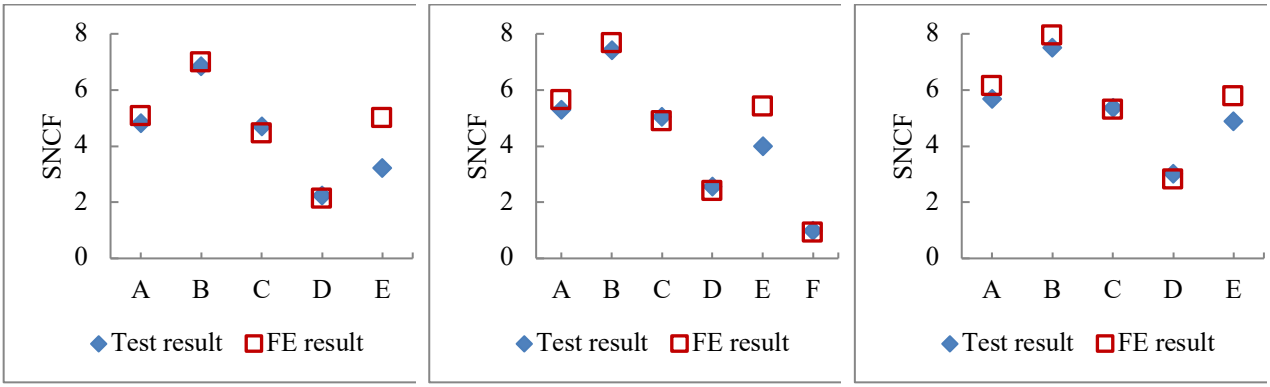

$\frac{\text{Test result}}{\text{FE result}}$ $\frac{\text{Test result}}{\text{FE result}}$ $\frac{\text{Test result}}{\text{FE result}}$

Mean = 0.938 COV = 0.185 Mean = 0.970 COV = 0.128 Mean = 0.960 COV = 0.090

(g) X-0.5 (h) XF-0.5 (i) XC-0.5

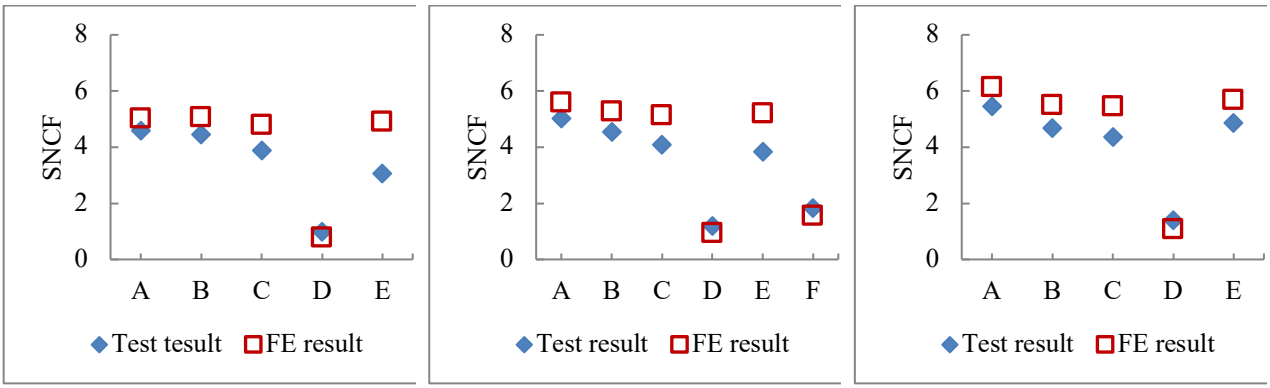

$\frac{\text{Test result}}{\text{FE result}}$ $\frac{\text{Test result}}{\text{FE result}}$ $\frac{\text{Test result}}{\text{FE result}}$

Mean = 0.894 COV = 0.252 Mean = 0.958 COV = 0.229 Mean = 0.936 COV = 0.214

(j) X-0.7 (k) XF-0.7 (l) XC-0.7

Figure 2.6. Comparison of SNCFs values obtained from experiments and FE analyses for X-connections

2.5. Development and verification of finite element modelling

2.5.1. Modelling of X-connections under branch axial loading

For initial validation of the modelling approach, the measured geometric properties of the six connection specimens and the boundary conditions in the test setup were used to develop replicate FE models in ABAQUS [22]. The details of a typical FE model are shown in Figure 2.7. Previous numerical research on regular RHS connections by van Wingerde [42], square bird-beak RHS connections by Cheng et al. [43], and diamond bird-beak RHS connections by Tong et al. [31,32] showed that the stress concentrations at the joint location could be influenced by the weld dimensions. As the weld leg size-over-branch wall thickness ratio increased from 1.0 to 1.5, an average decrease of 9% in SCF-values was observed by Tong et al. [31,32]. At the locations where the branch member wall is perpendicular to the chord surface, Cheng et al. [43] used the weld sizes shown in Figure 2.8. The sizes are consistent with the prequalified weld details provided by AWS D1.1 [33]. The same weld size was used by Tong et al. [31,32]. In this research, the profile in Figure 2.8 was used to model the weld. Linear elastic properties were applied to both the steel and weld materials in the FE models, where Young's modulus (E) = 200 GPa, and Poisson's ratio (ν) = 0.3. The stress contours were carefully monitored to ensure that the SCFs at the locations of interests are not influenced by different load levels within the elastic range. All modelling details conform to the recommendations in CIDECT Design Guide 8 [21]. In general, four layers of solid elements (C3D20R in ABAQUS) through the branch and chord wall thickness were used. The same solid elements were used to model the weld. These ensured the modelling accuracy and provided convergent initial stiffness and load-deformation responses for all six connections. In particular, a sensitivity analysis was performed to determine the suitable level of mesh refinement in the adjacent area of the vent and drain holes. The aim was to ensure that the refinement of the mesh was appropriate such that any further refinement did not result in a substantial change of the stress distribution. Based on the sensitivity analysis, the length of all sides of any solid element at the hole location were forced to be no larger than 0.5 mm. From the adjacent area of the hole to the welded joint, and then to the locations away from the joint, the element size increases, with a biased mesh pattern ensuring a smooth transition between the areas of fine and coarse meshes.

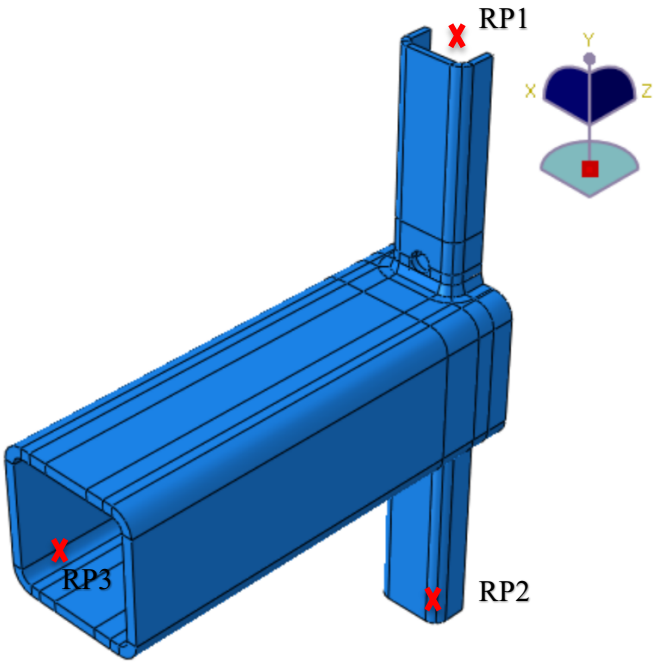

(a) Typical connection model

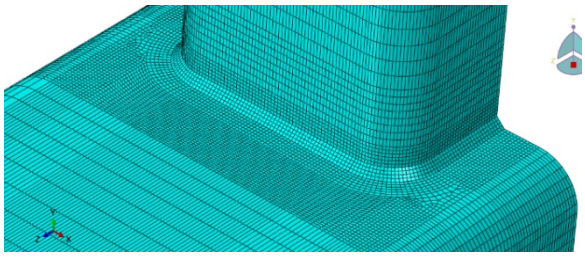

(b) Typical mesh pattern for connection without vent and drain holes

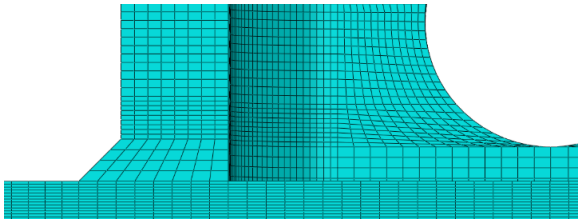

(c) Typical mesh pattern at weld and hole locations

Figure 2.7. Typical FE RHS-to-RHS X-connection geometry and mesh layout

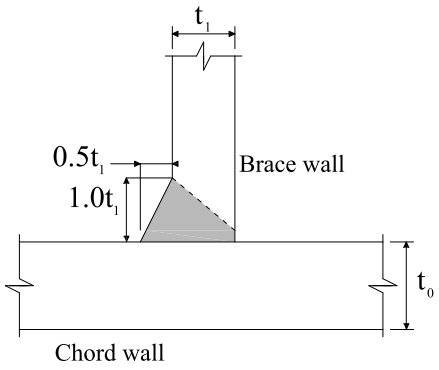

Figure 2.8. Weld simulation using profile suggested by Cheng et al. [43] and Tong et al. [31,32]

2.5.2. Verification of finite element modelling

For validation of the modelling approach used herein, quadratic extrapolation following the recommendations in CIDECT Design Guide 8 [21] was performed on the FE models to determine the SNCFs at the same locations where chain strain gauges were installed on the chord and branch members. The FE values are compared to the experimentally obtained SNCFs in Figure 2.6. As shown, the SNCFs values obtained from experiments and FE analyses agree well. In general, the FE values are slightly larger than the test results, which is favourable for fatigue assessment since a higher SNCF gives a conservative estimate of fatigue life. Hence, the accuracy of the modelling approach is confirmed.

Further credence was given to the modelling approach by checking the stress contours at the welded joints of the models. For both experimentally tested and numerically simulated connections, an axial compression was applied to the top branch end. According to the strain gauge readings and the numerical simulation results, maximum compressive stresses were observed in the two branch side walls at the welded joint location. On the other hand, tensile stresses were observed near the center of the two branch transverse walls. An example is provided in Figure 2.9. This is consistent with the findings by [36-38] during connection testing under small branch axial compression loads, due to geometric compatibility. The mechanism is illustrated in Figure 2.10. As shown, the deformation of the chord cross section is restrained by the branch. In other words, the branch member, through the weld, pulls up the chord face. Therefore, tensile stresses are developed at the center of the branch transverse walls. It should be noted that, although the stresses on Line F were tensile, following the suggestions by [30-32], positive SNCF-values are shown in Figure 2.6 for connection specimens XF-0.5 and XF-0.7 for simplification.

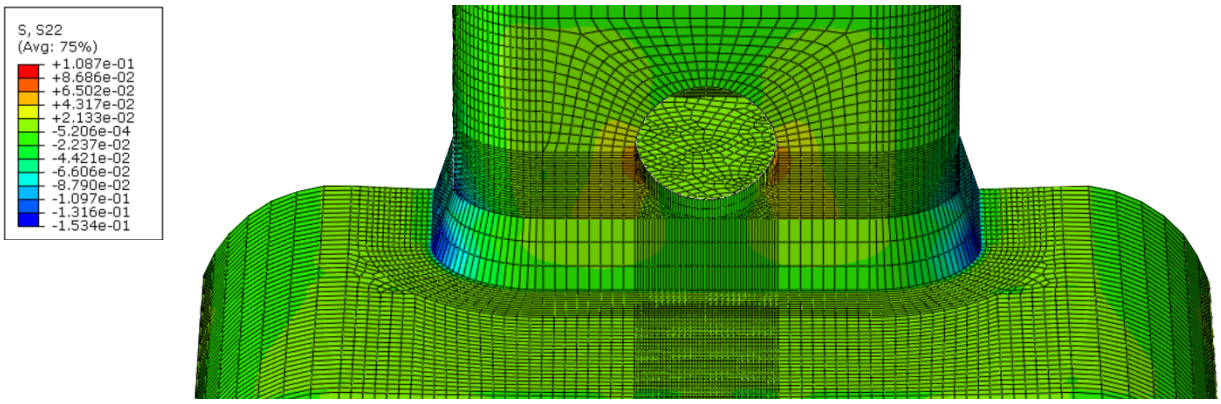

Figure 2.9. FE stress contour of connection with hole at center of branch transverse wall

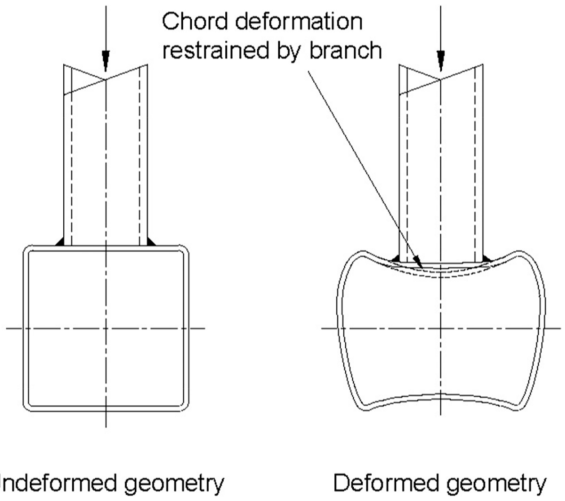

Figure 2.10. Geometric compatibility for RHS-to-RHS connection (adapted from [41])

2.5.3. Modelling of T-connections under branch in-plane bending

After validation of the X-connection models against the experimental data, the lower branches were removed to create the T-connection models listed in Table 2.2. The connection ID components are similar to those in Table 2.1. The first distinguishes the FE model by its configuration, where T = T connection with no hole; TF = T connection with holes at the center of branch flat faces, TC = T connection with holes at corners. The second component is the branch-to-chord width ratio of the connection. Previous

research [38-40] showed that the chord length and boundary conditions could influence the connection behaviour. Hence, to prevent these factors from having an excessive influence on the experimental or numerical results, special attention must be paid in research. Therefore, investigations have been conducted in this regard [38-40] to capture the effects of different chord length and boundary conditions so that the isolated connection behaviour can be linked to the general frame behaviour. In this research, the approach for modelling T-connections under branch axial bending followed the recommendations in the above investigations.

Table 2.2. Nominal geometry of verified T-connection models

Connection ID	Chord ($b_0 \times h_0 \times t_0$) (mm)	Branch ($b_1 \times h_1 \times t_1$) (mm)	$\beta = b_1/b_0$	$2\gamma = b_0/t_0$	$\tau = t_1/t_0$
T-0.5	178×178×12.7	89×89×9.53			
TF-0.5	178×178×12.7	89×89×9.53	0.5	14	0.75
TC-0.5	178×178×12.7	89×89×9.53			
T-0.7	178×178×12.7	127×127×9.53			
TF-0.7	178×178×12.7	127×127×9.53	0.7	14	0.75
TC-0.7	178×178×12.7	127×127×9.53			

In particular, the FE boundary conditions for the models were modified to simulate a typical setup for testing of welded hollow section T-connections under branch in-plane bending (see Figure 2.11 for an example [29]). The modelling approach used by [41,42] was used in this study. A rigid body constraint was first defined for each chord end, which was later used to slave all nodes on each end to a reference point (RP in Figure 2.12) located at the centre of the cross section. Different restraint conditions were then applied at the two reference points to simulate the behaviours of the pin and roller supports. All translational degrees of freedom were restrained for the reference point at the pin support location. On the other hand, only the two translational degrees of freedom perpendicular to the longitudinal axis of the chord member were restrained for the reference point at the roller support location.

A small lateral load was then applied to a reference point attached to all nodes of the top branch member end to generate the branch in-plane bending. A linear elastic behaviour was ensured. For all connection models, the chord member lengths equal to $6b_0$ to ensure that the joint was sufficiently far away from the support to mitigate the effects of end constraints on the stress distribution at the joint [41,42]. Similarly, the branch lengths equal to $4b_1$ to avoid possible end effects.

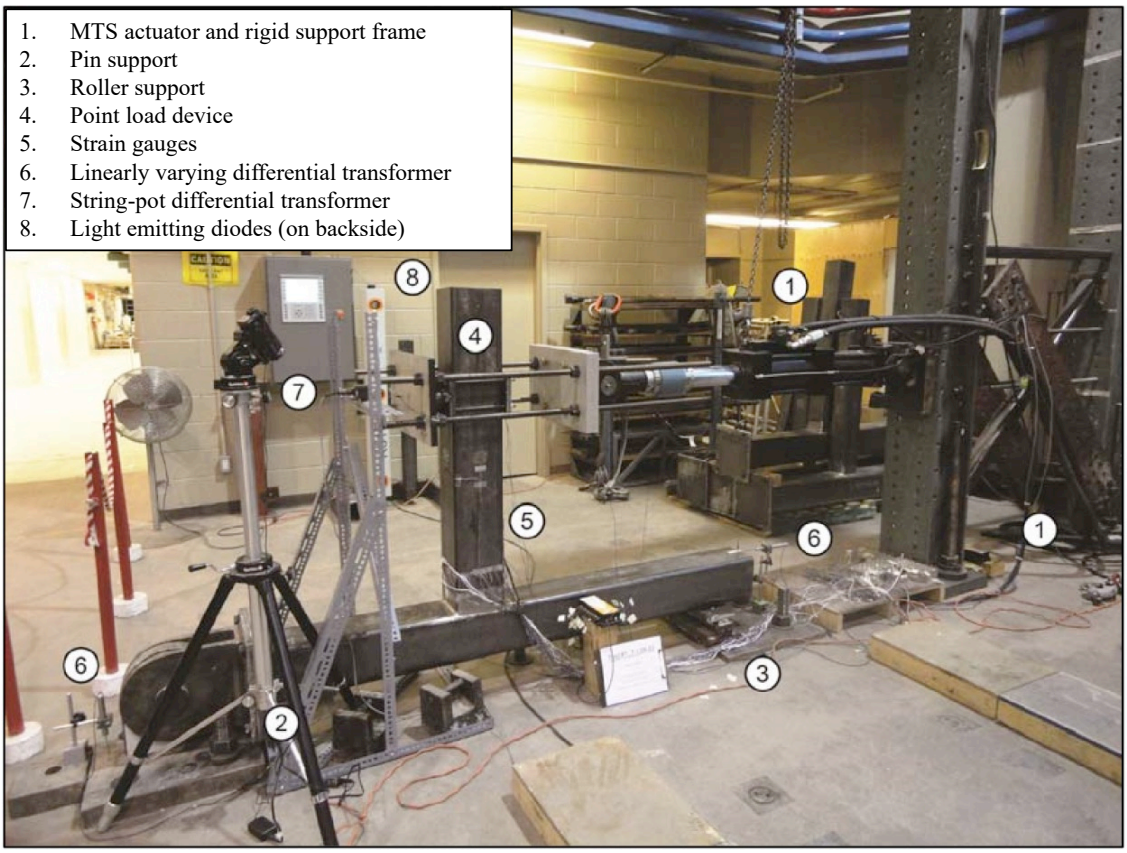

Figure 2.11. RHS-to-RHS moment T-connection experimental test setup [29]

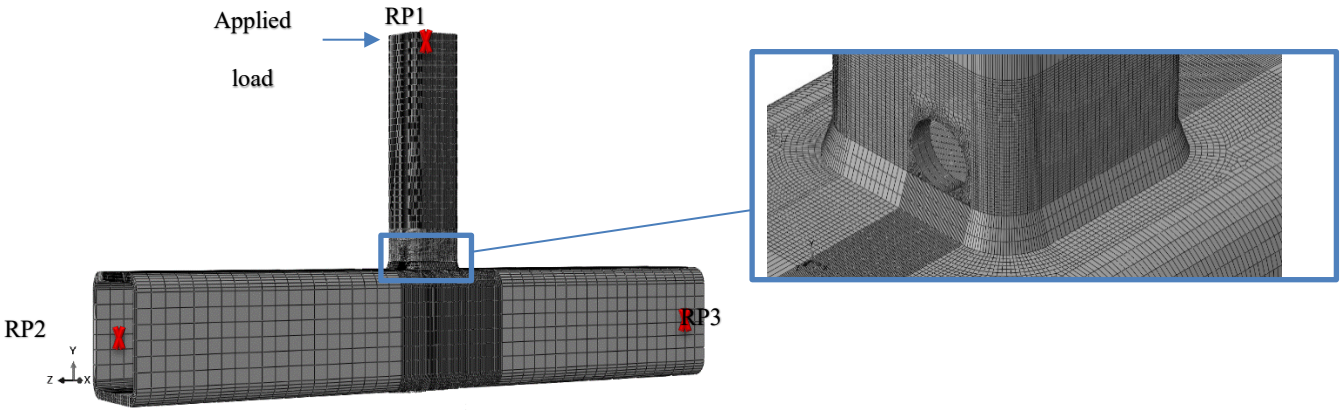

Figure 2.12. Typical FE RHS-to-RHS T-connection geometry, mesh layout and load application

2.5.4. Comparison with FE results using relevant design formulae

For each FE T-connection model, the hot spot stresses (S_{rhs}) at different locations were obtained using the extrapolation method. The branch nominal stress ($S_{n,b}$) was determined by dividing the in-plane bending moment by the branch elastic section modulus. The comparison of the predicated S_{rhs} / $S_{n,b}$-values by CIDECT Design Guide 8 [21] with the numerical results from the six verified FE T-connection models is shown in Figure 2.13. As shown, the CIDECT predictions are conservative for connections without vent and drain holes. On the other hand, for connections with holes at the center of the branch flat faces, the safety margin is inadequate. For connections with holes at the branch corner regions, the CIDECT predictions are unsafe. Since only the branch-to-chord width ratio ($\beta = b_1/b_0$) varies in Figure 2.13, a parametric study is desirable to: (i) explore the influences of the other non-dimensional geometric parameters including the chord width-to-thickness ratio ($2\gamma = b_0/t_0$), and branch-to-chord thickness ratio ($\tau = t_1/t_0$); and (ii) establish general conclusions and develop new parametric formulae for better prediction of SCFs in galvanized RHS connections with vent and drain holes.

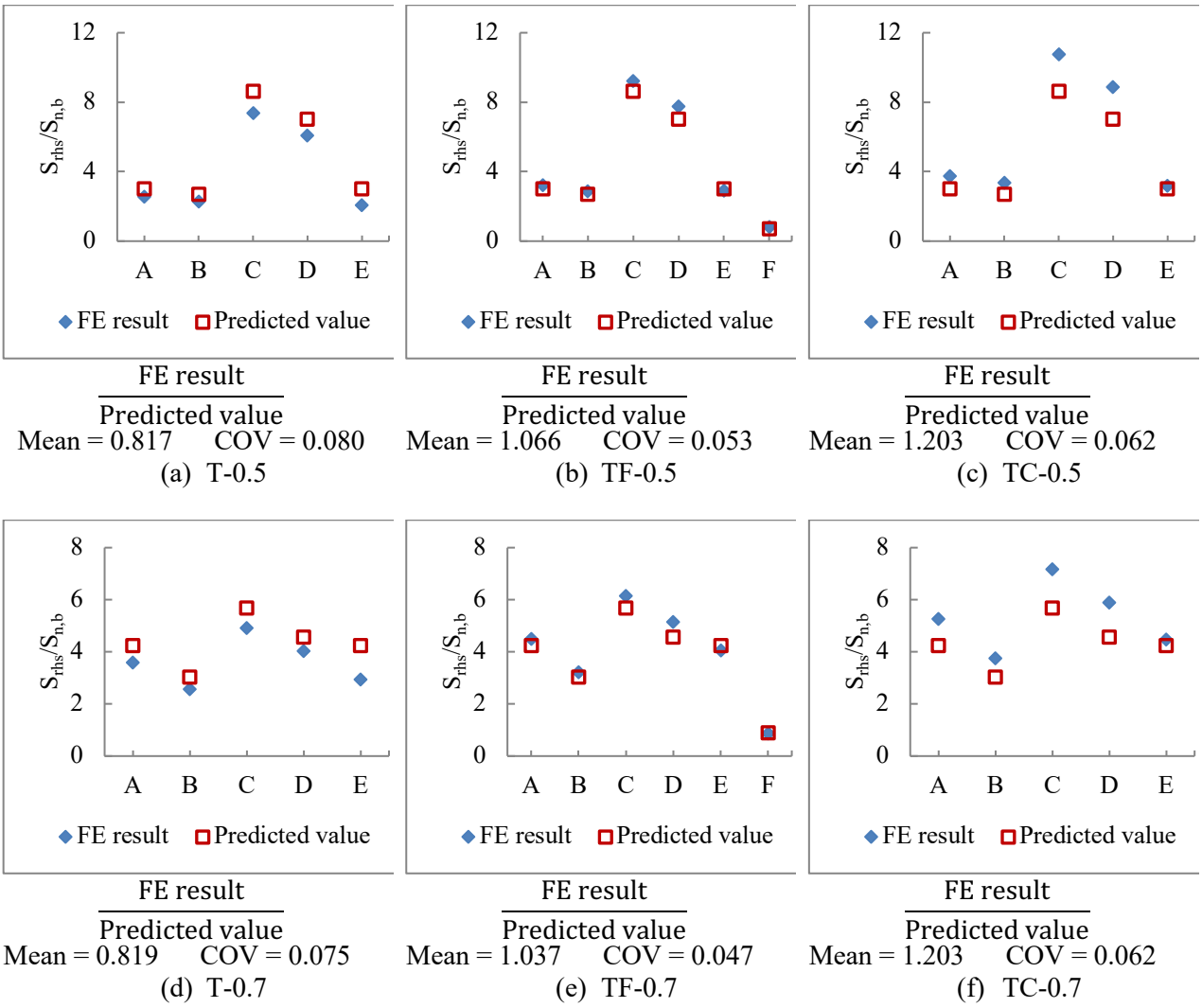

Figure 2.13. Comparison of predicated Srhs / Sn,b-values by CIDECT Design Guide 8 [21] with numerical results from calibrated FE T-connection models

2.6. Numerical parametric study

2.6.1. Ranges of parameters

Similar to the preliminary FE analysis, for the parametric study, the profile in Figure 2.12 was used to model the weld. Linear elastic properties were applied to both the steel and weld materials in the FE models, where Young's modulus (E) = 200 GPa, and Poisson's ratio (ν) = 0.3. The stress contours were carefully monitored to ensure that the SCFs at the locations of interests are not influenced by different load levels within the elastic range. All modelling details conform to the recommendations in CIDECT Design Guide 8 [21]. Following the recommendation in AISC Design Guide 24 [20], a 25-mm diameter was applied to all galvanizing holes in all FE parametric models. The branch-to-chord angles of all models were kept 90°. The variations of non-dimensional parameters are listed in Table 2.3. The parameters are within the ranges of validity adopted by CIDECT Design Guide 8 [21]. These parameters were used to develop a total of 192 square RHS-to-RHS moment T-connections models, including: (1) 64 connection models with no hole; (2) 64 connection models with a pair of holes at the centre of the two branch transverse wall; and (3) 64 connection models with a pair of holes at the corner regions of the two branch transverse wall. All FE models have the same chord member width (b_0) of 200 mm. The other dimensions of the parametric models vary according to the selected non-dimensional parameters. All chord member lengths were set to be $6b_0$ and all branch members lengths to $4b_1$ to avoid "end effects" [29-32,38-42]. With the selected non-dimensional parameters, the branch and chord member sizes of all FE models are in general within the range of practical applications.

Table 2.3. Non-dimensional parameters for FE analysis

$\beta = b_1/b_0$	$2\gamma = b_0/t_0$	$\tau = t_1/t_0$
0.35	12.5	0.25
0.50	16.0	0.50
0.65	20.0	0.75
0.80	25.0	1.0

2.6.2. Results of parametric study

For all FE models, the stresses on both branch and chord sides around the entire perimeter of the welded joint were carefully monitored, especially those at the critical locations shown in Section 2.4 including those near the galvanizing holes. The findings of the parametric study are consistent with those from the preliminary FE analysis shown in Figure 2.13. Typical stress contours of FE models are shown in Figure 2.14, in which the three FE connections have the same chord and branch sizes and are subject to in-plane bending moment of the same magnitude. It can be seen that the galvanizing holes can sometimes significantly increase the stresses at the welded joint location. Based on the results from the 192 parametric models, it was found that:

(1) For the 64 connections with holes on the branch transverse walls, the Srhs / Sn,b-values at location F never governed. Hence, it can be concluded that Line F is not a line of interest. In other words, it was confirmed via the parametric analysis that the critical hot spot stress locations are the same for connections with and without holes (i.e. locations A to E in Fig. 3).

(2) Comparing to the connections with no hole, the Srhs / Sn,b-values in the connections with holes at the branch flat face are on average 37% and 32% higher on the branch side and on the chord side, respectively. Comparing to the connections with no hole, the Srhs / Sn,b-values in the connections with holes at the branch corner region are on average 59% and 56% higher on the branch side and on the chord side, respectively. Hence, the stress concentration can be significantly affected by the presence of the hole.

(3) For the 64 connections with no hole, the Srhs / Sn,b-values in the branch and chord are on average 75% and 82% of the predicted values calculated using the CIDECT formulae [21]. For the 64 connections with holes on the branch flat faces, the Srhs / Sn,b-values in the branch and chord are on average 3% lower and 8% higher than the predicted values. For the 64 connections with holes at the branch corner regions, the Srhs / Sn,b-values in the branch and chord are on average 19% and 28% higher than the predicted values. Hence, it is unsafe to use the existing formulae for such connections, and new formulae that take vent and drain holes into account need to be proposed.

The S_{rhs} / $S_{n,b}$-values for different non-dimensional parameters are shown in Figure 2.15 to Figure 2.17. In general, the highest SCFs are found for medium β-ratios. The lower the 2γ-ratio, the lower is the SCF. The lower the τ-ratio, the lower is the SCF in the chord, but it has less effect on the branch. For the connections without vent and drain holes, high SCFs often occur in the chord at locations B and C. On the other hand, for the connections with vent and drain holes, high SCFs can often occur at other locations as well, such as locations D and E. In general, the trends in these figures agree well with the design charts in the CIDECT Design Guide 8 [21]. It can be seen from the results of the parametric study that a galvanizing hole at the corner region of an RHS branch can sometimes lead to significant increases in SCF-values. The increases in SCF-values due to a galvanizing hole at the center of the branch flat face are large as well but relatively smaller. Hence, it is recommended that for hot-dip galvanizing of a planar truss, the galvanizing holes should be specified that the center of the branch transverse wall (see Figure 2.2(a) for an example). At the same time, when hanging the planar truss, it should be oriented to have the vent hole at the highest point and the drain hole at the lowest point of the branch member during galvanizing. However, for galvanizing of a multiplanar truss, it may be necessary to specify vent and drain holes at the branch corner regions (see Figure 2.2(b) for an example).

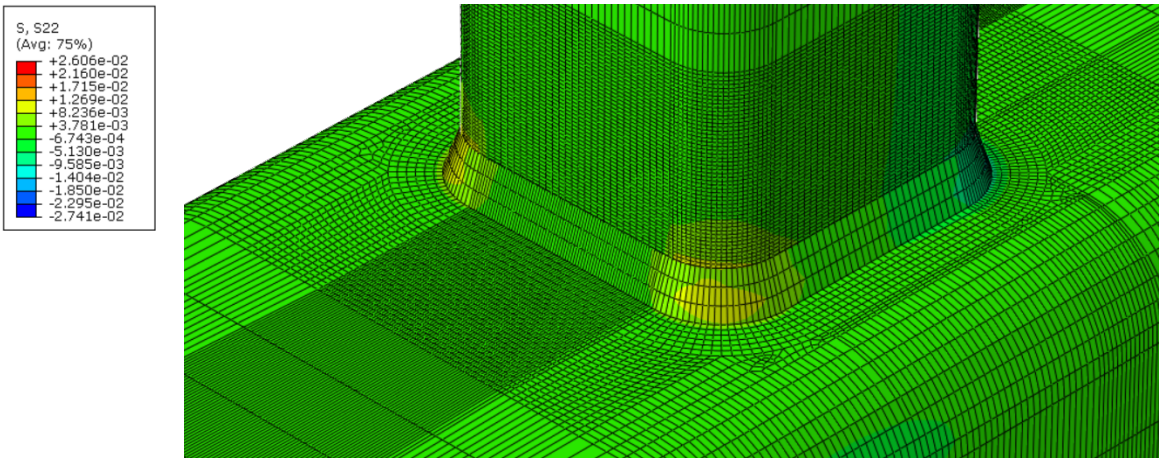

(a) Connection with no hole

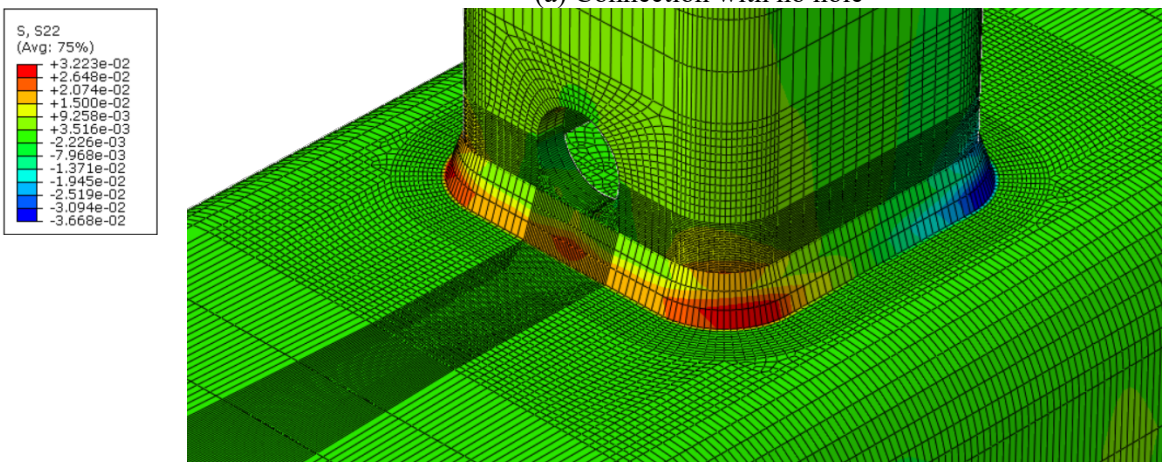

(b) Connection with holes at branch flat faces

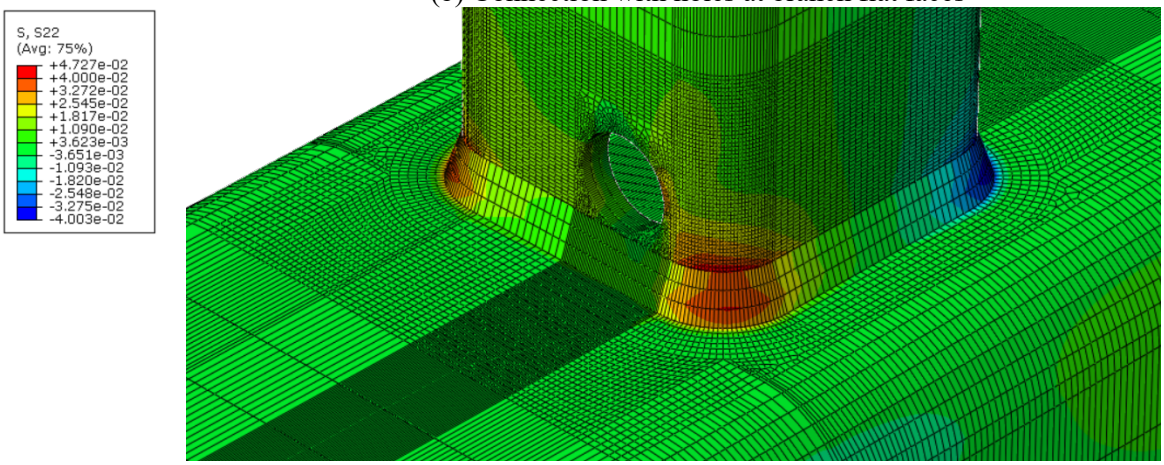

(c) Connection with holes at branch corner regions

Figure 2.14. Typical stress contours of FE RHS-to-RHS moment T-connection models

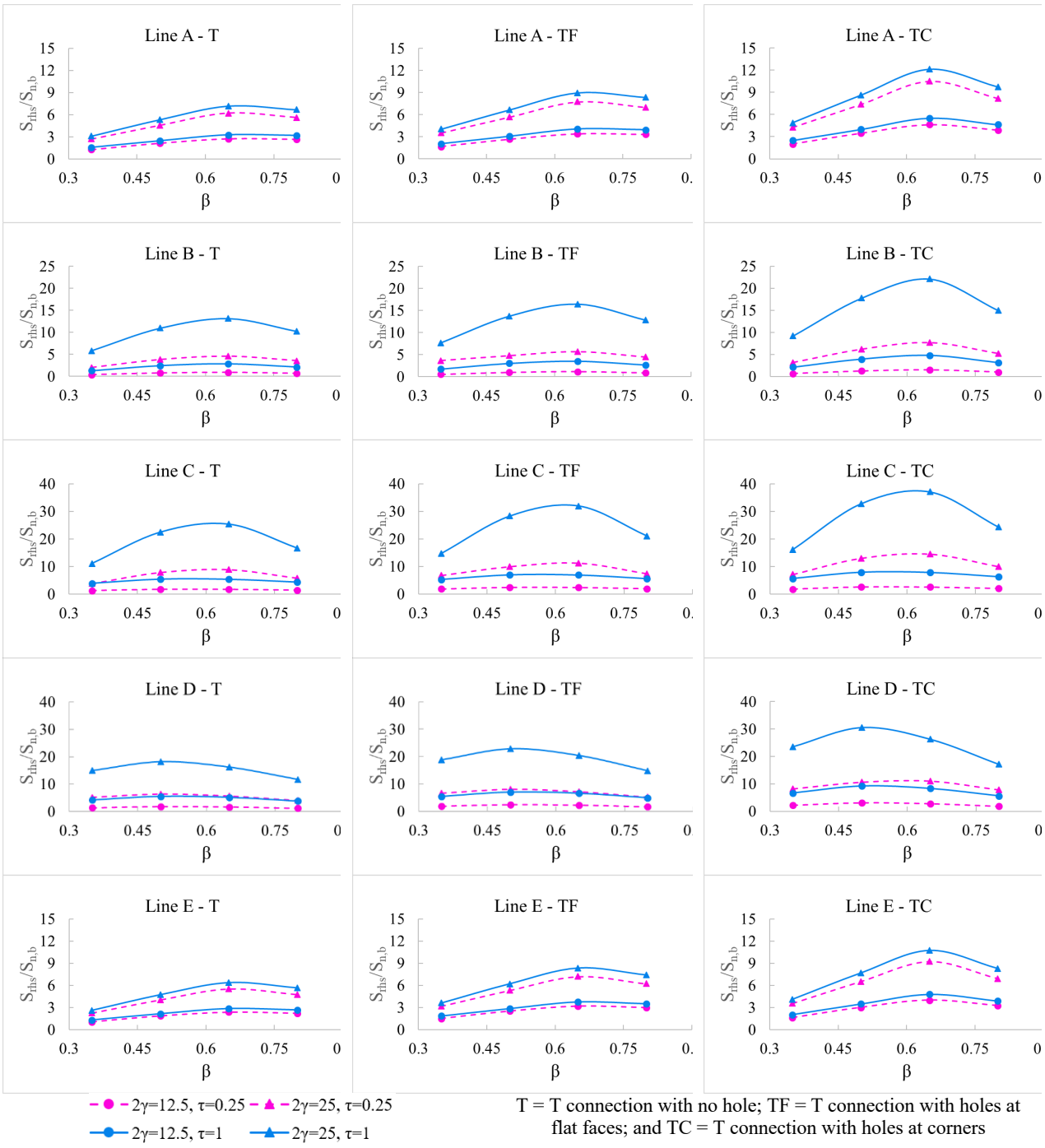

Figure 2.15. Influence of β on SCFs in RHS connections with and without holes under branch in-plane loading

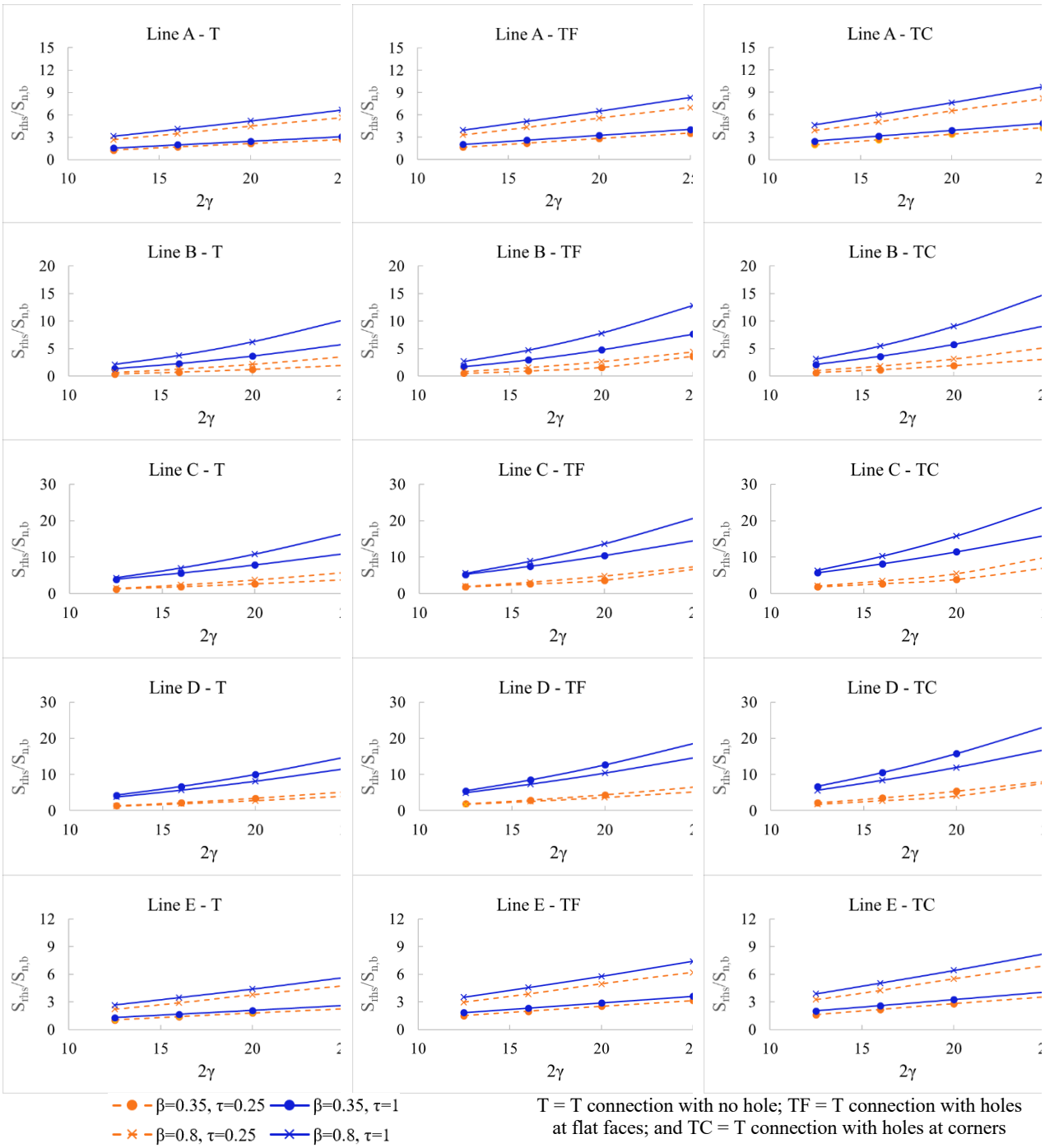

Figure 2.16. Influence of 2γ on SCFs in RHS connections with and without holes under branch in-plane loading

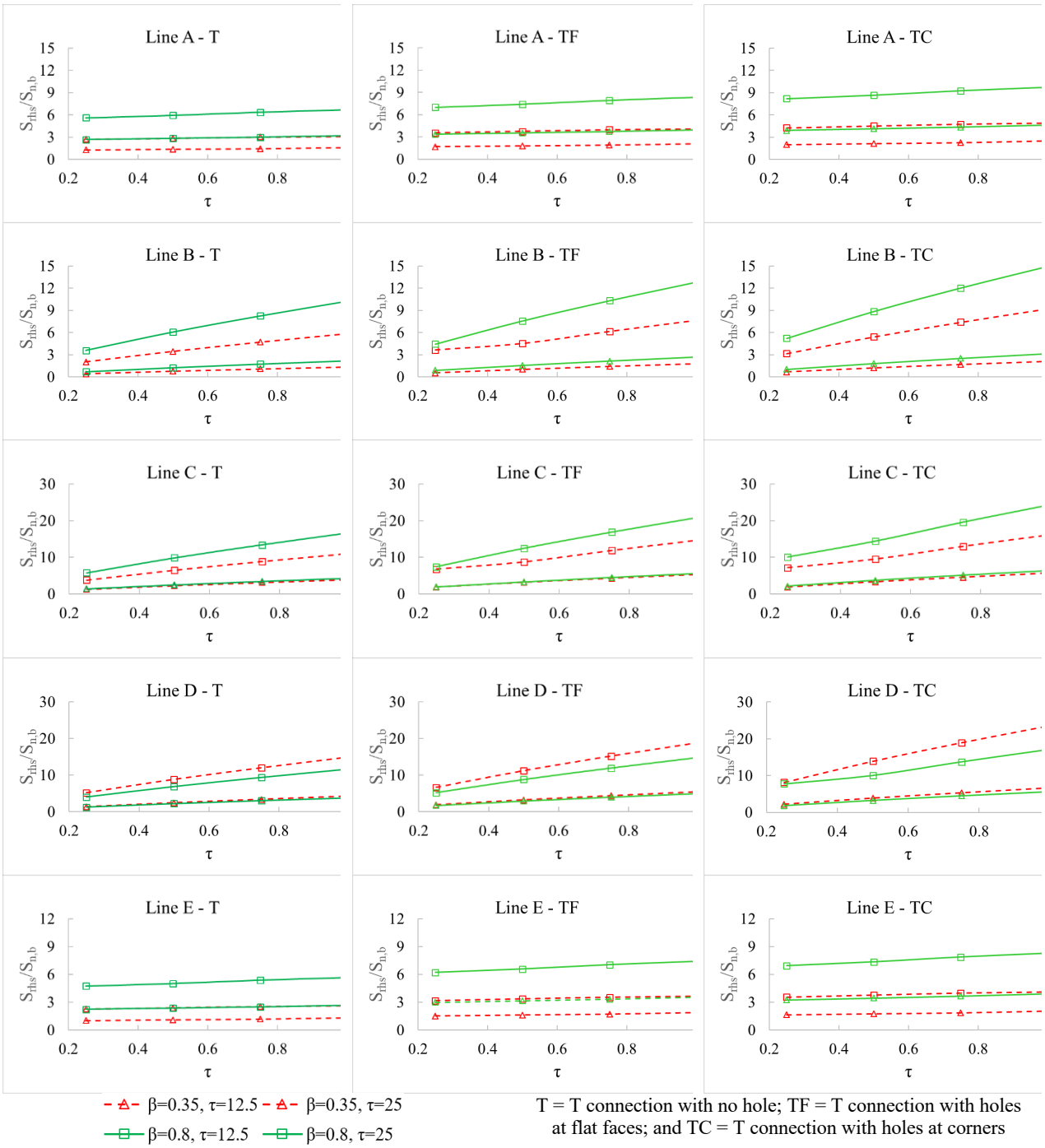

Figure 2.17. Influence of τ on SCFs in RHS connections with and without holes under branch in-plane loading

2.6.3. Procedures for development of SCF formulae

This section discusses the procedures for:

(1) development of formulae for $SCF_{ipb\text{-}in\text{-}branch}$ in Equation 2.10 for calculation of hot spot stresses (S_{rhs}) in branch under branch in-plane bending; and

(2) development of formulae for $SCF_{ipb\text{-}in\text{-}branch}$ and $SCF_{chord\text{-}loading}$ in Equation 2.12 for calculation of hot spot stresses (S_{rhs}) in chord under branch in-plane bending and chord loading.

These new formulae are developed using the data from the parametric study, and are listed in Section 2.6.4. The new formulae can be used for galvanized RHS moment connections, considering the increase in hot spot stresses due to specification of vent and drain holes at different branch locations. The approach used by van Wingerde et al. [42], which was used to develop the formulae in CIDECT Design Guide 8 [21], was adopted in this research.

2.6.3.1. SCFs in branch

For branch member, the in-plane bending moment at the welded joint location is calculated by multiplying the lateral force by the vertical distance between the line of application of the force and the top face of the chord (see Figure 2.18). The branch nominal stress ($S_{n,b}$) was calculated using Equation 2.9.

$$S_{n,b} = \frac{P_1 \cdot L_1}{W_1} \qquad \text{Equation 2.9}$$

where W_1 is the elastic section modulus for the branch member. For each FE connection model, the hot spot stresses (S_{rhs}) along Lines A and E at the weld toe locations were calculated using the extrapolation method. The SCF-values at these locations were then determined using the relationship in Equation 2.10.

$$S_{rhs} = SCF_{ipb-in-branch} \cdot S_{n,b} \qquad \text{Equation 2.10}$$

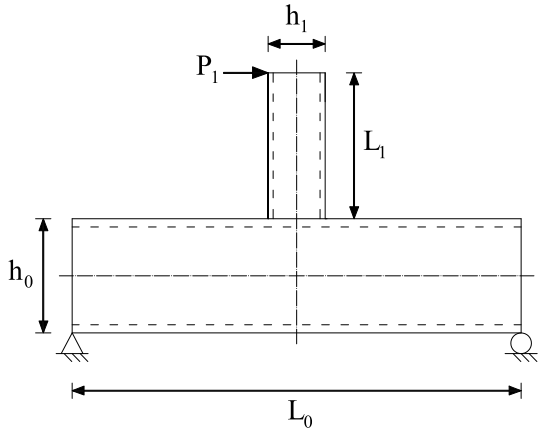

Figure 2.18. planar RHS-to-RHS T-connection under branch in-plane bending

Using the FE data from the parametric models under P_1 (see Figure 2.18), following the procedures adopted by [29,32], multiple regression analysis were performed to develop the formulae for $SCF_{ipb\text{-}in\text{-}branch}$ in Equation 2.10 for calculation of hot spot stresses in branch under branch in-plane bending for RHS T- and X-connections with vent and drain holes at different locations. Equation 2.11 suggested by [4,29,32] was used in this study as the general format.

$$SCF = (a + b \cdot \beta + c \cdot \beta^2 + d \cdot 2\gamma) \cdot (2\gamma)^{(e+f \cdot \beta + g \cdot \beta^2)} \cdot (\tau)^h \quad \text{Equation 2.11}$$

where the constants a to h can be determined by multiple regression analysis.

2.6.3.2. SCFs in chord

The CIDECT Design Guide 8 [21] formulae for calculation of total hot spot stresses in chord member of planar RHS-to-RHS X- or T- connection under branch in-plane bending and chord loading is listed here as Equation 2.12.

$$S_{rhs} = SCF_{ipb-in-branch} \cdot S_{n,b} + SCF_{chord-loading} \cdot S_{n,ch} \quad \text{Equation 2.12}$$

where $S_{n,ch}$ is the chord nominal stress due to chord axial force or bending. It should be noted that CIDECT Design Guide 8 [21] uses the same formulae (Equation 2.6 to Equation 2.8) for calculation of SCFs in chord due to two different chord loading conditions: (i) chord axial force, and (ii) chord in-plane bending. This is because fatigue design check is performed on the connecting face (e.g. top chord surface in Figure 2.18). Both chord axial force and chord bending moment produce on the connecting face chord nominal stress in the axial direction. The hot spot stresses result from these chord nominal stresses due to the same geometric influences at the joint locations [21].

In experimental and numerical research on HSS connections, isolated connections are usually studied, where the total hot spot stresses at the critical locations can be determined. In theory, the hot spot stress range at one location under one load case is the product of the nominal stress range and the corresponding SCF. Superposition of the hot spot stress ranges at the same location can be used for combined load cases. As discussed previously, in this research the approach used by van Wingerde et al. [42], which was used to develop the formulae in CIDECT Design Guide 8 [21], was used to determine the SCFs due to both branch in-plane bending and chord loading. Specifically, $SCF_{chord\text{-}loading}$ in Equation 2.12 was first determined. By subtracting $SCF_{chord\text{-}loading} \cdot S_{n,ch}$ from the total hot spot stress (S_{rhs}), $SCF_{ipb\text{-}in\text{-}branch}$ in Equation 2.12 was then determined.

In this research, another set of 192 FE models with only chord axial force, P_0 in Figure 2.19, were developed. The chord nominal stress due to P_0 was calculated using Equation 2.13.

$$S_{n,ch} = \frac{P_0}{A_0} \quad \text{Equation 2.13}$$

where A_0 is the cross-sectional area of the chord member. The chord hot spot stresses at the locations of interest under P_0 only were determined from FE analysis.

Using the chord hot spot stress data from the parametric models under P_0 (see Figure 2.19), multiple regression analysis were performed to develop the formulae for $SCF_{chord\text{-}loading}$ in Equation 2.12. Equation 2.14 recommended by CIDECT Design Guide 8 [21] was used in this study as the general format.

$$SCF_{chord-loading} = a \cdot (2\gamma)^{e\cdot\beta} \cdot (\tau)^{h}$$ Equation 2.14

where the constants a to h can be determined by multiple regression analysis.

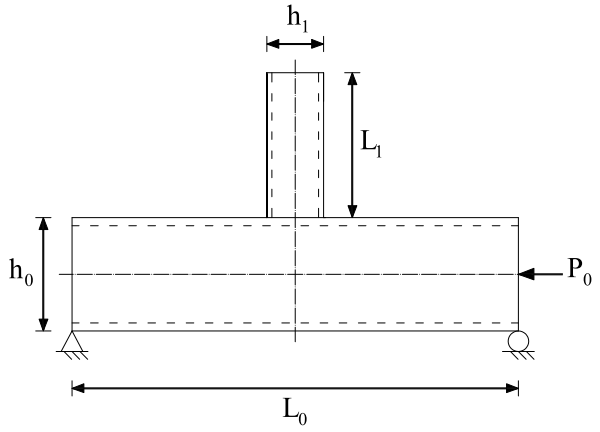

Figure 2.19. Planar RHS-to-RHS T-connection under chord axial force

For determination of $SCF_{ipb\text{-}in\text{-}branch}$ in Equation 2.12, the original set of 192 FE models under branch in-plane bending (illustrated in Figure 2.18) was used. The total hot spot stresses (S_{rhs} in Equation 2.12) at the locations of interest on the chord member can be directly obtained using the extrapolation method in FE analysis. It should be noted that S_{rhs} in this case results from: (i) branch in-plane bending; and (ii) chord bending due to support reactions. $S_{n,b}$ in Equation 2.12 can be calculated using Equation 2.9. $S_{n,ch}$, which in this case is the chord nominal stress at the welded joint side of critical cross section of the chord member due to chord loading, can be calculated using the simple beam theory and Equation 2.15.

$$S_{n,ch} = \frac{\left[\frac{P_1 \cdot \left(L_1 + {h_0}/{2}\right)}{L_0}\right] \cdot \left(\frac{L_0 - h_1}{2}\right)}{W_0}$$ Equation 2.15

where W_0 is the elastic section modulus of the chord member.

Since $SCF_{chord\text{-}loading}$ can be calculated using the already derived Equation 2.14, for each FE connection model, the only unknown in Equation 2.12 is $SCF_{ipb\text{-}in\text{-}branch}$, which can then be easily calculated. Using the $SCF_{ipb\text{-}in\text{-}branch}$ data from the parametric study, multiple regression analysis can be performed to develop the SCF formulae, using Equation 2.11 as the general format.

2.6.4. Proposed SCF formulae

Following the procedures discussed in Section 2.6.3, the SCF formulae for planar RHS-to-RHS moment T-connection *with vent and drain holes on the center of branch transverse walls* are listed in Table 2.4.

The SCF formulae for such connection *with vent and drain holes at the branch corner regions* are listed in Table 2.5.

Table 2.4. RHS moment T-connection with vent and drain holes on branch flat faces

Load condition 1: in-plane bending on the branch	
For branch member (lines A and E):	
$SCF_A = (-0.227 + 1.309\beta - 1.172\beta^2 - 0.002\gamma)(2\gamma)^{(1.992-3.053\beta-3.309\beta^2)}\tau^{0.119}$	Equation 2.16
$SCF_E = (-0.187 + 1.131\beta - 1.016\beta^2 - 0.002\gamma)(2\gamma)^{(1.758-2.208\beta+2.572\beta^2)}\tau^{0.118}$	Equation 2.17
For joints with fillet welds:	
Multiply branch $SCF_{A\ and\ E}$ by 1.4	
For chord member (lines B, C and D):	
$SCF_B = (-0.012 + 0.088\beta - 0.079\beta^2)(2\gamma)^{(1.759+1.113\beta-0.601\beta^2)}\tau^{0.75}$	Equation 2.18
$SCF_C = (0.134 - 0.308\beta + 0.183\beta^2)(2\gamma)^{(0.0471+3.839\beta-1.501\beta^2)}\tau^{0.75}$	Equation 2.19
$SCF_D = (-0.43 - 0.49\beta - 0.36\beta^2 + 1.136\gamma)(2\gamma)^{(-0.527+1.63\beta-1.501\beta^2)}\tau^{0.75}$	Equation 2.20
Load condition 2: chord loading (axial and bending)	
For branch member (lines A and E):	
$SCF_A = 0$ (negligible)	Equation 2.21
$SCF_E = 0$ (negligible)	Equation 2.22
For joints with fillet welds:	
Multiply branch $SCF_{A\ and\ E}$ by 1.4	
For chord member (lines B, C and D):	
$SCF_B = 0$ (negligible)	Equation 2.23
$SCF_C = 0.804 \cdot (2\gamma)^{0.253\cdot\beta} \cdot (\tau)^{0.192}$	Equation 2.24
$SCF_D = 2.242 \cdot (2\gamma)^{0.205\cdot\beta} \cdot (\tau)^{0.240}$	Equation 2.25
The range of validity for Equation 2.16 to Equation 2.25 are as follows:	
$0.35 \leq \beta \leq 1.0$	
$12.5 \leq 2\gamma \leq 25.0$	
$0.25 \leq \tau \leq 1.0$	
A minimum SCF of 2.0 is recommended for all locations.	

Table 2.5. RHS moment T-connection with vent and drain holes at branch corner regions

Load condition 1: in-plane bending on the branch	
For branch member (lines A and E):	
$SCF_A = (-0.507 + 2.558\beta - 2.285\beta^2 - 0.003\gamma)(2\gamma)^{(2.304-4.476\beta+4.645\beta^2)}\tau^{0.119}$	
$SCF_E = (-0.473 + 2.290\beta - 2.029\beta^2 - 0.002\gamma)(2\gamma)^{(2.492-5.022\beta+5.075\beta^2)}\tau^{0.121}$	Equation 2.26
For joints with fillet welds:	
Multiply branch $SCF_{A\ and\ E}$ by 1.4	
For chord member (lines B, C and D):	
$SCF_B = (0.023 - 0.036\beta - 0.09\beta^2 + 0.038\gamma)(2\gamma)^{(0.656+1.292\beta-0.79\beta^2)}\tau^{0.75}$	Equation 2.27
$SCF_C = (0.783 - 2.440\beta + 1.878\beta^2 + 0.038\gamma)(2\gamma)^{(-0.677+6.124\beta-4.948\beta^2)}\tau^{0.719}$	Equation 2.28
$SCF_D = (0.068 + 0.221\beta - 0.324\beta^2 + 0.002\gamma)(2\gamma)^{(1.076+1.266\beta-0.790\beta^2)}\tau^{0.744}$	Equation 2.29
Load condition 2: chord loading (axial and bending)	
For branch member (lines A and E):	
$SCF_A = 0$ (negligible)	Equation 2.30
$SCF_E = 0$ (negligible)	Equation 2.31
For joints with fillet welds:	
Multiply branch $SCF_{A\ and\ E}$ by 1.4	
For chord member (lines B, C and D):	
$SCF_B = 0$ (negligible)	Equation 2.32

$$SCF_C = 0.945 \cdot (2\gamma)^{0.253 \cdot \beta} \cdot (\tau)^{0.192}$$ Equation 2.33

$$SCF_D = 2.810 \cdot (2\gamma)^{0.205 \cdot \beta} \cdot (\tau)^{0.240}$$ Equation 2.34

The range of validity for Equation 2.26 to Equation 2.34 are as follows:

$0.35 \leq \beta \leq 1.0$

$12.5 \leq 2\gamma \leq 25.0$

$0.25 \leq \tau \leq 1.0$

A minimum SCF of 2.0 is recommended for all locations.

The SCFs determined using the proposed formulae (SCF_{FOR}) and those obtained from the FE analyses (SCF_{FE}) are compared in Figure 2.20. The comparisons show good correlation, indicating a good accuracy of the multiple regression analysis.

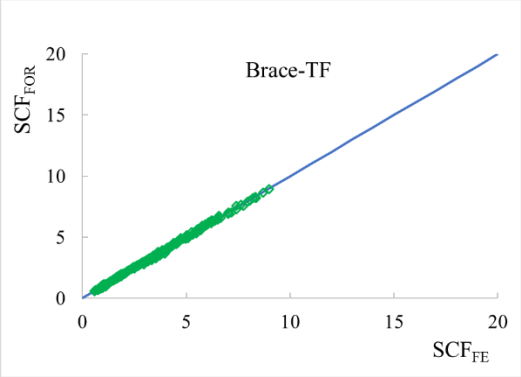

$SCF_{FOR/FE}$	Line A	Line E
Mean	1.000	1.002
COV	0.026	0.026

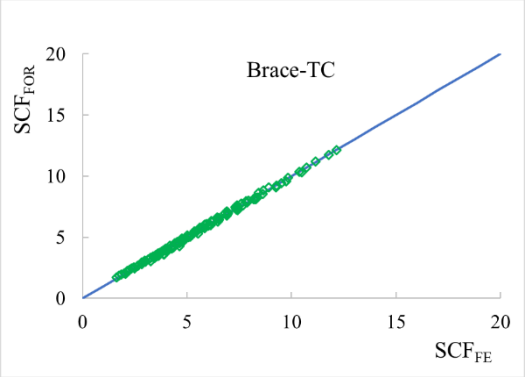

$SCF_{FOR/FE}$	Line A	Line E
Mean	1.001	1.001
COV	0.026	0.027

(a) SCFs for branch member under branch in-plane bending

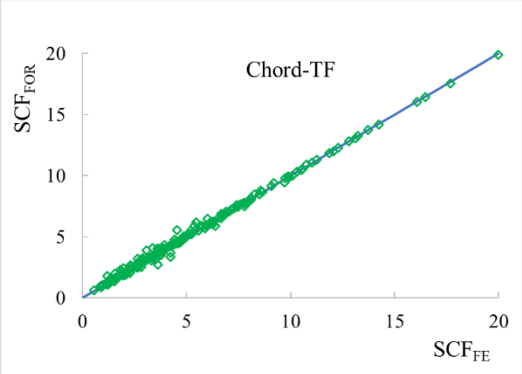

$SCF_{FOR/FE}$	Line B	Line C	Line D
Mean	1.013	0.993	1.035
COV	0.045	0.041	0.107

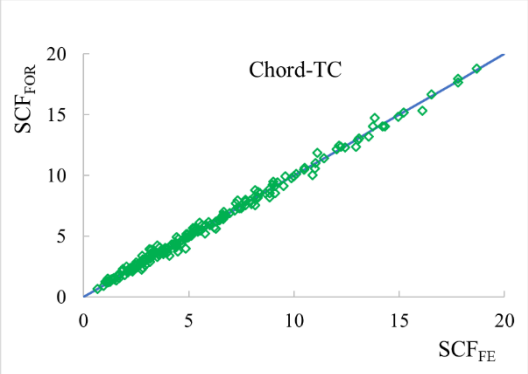

$SCF_{FOR/FE}$	Line B	Line C	Line D
Mean	1.004	1.011	1.026
COV	0.087	0.043	0.080

(b) SCFs for chord member under branch in-plane bending

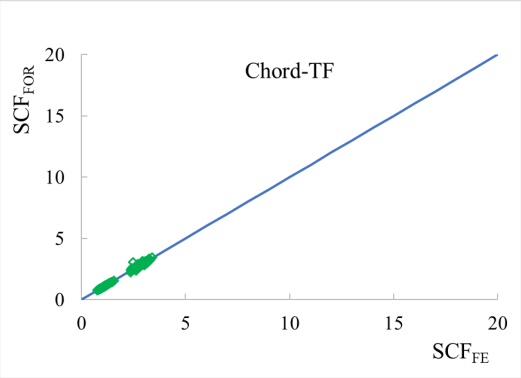

$SCF_{FOR/FE}$	Line C	Line D
Mean	0.999	1.000
COV	0.006	0.045

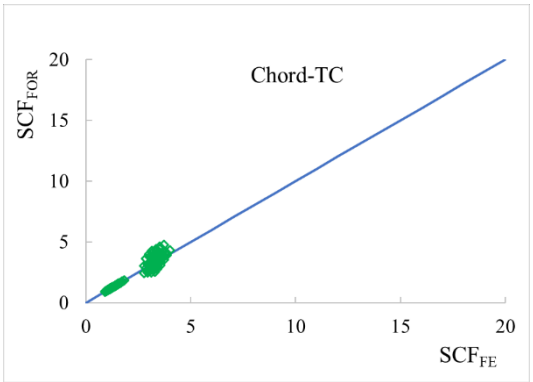

$SCF_{FOR/FE}$	Line C	Line D
Mean	0.999	1.046
COV	0.006	0.134

(c) SCFs for chord member under chord loading
TF = T connection with holes at branch flat faces; and TC = T connection with holes at branch corner regions

Figure 2.20. Comparison of SCF values determined by proposed formulae and FE analyses

2.7. Conclusions

For galvanizing of tubular steel trusses, sufficiently large vent and drain holes must be specified at the welded joint locations. In practice, the holes are generally specified at the branch flat face or corner region. Based on the experimental and numerical studies reported in this chapter, it was found that the CIDECT Design Guide 8 formulae often underestimates the Stress Concentration Factors (SCFs) in RHS-to-RHS T-connections with vent and drain holes under branch in-plane bending, which will in turn lead to unsafe prediction of connection fatigue resistance. Hence, a parametric study including a total of 192 finite element connection models, covering varied hole location, branch-to-chord width ratio, chord width-to-thickness ratio, and branch-to-chord thickness ratio, were performed. Modified formulae were proposed to provide accurate predictions of SCFs in such connections.

Chapter 3

3. RHS X-Connections near an Open Chord End

3.1. Introduction

Over the last 60 years, substantial work has been carried out to develop design recommendations for rectangular hollow section (RHS)-to-RHS and circular hollow section (CHS)-to-CHS connections under static [1-4] and fatigue [5,6] loading. These recommendations are the basis for design rules for tubular structures in Canada (via [7,8]), the United States (via [9-11]), and Europe (via [57]).

The design rules in [9-12] are predicated upon a hollow structural section (HSS) (RHS or CHS) chord member that is sufficiently long on both sides of the connection [i.e. the "end distance" (e), in Fig. 1a, is large] to avoid the effect of the chord boundary conditions (i.e. "end effects") on the connection behaviour [58].

Thus, at present, there are few established design rules for cases in which an HSS branch(es) is situated near an HSS chord end (i.e. an "end connection"), as shown in Figure 3.1b,c. When these arise (as they often do), designers invariably resort to strengthening the connection via cap plates (or end plates), doubler plates, or diaphragms [59]. This can be an expensive and inefficient practice, for both static loading and fatigue. For fabrication, un-strengthened (i.e. directly welded) connections are almost always preferred.

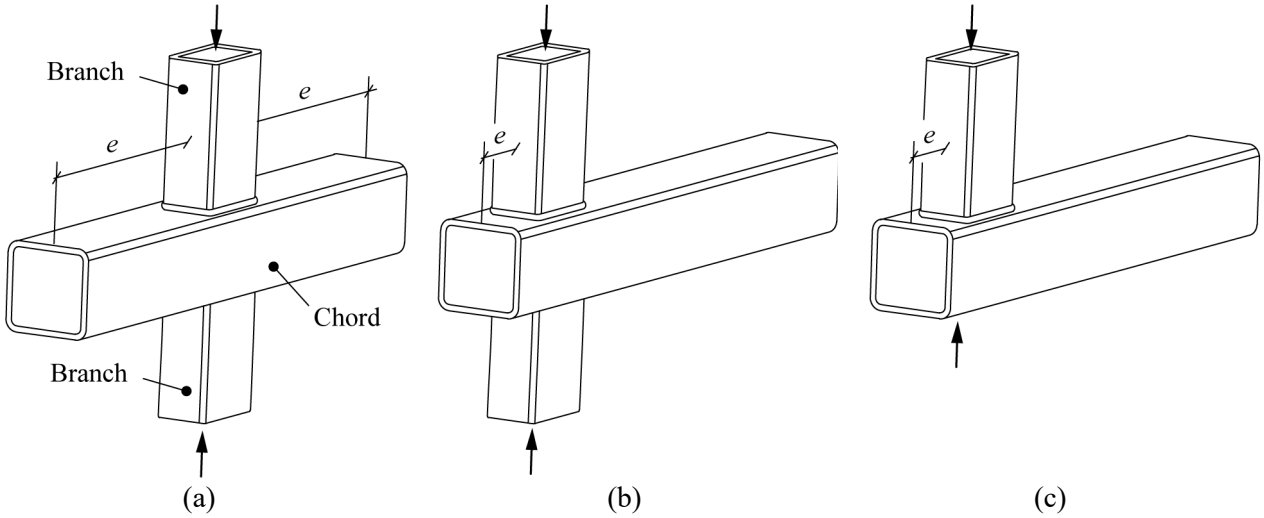

Figure 3.1. RHS-RHS X-connections: (a) standard connection; (b) and (c) end connections

As a step towards addressing this problem, this chapter presents a study to determine stress concentration factors (SCFs) for directly welded RHS-to-RHS axially loaded X-connections near an *open* chord end (e.g. Figure 3.1b,c). Two large-scale experiments are used to validate finite element (FE) models, and a parametric FE study is performed. The FE study consists of 256 FE models with variations in non-dimensional parameters [i.e. chord slenderness ($2\gamma = b_0/t_0$, where b_0 = chord width and t_0 = chord

thickness), branch-to-chord width ratio ($\beta = b_1/b_0$, where b_1 is the branch width), branch-to-chord thickness ratio ($\tau = t_1/t_0$, where t_1 is the branch thickness] and e (on *one side* of the of the connection) = 0.1, 0.25, 1.0 and 3.0 times b_0. This terminology (for RHS-to-RHS connections) is illustrated in Figure 3.2. For each connection, SCFs are determined. Existing formulae to predict SCFs in directly welded RHS-to-RHS X-connections given in CIDECT DG8 [21] are evaluated and shown to be over-conservative; hence, SCF reduction coefficients (ψ) – and parametric formula to estimate ψ (based on e/b_0, 2γ and β) – are derived.

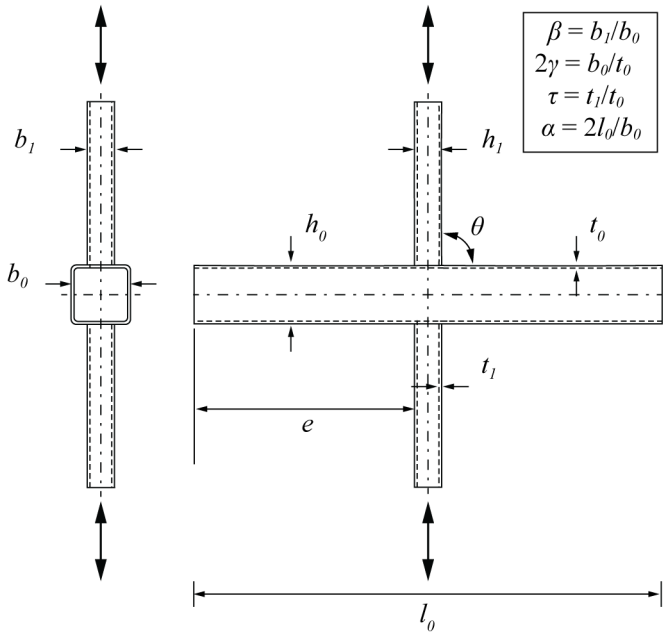

Figure 3.2. RHS-to-RHS X-connection terminology

3.2. Recent Research on HSS End Connections

Contemporary research on directly welded HSS-to-HSS end connections can be attributed to work by van der Vegte and Makino [61]. van der Vegte and Makino [61] studied CHS-to-CHS axially loaded T- and X-connections with variations in chord slenderness ($2\gamma = d_0/t_0$, where d_0 = chord diameter), branch-to-chord diameter ratio ($\beta = d_1/d_0$, where d_1 = branch diameter), chord length parameter ($\alpha = 2l_o/d_o$, where l_o = chord length), and chord boundary conditions [which were modelled as either "free" (simulating an open end) or "fixed" (simulating a capped end)]. This terminology (for CHS-to-CHS connections) is illustrated in Figure 3.3.

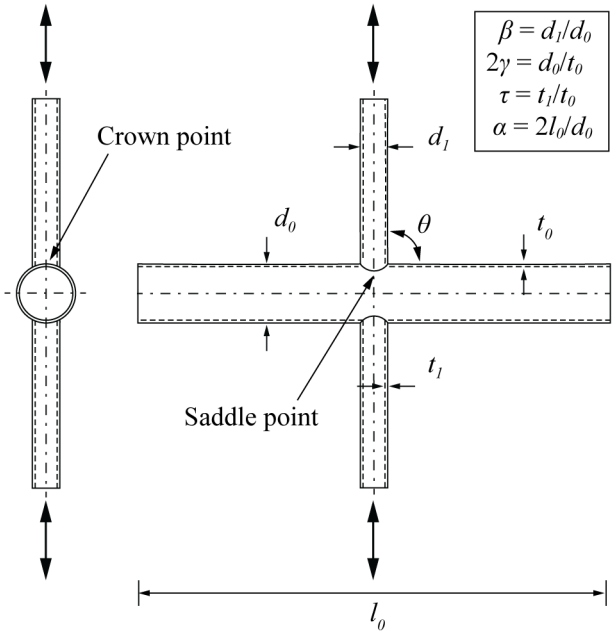

Figure 3.3. CHS-to-CHS X-connection terminology

In their research, van der Vegte and Makino [61] showed that the static strength of a CHS-to-CHS axially loaded T- or X-connection with low α, high 2γ, high β, and open chord ends could be much less than that of a similar connection with high α. To prevent end effects, they proposed simple limits of $\alpha \geq 20$ (for chords with $2\gamma > 25$) and $\alpha \geq 12$ (for chords with $2\gamma \leq 25$). These limits imply a minimum end distance (e_{min}), which was later confirmed for transverse branch plate-to-CHS T- and X-connections by Voth and Packer [16,17].

In response to this research [15-17], an amendment was made to EN 1993-1-8 [57] (via prEN1993-1-8 Clause 9.1.2(10) [64]), which stipulates:

"For joints with a chord end not connected to other members, the chord end shall be at a distance of at least $(2\gamma/10)d_0$ from the heel or toe of the closest branch, with a minimum of $2.5d_0$. For RHS chords, substitute d_0 by the largest of b_0 or h_0. Otherwise, the end shall be welded to a cap plate with a thickness of at least $1.5t_0$, at a minimum distance of $0.5d_0(1 - \beta)$ or $0.5b_0(1 - \beta)$ from the branch toe or heel of the joint".

Note that the term "branch" in prEN1993-1-8 [64] is synonymous with the term "branch" (see Figure 3.1a) (used herein).

The formula for e_{min} implied in the amendment (prEN1993-1-8 Clause 9.1.2(10) [64]) is verified for CHS-to-CHS and plate-to-CHS connections [15-17], and for welds in CHS-to-CHS connections designed as "fit-for-purpose" [65]; however, a speculative transcription (i.e. "substitute d_0 by the largest of b_0 or h_0") [64] was made for application to HSS connections with RHS chords. Additionally, the research discussed so far [15-17,19] caters only to connections that are symmetrical about the branch(es).

These issues were addressed by Fan and Packer [59], who experimentally studied the static strength of RHS-to-RHS axially loaded X-connections near an open chord end (on one side only). Akin to previous work [15,20-23], Fan and Packer [59] found that the static strengths of such connections near an open chord end were often much less than those of "standard" (or "control") connections with long chords ($e \geq 3b_0$, conservatively, on both sides). A yield-line model was developed, from which e_{min} was derived (for HSS connections with RHS chords). This research supported the e_{min} requirement already present in AISC 360-16 [55] Table K3.2A for RHS-to-RHS truss connections (Equation 3.1), which is (a) based on the "chord face plastification" limit state and (b) clearly much different (i.e. less) than e_{min} implied in prEN1993-18 Clause 9.1.2(10).

$$e_{min} = b_0\sqrt{1-\beta} \qquad \text{Equation 3.1}$$

While both prEN1993-1-8 Clause 9.1.2(10) [64] and AISC 360-16 (via the Commentary to Chapter K) [55] recognize providing a cap plate as a "commonly accepted alternative" to providing $e \geq e_{min}$, AISC 360-16 [55] also permits a reduction in the predicted connection strength by 50% for RHS-to-RHS or plate-to-RHS connections (as another alternative).

Bu and Packer [58] have shown recently that Equation 3.1 is, in fact, unconservative, since it is based solely on "chord face plastification" and does not consider other limit states. Based on their research, which considered "chord side wall buckling" in addition to "chord face plastification", Bu and Packer [58] proposed: (a) a new limit of $e_{min} = 0.75b_0$ for HSS connections with RHS chords and (b) a reduction in strength by 40% (instead of 50%) if $e < e_{min} = 0.75b_0$.

While research has hence aimed to establish design guidance for directly welded HSS "end connections" under static loading [13-17,19-23], research on "end connections" under fatigue loading is rare. Efthymiou and Durkin [70] showed that SCFs in CHS-to-CHS connections with short chords (i.e. low α) were often much smaller than those in "standard" connections (with long chords), which has formed the basis of some of the SCF formulae for CHS-to-CHS axially loaded X-connections in CIDECT DG8 [21] (which are discussed in Section 3.3.1 of this section). However, like most previous research [15-17,19], Efthymiou and Durkin's [70] work catered only to connections that are symmetrical about the branch(es).

3.3. Design of HSS Connections for Fatigue

For HSS-to-HSS connections subjected to fatigue, design is commonly done according to the "hot spot stress method" in CIDECT DG8 [21]. The procedure to apply this method is as follows:

1. Calculate the nominal stress ranges in the branch(es) and chord under service conditions.
2. Calculate the SCFs at the critical (hot spot) locations (for which formulae are provided in [21]).
3. Calculate the hot spot stress range at the critical locations (equal to: nominal stress range × SCF).
4. Determine the fatigue life of the connection by using hot-spot-stress vs. fatigue life (S-N) curves.

The SCFs needed for 2. are functions of connection geometry (e.g. α, β and 2γ) that can be determined by connection testing or FE analysis, or – for standard connections (e.g. Figure 3.1a) – by using formulae provided in CIDECT DG8 [21] or other HSS design guides. The terms "hot spot stress" and "hot spot stress range" used herein are synonymous with the terms "geometric stress" and "geometric stress range", which may be more familiar to some readers.

3.3.1. CHS X-Connections

For CHS-to-CHS axially loaded X-connections, the CIDECT DG8 [21] formulae for SCFs consider critical (hot spot) stress locations at the crown and saddle points (see Figure 3.3). These formulae are presented in Equation 3.2-Equation 3.11 using the nomenclature from CIDECT [21].

- For the chord:

$$SCF_{ch\_saddle,ax} = X_1 \cdot F_2 \qquad \text{Equation 3.2}$$

$$SCF_{ch\_crown,ax} = X_2 \qquad \text{Equation 3.3}$$

where $SCF_{,ch\_saddle,ax}$ = chord SCF at the saddle point; SC$F_{ch_crown,ax}$ = chord SCF at the crown point; and F_2 = reduction factor to account for "end effects" [70].

- For the branch(es):

$$SCF_{b\_saddle,ax} = X_3 \cdot F_2 \qquad \text{Equation 3.4}$$

$$SCF_{b\_crown,ax} = X_4 \qquad \text{Equation 3.5}$$

where $SCF_{,b\_saddle,ax}$ = branch SCF at the saddle point; and SC$F_{b_crown,ax}$ = branch SCF at the crown point.

The parameters X_1, X_2, X_3, X_4 and F_2 are given as:

$$X_1 = 3.87 \cdot \gamma \cdot \tau \cdot \beta \left[1.10 - \beta^{1.8}\right] \cdot (\sin\theta)^{1.7} \qquad \text{Equation 3.6}$$

$$X_2 = \gamma^{0.2} \cdot \tau \left[2.65 + 5 \cdot (\beta - 0.65)^2\right] - 3 \cdot \tau \cdot \beta \cdot \sin\theta \qquad \text{Equation 3.7}$$

$$X_3 = 1 + 1.9 \cdot \gamma \cdot \tau^{0.5} \cdot \beta^{0.9} \cdot \left(1.09 - \beta^{1.7}\right) \cdot \sin^{2.5}\theta \qquad \text{Equation 3.8}$$

$$X_4 = 3 + \gamma^{1.2} \cdot \left[0.12 \cdot \exp\left(-4 \cdot \beta\right) + 0.011 \cdot \beta^2 - 0.045 \right]$$ Equation 3.9

If $\alpha \geq 12$: $F_2 = 1.0$ Equation 3.10

If $\alpha < 12$: $F_2 = 1 - \left(1.43 \cdot \beta - 0.97 \cdot \beta^2 - 0.03\right) \cdot \gamma^{0.04} \cdot \exp\left(-0.71 \cdot \gamma^{-1.38} \cdot \alpha^{2.5}\right)$ Equation 3.11

where θ = acute angle between the branch and chord (in degrees) (see Fig. 3).

Equation 3.2-Equation 3.11 are valid within the range $0.2 \leq \beta \leq 1.0$, $15 \leq 2\gamma \leq 64$, $0.2 \leq \tau \leq 1.0$, $4 \leq \alpha \leq 40$, and $30° \leq \theta \leq 90°$, and apply to connections under branch axial loading.

As shown by the F_2 factor [Equation 3.11], CIDECT DG 8 [21] acknowledges "end effects" on SCFs for CHS-to-CHS axially loaded X-connections with low α (based on research by [70]). For typical axially loaded CHS-to-CHS X-connections, the factor F_2 is plotted against α in Figure 3.4a,b. As shown therein, F_2 can be quite small, indicating that "end effects" (according to CIDECT DG 8[21]) can reduce SCFs (significantly) in CHS-to-CHS X-connections. However, α = 4 is still large for a practical "end connection" [58] and that Equation 3.11 still caters to connections that are symmetrical about the branch(es).

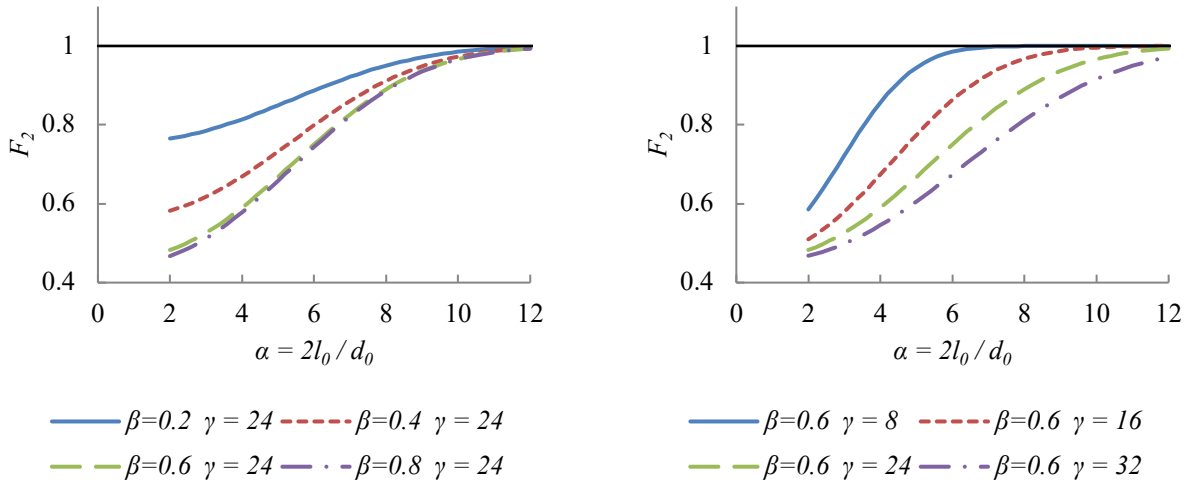

(a) Effect of β (γ = 24) (b) Effect of γ (β = 0.6)

Figure 3.4. Effects of chord length and non-dimensional parameters on SCFs in CHS-to-CHS axially loaded X-connections based on CIDECT DG8 [21]

3.3.2. RHS T- and X-Connections

For "standard" RHS-to-RHS axially loaded T- and X-connections, the CIDECT DG8 [21] formulae for SCFs consider five critical (hot spot) stress locations. These locations are labelled A – E in Figure 3.5.

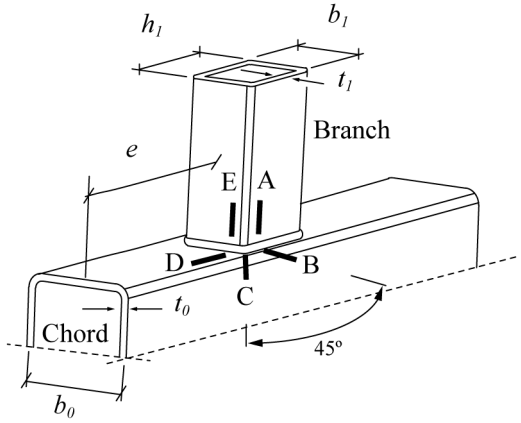

Figure 3.5. Critical (hot spot) stress locations for RHS-to-RHS T- and X-connections [21]

The formulae given in CIDECT [21] to calculate SCFs at the "hot spots" (A – E) are:

- For the chord:

$$SCF_B = \left(0.143 - 0.204\beta + 0.064\beta^2\right)(2\gamma)^{\left(1.377+1.715\beta-1.103\beta^2\right)}\tau^{0.75} \quad \text{Equation 3.12}$$

$$SCF_C = \left(0.077 - 0.129\beta + 0.061\beta^2 - 0.0006\gamma\right)(2\gamma)^{\left(1.565+1.874\beta-1.028\beta^2\right)}\tau^{0.75} \quad \text{Equation 3.13}$$

$$SCF_D = \left(0.208 - 0.387\beta + 0.209\beta^2\right)(2\gamma)^{\left(0.925+2.389\beta-1.881\beta^2\right)}\tau^{0.75} \quad \text{Equation 3.14}$$

where SCF_B, SCF_C, and SCF_D = chord SCFs at hot spot B, C, and D, respectively.

- For the branch(es):

$$SCF_A = SCF_E = \left(0.013 + 0.693\beta - 0.278\beta^2\right)(2\gamma)^{\left(0.790+1.898\beta-2.109\beta^2\right)} \quad \text{Equation 3.15}$$

where $SCF_A = SCF_E$ = branch SCF at hot spots A and E, respectively.

For connections with fillet welds, SCF_A and SCF_E are multiplied by 1.4, and for X-connections with β = 1.0, SCF_C is multiplied by 0.65 and SCF_D is multiplied by 0.50.

According to CIDECT [21], Equation 3.12-Equation 3.15 are valid within the range $0.35 \le \beta \le 1.0$, $12.5 \le 2\gamma \le 25$, $0.25 \le \tau \le 1.0$, for connections under branch axial loading. And, as the factor F_2 is absent, there is no benefit/penalty for "end effects". Part of this issue, concerning end effects for RHS-to-RHS axially loaded X-connections near an open chord end, is herein addressed. It should be noted that, unlike

Equation 3.6-Equation 3.8, the CIDECT DG8 formulae for RHS-to-RHS connections are not functions of the branch-to-chord angles.

3.4. SCFs for RHS X-Connections near an Open Chord End

3.4.1. Experimental Testing

Two large-scale, directly welded RHS-to-RHS axially loaded X-connections were tested in this research. Their general layout is shown in Figure 3.6. The connections were fabricated with RHS members produced to CSA G40.20/G40.21 [26] Grade 350W Class C; they were symmetrical about the branches and had $e = 3b_0$ (on each side) (see Figure 3.6). The branch and chord members were joined by partial joint penetration groove welds, using a semi-automatic flux cored arc welding process (the most common process in high-production structural welding). Nominal geometrical properties of the connections are given in Table 3.1. The specimen IDs (first column in Table 3.1) are described in the footnote.

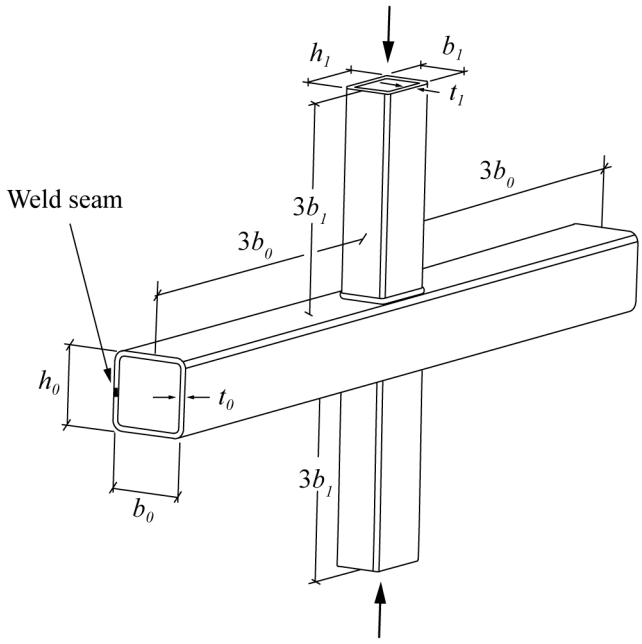

Figure 3.6. Layout of test specimens

Table 3.1. Nominal geometrical properties of test specimens

Specimen ID[1]	Chord ($b_0 \times h_0 \times t_0$) (mm×mm×mm)	Branch ($b_1 \times h_1 \times t_1$) (mm×mm×mm)	$\beta = b_1/b_0$	$2\gamma = b_0/t_0$	$\tau = t_1/t_0$
X-0.5	178×178×12.7	89×89×9.53	0.5	14	0.75
X-0.7	178×178×12.7	127×127×9.53	0.7	14	0.75

[1] ID: connection configuration (i.e. "X") - β-ratio.

The aim of this initial, experimental work was to produce test results that could be used to validate subsequent FE models. Hence, a procedure recommended by CIDECT DG8 [21], and used in previous test programs (with similar aims) [26,27], was adopted.

Quasi-static axial compression was applied to the end of each branch by using a Universal Testing Machine (UTM) (Figure 3.7a), under force control, at a rate of 10 kN/min. For both tests, the load was paused at four stages (30, 40, 50 and 60 kN). At each stage, the connections remained elastic (this was verified by previous FE modelling), and strain concentration factors (SNCFs) were determined. SNCFs are defined as the ratio: hot spot strain / branch nominal strain [21]. Linear strain gauges (SGs) (four total) were installed at the mid-walls of one RHS branch (in each connection) to determine branch nominal strain. These were taken as the average over the four SG readings. Hot spot strains were determined using "chain strain gauges" (CSGs), situated along lines A1 – E1 and A2 – E2 (see Figure 3.7b,c), and within the dimensions $L_{r,min}$ and $L_{r,max}$ recommended by CIDECT DG8 [21] (see Figure 3.8). These dimensions ($L_{r,min}$ and $L_{r,max}$) are defined by CIDECT DG8 [21] as follows: $L_{r,min}$ is the greater of 0.4 times t_0 or t_1 (for CSGs on the chord and branch, respectively) and 4 mm, and $L_{r,max}$ is equal to $L_{r,min}$ plus t_0 or t_1 (again, for CSGs on the chord and branch, respectively).

Using quadratic extrapolation (in accordance with CIDECT DG8 [21]), the measured strains obtained with the CSGs were used to the calculate hot spot strains and the corresponding SNCFs. Then, the average SNCF (at each of five locations, A – E) was calculated by taking an average of the values on each side of the connection across all load levels. The average SNCFs, for connections X-0.5 and X-0.7, are plotted as filled diamonds in Figure 3.9.

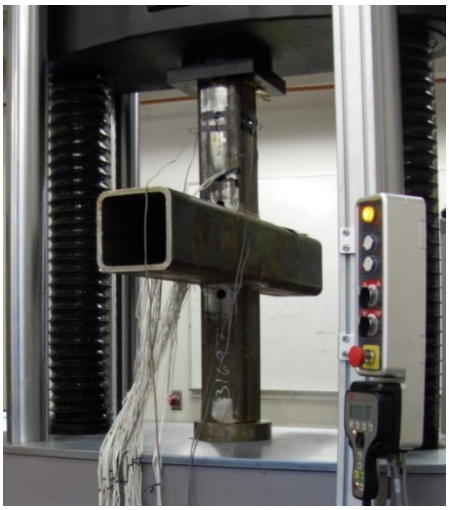

(a) UTM

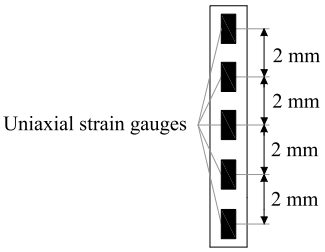

(b) CSG dimensions

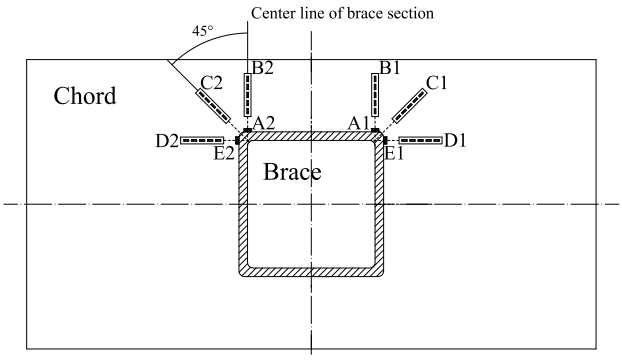

(c) CSG locations

Figure 3.7. Test setup and instrumentation

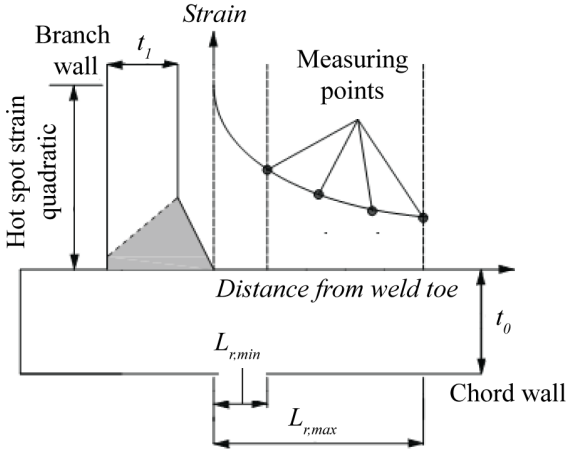

Figure 3.8. Strain vs. distance from the weld toe (adapted from [21])

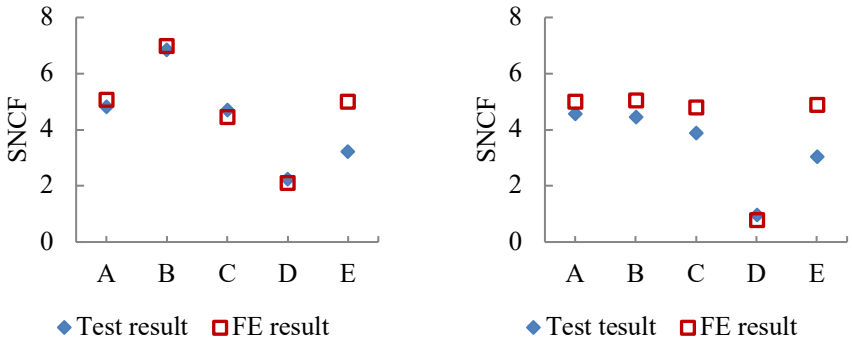

Figure 3.9. Comparison of SNCFs values obtained from experiments and FE analyses

3.4.2. Finite Element Modelling

Two FE models were developed in ABAQUS [43] to replicate the nominal geometrical properties of the RHS-to-RHS axially loaded X-connections described in Table 3.1. For both models, the inner and outer corner radii of the RHS members (r_i and r_o, respectively) were taken as one and two times the nominal wall thickness, and the total chord length (l_o) was taken as $6b_0+b_1$ (i.e. $e = 3b_o$ on both sides of the connection, as shown in Figure 3.6, like the experiments). The modelled weld geometry followed Figure 3.10 (which corresponds to the weld geometry in the experiments and in previous studies [27,28,30]).

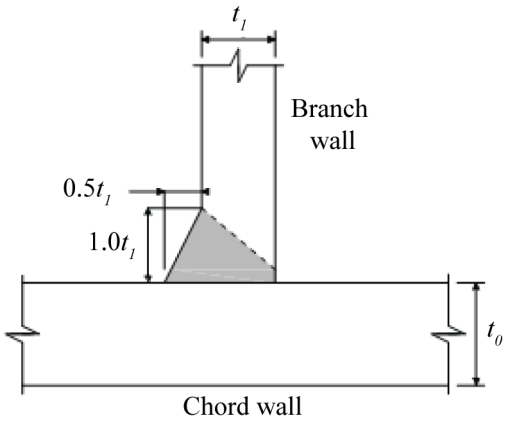

Figure 3.10. Weld dimensions (adapted from [27,28,30])

The FE models were partitioned in order to allow calculation of the SNCFs at the locations A1 – E1 and A2 – E2 (see Figure 3.7c, shown previously). The region partition of a typical FE model is shown in Figure 3.11a. Locations A2 – E2 are not shown in Fig. 11a, but they can be inferred from Figure 3.7c. Linear elastic material properties [Young's modulus (E) = 200 GPa and Poisson's ratio = 0.3] were applied to the RHS branch(es), chord, and weld materials in accordance with approaches used by previous investigators [26-28,30].

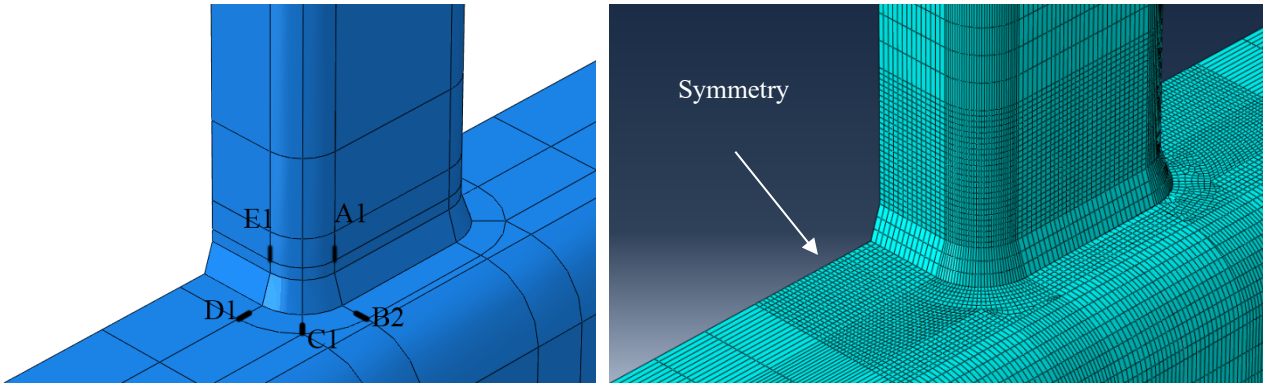

(a) Region partition (b) Mesh pattern at joint location

Figure 3.11. FE model details

Four layers of through-thickness solid elements (C3D20R in ABAQUS) were used for the branch(es) and the chord, and a "one-half model" (which was permissible due to symmetry in geometry, loading and boundary conditions along the "cut face"), as shown in Figure 3.11b, was used. A "symmetry boundary condition" was applied to all nodes on the "cut face". The nodes at the bottom of the lower branch were "fixed", and the nodes at the top of the upper branch were "free", with loads applied thereto in compression.

For both FE models, SNCFs were obtained by dividing the hot spot strains (calculated using "quadratic extrapolation" [21]) by the branch nominal strain (taken as the applied force divided by the branch cross-sectional area multiplied by E, under a 50 kN axial compression force in the branch). These are compared to SNCFs from the experiments in Figure 3.9a,b (where they are plotted as unfilled squares), and show good agreement with them (hence, validating the FE models). A preliminary FE study on "end effects" in RHS-to-RHS axially loaded X-connections near an open chord end was thus performed by using the validated models.

3.4.2.1. Preliminary Study on End Effects

Two "control models", with different β, and $e = 3b_0$, served as the basis for the preliminary study. From each of the two "control models", three new models were created with $e = b_0$, $0.5b_0$ and $0.1b_0$ on *one side only* of the connection (i.e. $e = 3b_0$ was maintained on the other side of the connection, as shown in Figure 3.12). The lower bound of $0.1b_0$ chosen represents the smallest practical value of e for an "end connection" [58]. Geometrical properties of these eight models are listed in Table 3.2. The model IDs

(first column in Table 3.2) are described in the footnote. Figure 3.13a shows a typical “control models” and Figure 3.13b shows a typical “end connection”.

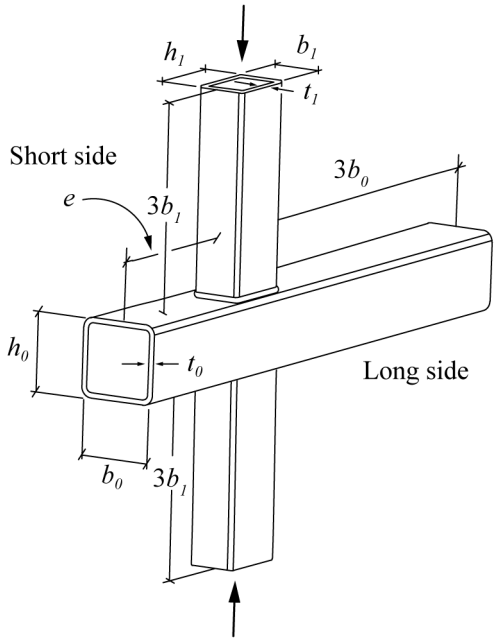

Figure 3.12. Schematic diagram of the FE models

Table 3.2. Geometrical properties of preliminary connection models

Model ID [1]	Chord (b_0×h_0×t_0) (mm×mm×mm)	Branch (b_1×h_1×t_1) (mm×mm×mm)	$\beta=b_1/b_0$	$2\gamma=b_0/t_0$	$\tau=t_1/t_0$	e (mm)
X-0.35-3b_0	200×200×16	70×70×8	0.35	12.5	0.5	600
X-0.35-1b_0						200
X-0.35-0.5b_0						100
X-0.35-0.1b_0						20
X-0.65-3b_0	200×200×16	130×130×8	0.65	12.5	0.5	600
X-0.65-1b_0						200
X-0.65-0.5b_0						100
X-0.65-0.1b_0						20

[1] ID: connection configuration (i.e. “X”) - β-ratio – e (see Fig. 12).

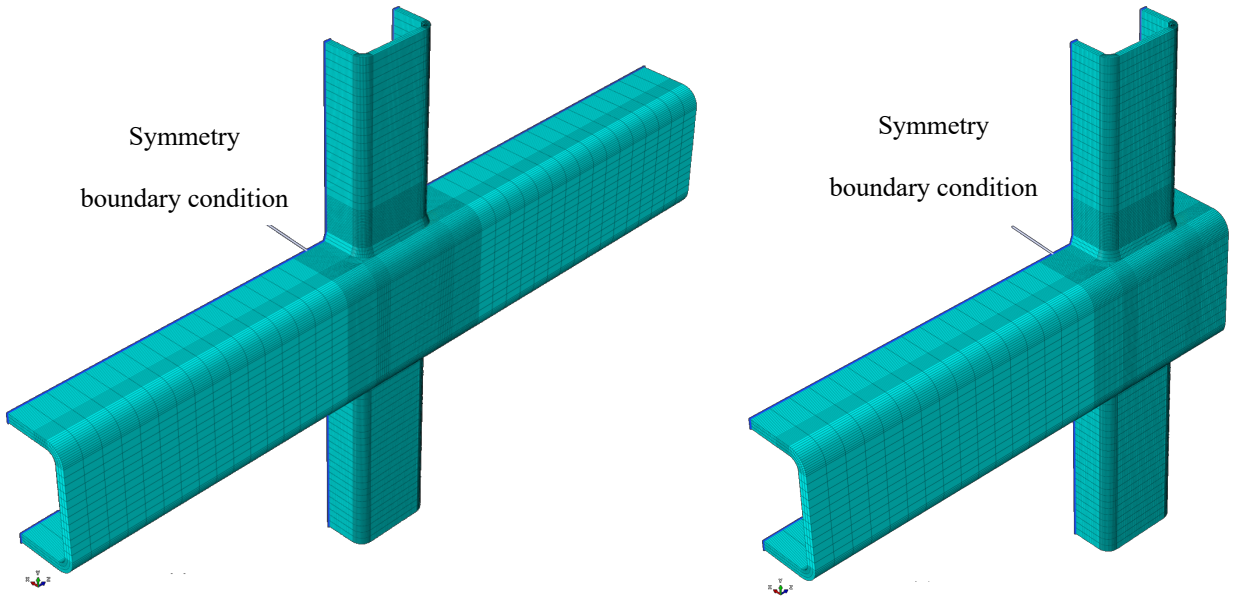

(a) Control model ($e = 3b_0$) (X-0.65-3b$_0$)

(b) End connection ($e = 0.1b_0$) (X-0.65-0.1b$_0$)

Figure 3.13. RHS-to-RHS axially loaded X-connection models with different end distances

For the "control models", with $e = 3b_0$, the SCF formulae in CIDECT DG8 [21] [i.e. Equation 3.12 to Equation 3.15] are theoretically valid. For the "end connections", following the recommendations in Appendix C of CIDECT DG8 for determinations of SCFs by finite element analysis [21], the hot spot stresses at the weld toe at the critical locations A1 – E1 and A2 – E2 (i.e. on both the "long" side and the "short" side of the connection, as labelled in Figure 3.11) were calculated using the stress readings within the extrapolation zones. SCFs were then calculated by dividing the hot spot stresses by the nominal stress. The nominal stress was calculated by dividing the branch force by its cross-sectional area.

For the "control models", corresponding SCFs on each side of the connection (e.g. A1 and A2) were the same due to symmetry. For the "end connections", these differed on the "long side" and "short side" of the connection as shown in Figure 3.12. The SCFs for all eight connections, at all 10 hot spots, are plotted in Figure 3.14 and Figure 3.15. As pointed out by Efthymiou and Durkin [70], for regular connections, the chord deformation resulting from the branch axial loading decays as the distance from the welded joint increases. If this natural decay is interrupted by using short chords, the SCFs will be affected. It can be seen from Figure 3.14 and Figure 3.15 that "end effects" can reduce SCFs in RHS-to-RHS axially loaded X-connections near an open chord end. This is similar to findings by Efthymiou and Durkin's [70], as implied by the F_2 factor [Equation 3.11] for CHS-to-CHS axially loaded X-connections in CIDECT DG8 [21].

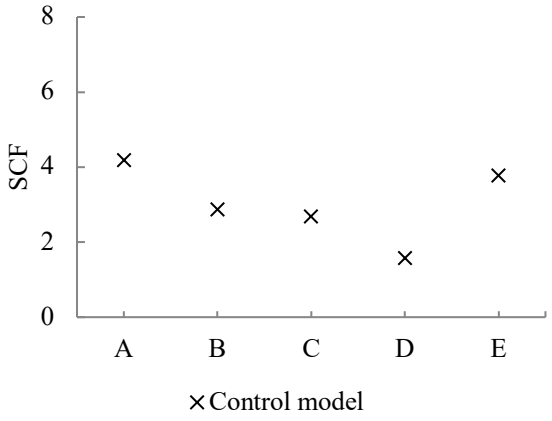

(a) Control model ($e = 3b_0$)

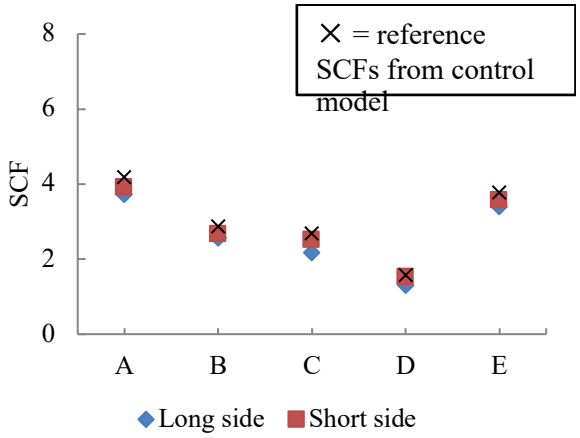

(b) End connection model ($e = 1.0b_0$)

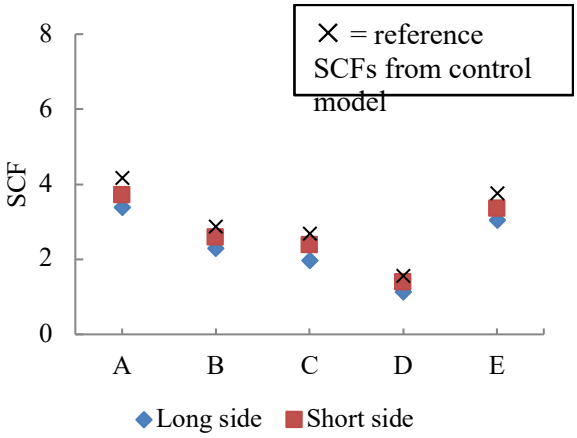

(c) End connection model ($e = 0.5b_0$)

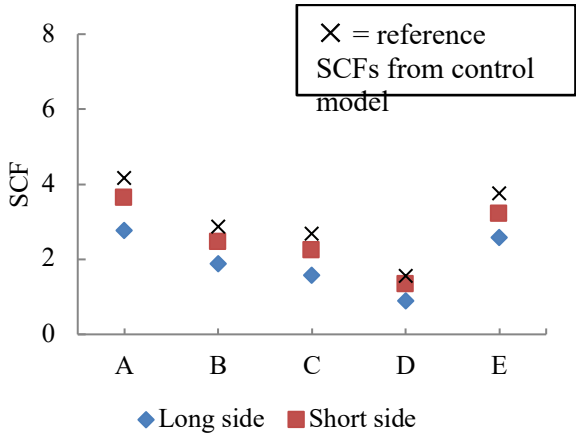

(d) End connection model ($e = 0.1b_0$)

Figure 3.14. SCFs for connection models in Table 3.2 with $\beta = 0.35$

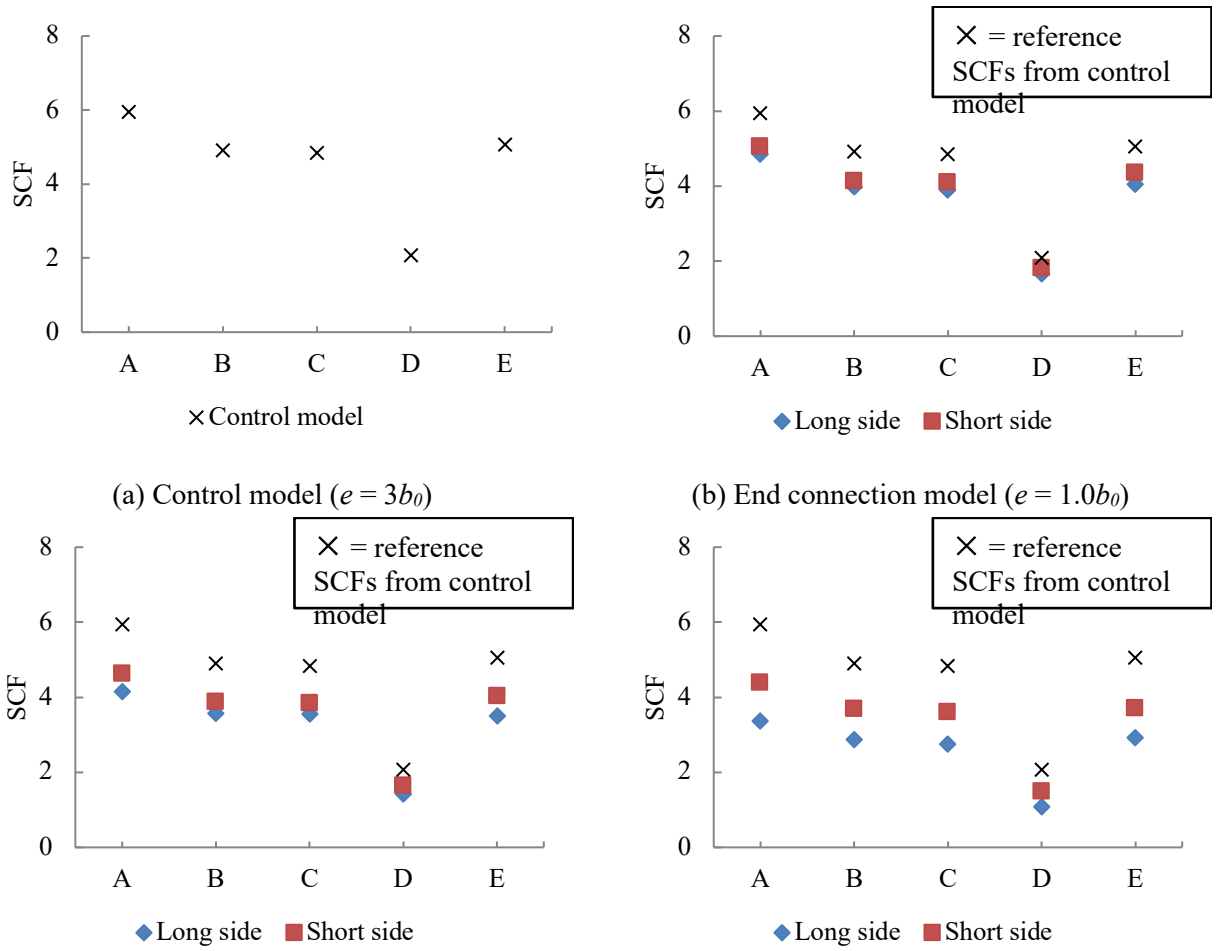

(a) Control model ($e = 3b_0$)

(b) End connection model ($e = 1.0b_0$)

(c) End connection model ($e = 0.5b_0$)

(d) End connection model ($e = 0.1b_0$)

Figure 3.15. SCFs for connection models in Table 3.2 with $\beta = 0.65$

Figure 3.14 and Figure 3.15 also show that the SCFs on the "long side" and the "short side" of the connections are similar, with the SCFs on the "short side" always being slightly greater. This was confirmed for all the FE models in Section 3.3.5, where only the SCFs on the "short side" of the connection are presented.

3.4.3. Parametric Study

Based on the results of the preliminary study, a follow-up (parametric) FE study was deemed necessary to quantify the effect of β, 2γ, τ, and the end distance (e) on SCFs in RHS-to-RHS axially loaded X-connections near an open chord end. The goal of this study was to develop a generalized design approach for RHS-to-RHS axially loaded X-connections (i.e. RHS-to-RHS X-connections under branch axial loading) near an open chord end, for fatigue, using the "hot spot stress method" [21].

The FE parametric study consisted of 256 FE models with chord members of constant outer dimensions ($h_0 = b_0$) of 200 mm. Other dimensions (e.g. t_0, t_1, and l_0) were determined from non-dimensional

parameters (β, 2γ and τ), and the end distance (e). Considering the limits of validity of the SCF equations for RHS-to-RHS X-connections in CIDECT DG 8 [21] [Equation 3.12-Equation 3.15], the non-dimensional parameters (β, 2γ and τ) were taken as 2γ = 12.5, 16, 20 and 25; β = 0.35, 0.5, 0.65, and 0.8; and τ = 0.25, 0.5, 0.75, and 1.0. The end distance (e) was varied between $0.1b_0$, $0.5b_0$, $1.0b_0$ and $3.0b_0$, with $3.0b_0$ representing a conservative upper limit for which "end effects" could be safely ignored [58].

3.4.3.1. Results

For the parametric study, the SCFs in the end connections models are divided by those in the control models. The values are denoted as ψ. Representative results of ψ at the five critical (hot spot) locations on the "short side" of the connections are shown in Figs. 16-18. It can be seen in Figure 3.16 that ψ decreases as β increases. Figure 3.17 shows that the smaller the 2γ ratio, the smaller are the ψ-values. According to Figure 3.18, for different values of e/b_0, the variation in τ has only a minor effect on the ψ-values. This is consistent with observations by Bu and Packer [58], as well as Equation 3.11, which considers "end effects" on SCFs in CHS-to-CHS axially loaded X-connections. [As shown previously, Equation 3.11 is a function of 2γ and β, but not τ]. It can also be noted that these plots of ψ vs. e/b_0 in Figure 3.16 and Figure 3.17 exhibit trends similar to those in the plots of F_2 vs. α in Figure 3.4a,b.

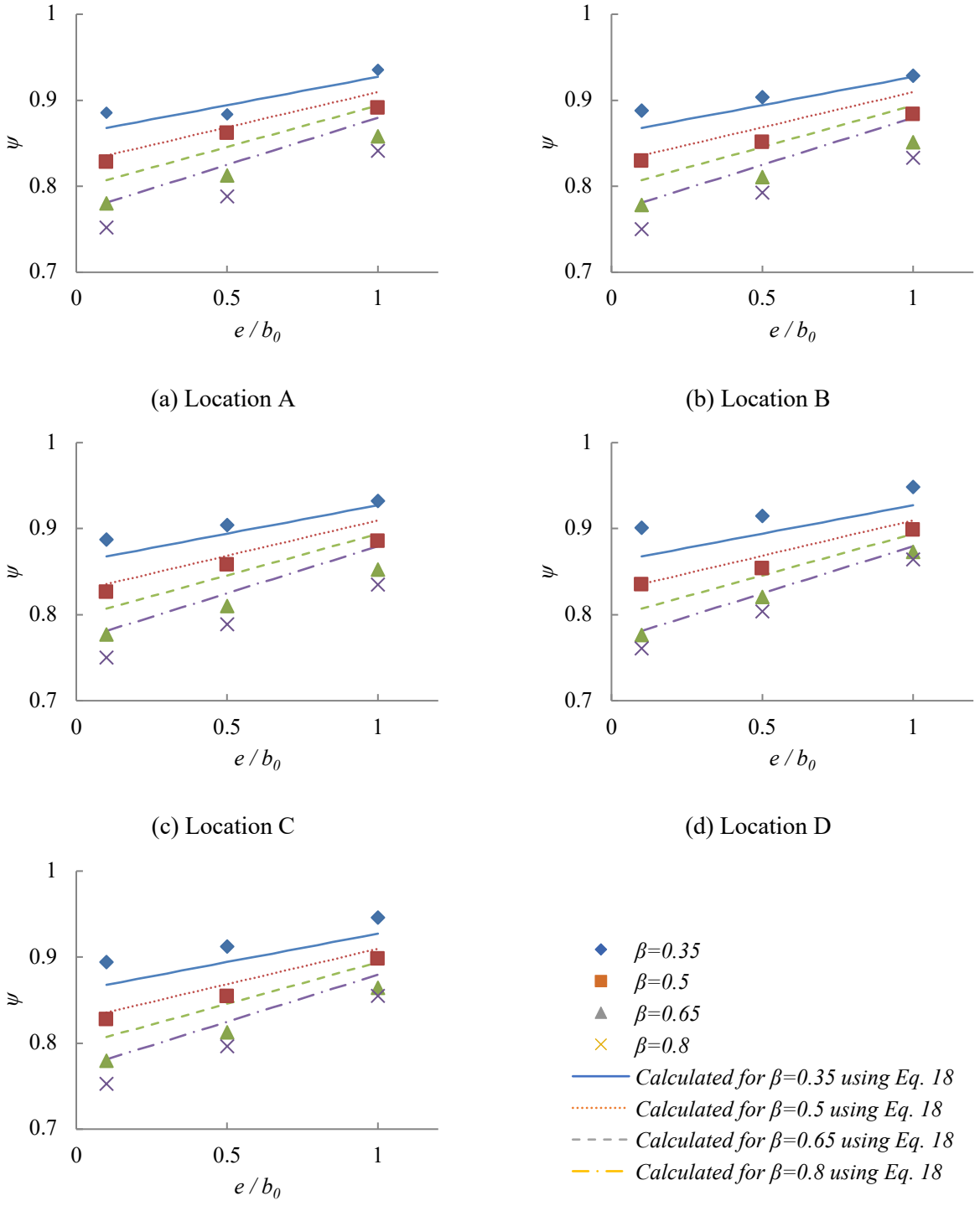

(a) Location A

(b) Location B

(c) Location C

(d) Location D

(e) Location E

Figure 3.16. Effects of e/b_0 and β on SCFs in connections (2γ=20 and τ=0.75)

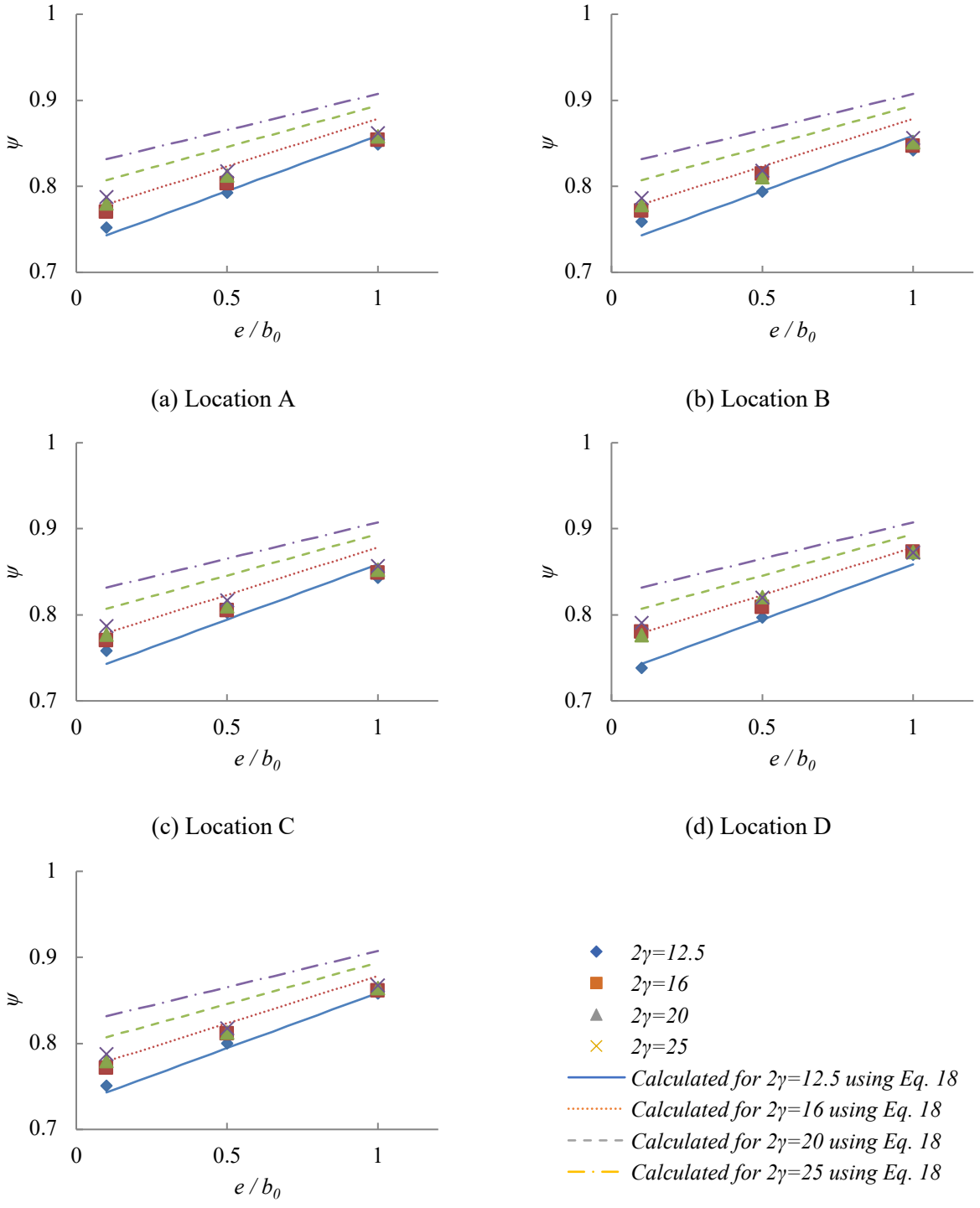

Figure 3.17. Effects of e/b_0 and 2γ on SCFs in connections (β=0.65 and τ=0.75)

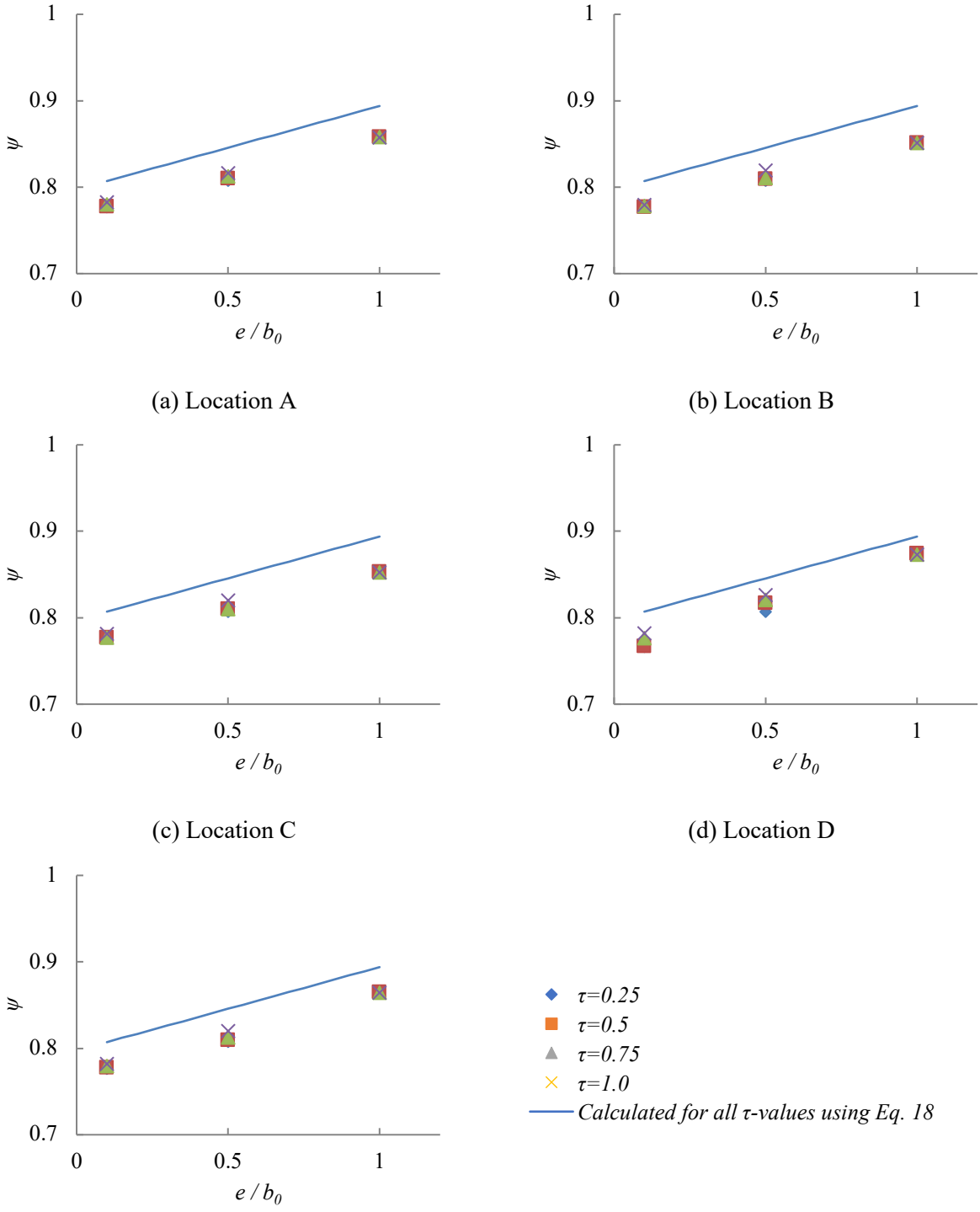

Figure 3.18. Effects of e/b_0 and τ on SCFs in connections (β=0.65 and 2γ=20)

3.5. Design Approach

SCF formulae for directly welded RHS-to-RHS axially loaded X-connections are readily available, such as those recommended by CIDECT DG8 [21]; however, as noted in Section 3.2, they do not consider "end effects". The proposed design approach for RHS-to-RHS axially loaded X-connections (i.e. RHS-to-RHS X-connections under branch axial load) near an open chord end hence aims to utilize existing formulae [Equation 3.12-Equation 3.15] through the introduction of a reduction coefficient (ψ) [like F_2, given by Equation 3.11] to consider "end effects"; i.e.:

$$SCF_{end,i} = SCF_i \cdot \psi \qquad \text{Equation 3.16}$$

where $SCF_{end,i}$ = SCF at hot spot i in a RHS-to-RHS axially loaded X-connection near an open chord end; SCF_i = SCF at hot spot i in a RHS-to-RHS axially loaded X-connection [determined using Equation 3.12, Equation 3.13, Equation 3.14 or Equation 3.15]; and i = parameter used to designate a critical (hot spot) location (= A, B, C, D or E).

As discussed in Section 3.4.3.1, the reduction factors (ψ) for all critical (hot spot) locations (A – E) for the end connection models have been determined by dividing the $SCF_{end,i}$ by SCF_i determined from the corresponding control connections with $e = 3b_0$. For the parametric study, ψ ranges from 0.57 to 0.96.

Also, ψ is nearly constant across all 5 critical (hot spot) locations in each connection, and a mean variation of 1% between ψ at a critical hot spot and the maximum value of ψ at any hot spot in the same connection can be noted. A non-linear regression analysis to relate the maximum value of ψ at any hot spot to non-dimensional connection parameters was hence performed by using Equation 3.17 as basis:

$$\psi = 1 - a\left(b - e/b_0\right)/\left(2\gamma/\beta\right)^c \qquad \text{Equation 3.17}$$

where a, b, and c = regression constants.

The arrangement of variables in Equation 3.17 was determined empirically and considers the relationships between e/b_o, 2γ and β and the SCFs presented in Figure 3.16Figure 3.18. The values of a, b and c were determined by least-squares regression of 192 data points with e/b_0 = 0.1, 0.5 and 1, 2γ = 12.5, 16, 20 and 25; β = 0.35, 0.5, 0.65, and 0.8; and τ = 0.25, 0.5, 0.75, 1.0. As noted, ψ (the dependent variable) taken as the maximum value of ψ at any hot spot in the same connection (which is hence conservative for all other hot spots). The "best-fit" equation is given by Equation 3.18:

$$\psi = 1 - 0.78\left(2.10 - e/b_0\right)/\left(2\gamma/\beta\right)^{0.61} \qquad \text{Equation 3.18}$$

Equation 3.18 gives a mean value of actual-to-predicted maximum value of ψ of 1.00 with a COV of 0.03, and a mean value of actual-to-predicted value of ψ (at any hot spot) of 0.99, also with a COV of 0.03. Equation 3.18 implies a minimum distance of $e = 2.1b_0$ to avoid "end effects" on the fatigue life of RHS-to-RHS axially loaded X-connections.

It is hence recommended that Equation 3.18 be multiplied by the appropriate SCF equation(s) from CIDECT DG8 [21] (or other design guides) to determine SCFs for RHS-to-RHS axially loaded X-

connection near an open chord end. By using previously determined SCF equations for “standard connections”, the proposed formula for ψ [Equation 3.18] is expected to provide the same level of reliability for fatigue life predictions of “end connections”. The foregoing recommendation is summarized in Figure 3.19. To be consistent with CIDECT DG8 [21], a minimum SCF-value of 2.0 is also recommended.

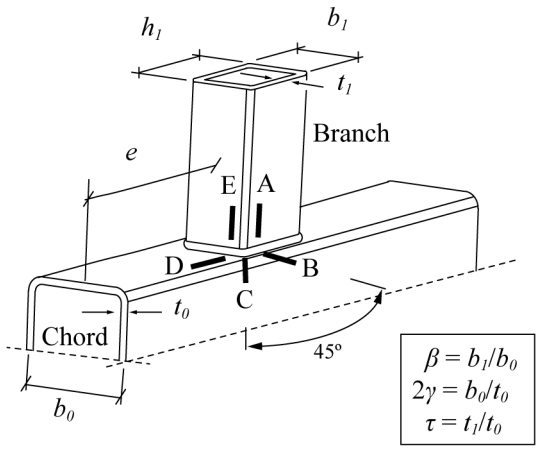

Range of Validity

$0.35 \le \beta \le 1.0$
$12.5 \le 2\gamma \le 25$
$0.25 \le \tau \le 1.0$
and
$0.1 \le e/b_0$

Load Condition: Axial Force on Branch(es)

Chord (lines B, C and D):

$$SCF_B = \left(0.143 - 0.204\beta + 0.064\beta^2\right)(2\gamma)^{\left(1.377+1.715\beta-1.103\beta^2\right)}\,\tau^{0.75}\psi$$

$$SCF_C = \left(0.077 - 0.129\beta + 0.061\beta^2 - 0.0006\gamma\right)(2\gamma)^{\left(1.565+1.874\beta-1.028\beta^2\right)}\,\tau^{0.75}\psi$$

$$SCF_D = \left(0.208 - 0.387\beta + 0.209\beta^2\right)(2\gamma)^{\left(0.925+2.389\beta-1.881\beta^2\right)}\,\tau^{0.75}\psi$$

For X-connections with $\beta = 1.0$:
SCF_C is multiplied by a factor of 0.65, and
SCF_D is multiplied by a factor of 0.50.

Branch (Lines A and E):

$$SCF_A = SCF_E = \left(0.013 + 0.693\beta - 0.278\beta^2\right)(2\gamma)^{\left(0.790+1.898\beta-2.109\beta^2\right)}\,\psi$$

For X-connections with fillet welds:
multiply branch SCF_A and SCF_E by 1.40 for the branch side of the weld.

For X-connections with $\beta \le 0.8$:

if $e/b_0 \ge 2.1$: $\psi = 1$

if $e/b_0 < 2.1$: $\psi = 1 - 0.78\left(2.10 - e/b_0\right)\Big/\left(2\gamma/\beta\right)^{0.61}$

Otherwise:
$\psi = 1$

Figure 3.19. Recommended SCFs for RHS-to-RHS axially loaded X-connections

3.6. Conclusions

An FE parametric study consisting of 256 linear FE models was conducted to determine SCFs for directly welded RHS-to-RHS axially loaded X-connections near an open chord end. The FE analyses were validated by comparison to two large-scale (experimental) tests. The following conclusions are made:

(1) SCFs in RHS-to-RHS axially loaded X-connections near an open chord end are lower than those in "standard" RHS-to-RHS X-connections with sufficient chord continuity (i.e. $e/b_0 \geq 2.1$ on both sides of the connection, as determined in this study);

(2) SCFs in RHS-to-RHS axially loaded X-connections near an open chord end become smaller (and hence less critical) as e/b_0 becomes smaller, and as 2γ becomes larger;

(3) The highest SCFs in RHS-to-RHS axially loaded X-connections near an open chord end are found in connections with medium values of β; and

(4) For different value of $e/b_0 \leq 2.1$, τ has a negligible effect on the SCFs.

SCF reduction factors (ψ) were derived from the FE results and regression analyses were conducted to derive a parametric formula to estimate ψ based on e/b_0, 2γ and β. As demonstrated in Figure 3.19, the ψ formula derived from this work can be used in conjunction with existing SCF formulae in CIDECT DG8 [21] (or other design guides) to estimate SCFs for RHS-to-RHS axially loaded X-connections near an open chord end. The results of this study are valid for $0.1 \leq e/b_0 \leq 3.0$, $12.5 \leq 2\gamma \leq 25$, $0.35 \leq \beta \leq 0.8$, and $0.25 \leq \tau \leq 1.0$.

Chapter 4

4. Chord-End RHS X-Connections with Cap Plates

4.1. Introduction

Current design standards and guidelines [1-9] for welded hollow structural section (HSS) connections tabulate limit states, associated formulae (for calculation of connection strength), and ranges of validity for formulae; however, these provisions assume a chord member (as labelled in Figure 4.1a and Figure 4.1d) with sufficient continuity on both sides of the connection [i.e. large end distances (e)]. Such connections are referred to in this paper as "regular" connections.

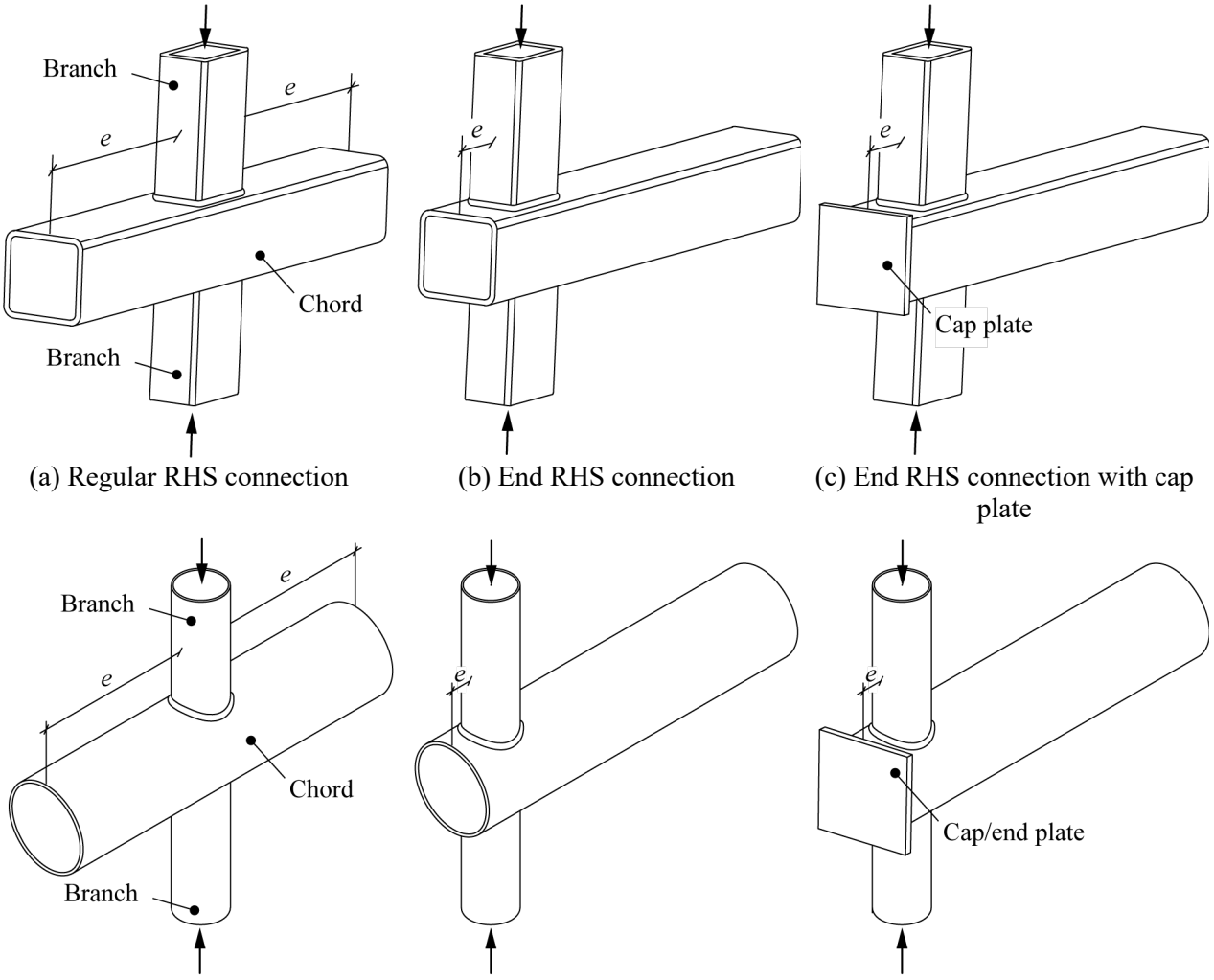

(a) Regular RHS connection (b) End RHS connection (c) End RHS connection with cap plate

(d) Regular CHS connection (e) End CHS connection (f) End CHS connection with cap plate

Figure 4.1. Different types of RHS-to-RHS and CHS-to-CHS X-connections

The chord-continuity assumption inherent to current design provisions is important for connection strength calculations for several limit states, e.g. chord plastification for Rectangular Hollow Section (RHS)-to-RHS and Circular Hollow Section (CHS)-to-CHS connections, and sidewall buckling for RHS-to-RHS connections. In such cases, sufficient end distances (e) are required on both sides of the connection to develop the predicted failure mechanism(s) and, in turn, the full (predicted) connection strength.

For connections at the end of a truss/girder, branch(es) are usually situated near a chord end (as shown in Figure 4.1b,c and Figure 4.2b,c). In such cases, existing design formulae (e.g. in [1-9]) do not apply (because the chord-continuity assumption is violated). Guidance on design of these so-called "end" connections has become increasingly sought after.

To address the challenge of designing end connections, research was performed by [10-16] on directly welded RHS-to-RHS, CHS-to-CHS, and branch plate-to-CHS end connections near an open (uncapped) chord end. It was found (by [10-16]) that the static strength of the connections (and welds thereto) were reduced relative to their regular-connection counterparts. In light of this, amendments were made to EN 1993-1-8 [71] (via prEN1993-1-8 Clause 9.1.2(10) [63]), and Tables K2.1A, K3.1A and K3.2A of AISC 360-16 [55], giving requirements for so-called minimum end distances (e_{min}). A review of the above research can be found in [18,19].

When the distance from the near side of a connecting HSS branch member (or branch plate) to the open end of a chord (e in Figure 4.1b) is less than e_{min}, AISC 360-16 [55] suggests (via the Commentary to Chapter K) a uniform reduction in predicted connection strength of 50% for RHS-to-RHS and plate-to-RHS connections; both prEN1993-1-8 Clause 9.1.2(10) [63] and AISC 360-16 [55] also suggest that providing a chord-end cap plate (Figure 4.1c and Figure 4.1f) is an effective design alternative. For the latter (AISC 360-16), this allows a waiver of the connection strength reduction requirement.

Research has been performed by [18,19] to address fatigue design of RHS-to-RHS and CHS-to-CHS axially loaded X-connections near an open chord end. For the connections studied, [18,19] found that existing formulae in CIDECT Design Guide 8 (DG8) [21], for the calculation of Stress Concentration Factors (SCF) (for regular connections) can be highly inaccurate. SCF correction factors (ψ), and parametric formulae to estimate ψ based on e, and non-dimensional connection parameters, were proposed. (Use of the ψ factor is discussed in Section 4.3).

As another step towards developing comprehensive fatigue design rules for chord-end RHS-to-RHS X-connections, this chapter presents a FE parametric study to determine SCFs for such connections reinforced with cap plates. Using FE modelling approaches validated in previous investigations [18,19], this study consists of: 256 RHS connection models with variations in chord slenderness ($2\gamma = b_0/t_0$, where b_0 = chord width and t_0 = chord thickness), branch-to-chord width ratio ($\beta = b_1/b_0$, where b_1 is the branch width), branch-to-chord thickness ratio ($\tau = t_1/t_0$, where t_1 is the branch thickness] and e (on *one side* of the of the connection) = 0.1, 0.25, 1.0 and 3.0 times b_0. This terminology (for RHS-to-RHS connections) is illustrated in Figure 4.2 (on the following page). It should be noted that $e = 3.0d_0$ (the upper value of e, above) is a conservative upper limit beyond which end-distance effects can be safely ignored [10-16].

For each connection model, SCFs at the critical locations are determined numerically and compared to the predicted values by CIDECT DG 8 [21] (for regular connections) to examine the applicability of the

existing formulae. SCF correction coefficients (ψ) – and parametric formulae to estimate ψ (based on e/b_0, 2γ and β) – are then derived to increase the accuracy of the SCF predictions.

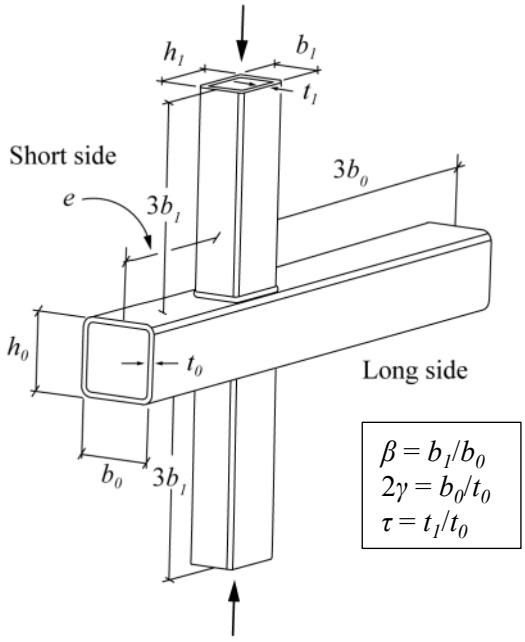

Figure 4.2. Connection terminology (end plate not shown, for clarity)

4.2. Relevant research on chord lengths and end conditions

In a recent experimental study on RHS-to-RHS connections with medium β-ratios [59], different yield line patterns were observed in regular connections and connections near an open chord end (see Figure 4.3). Due to the reduction in the total yield line length, the static strength of an RHS-to-RHS connection near an open chord end – for the "chord face plastification" limit state – was found to be significantly smaller than that of its regular-connection counterpart. The research done by [59] broadly supports the e_{min} requirement already present in AISC 360-16 [55] Table K3.2A for RHS-to-RHS truss connections (Equation 4.1), i.e.:

$$e_{\min} = b_0\sqrt{1-\beta} \qquad \text{Equation 4.1}$$

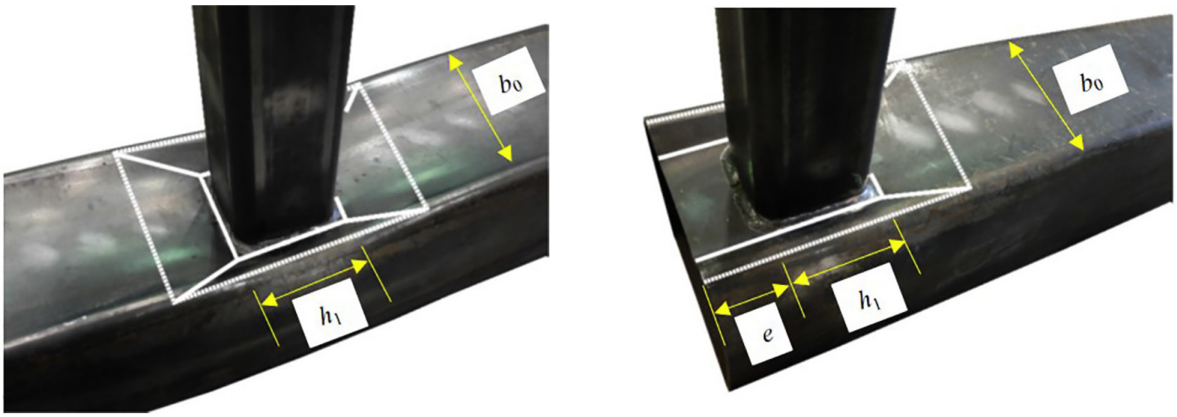

(a) Regular RHS connection (b) RHS connection near an open chord end

Figure 4.3. Typical yield line patterns (adapted from [59])

The study by [59] was extended by [58], via a FE parametric study to consider both the "chord side wall buckling" and the "chord face plastification" limit states. A new limit of $e_{min} = 0.75b_0$ was proposed for connections with RHS chords. A 40% strength reduction (instead of 50%) was recommended when $e < e_{min} = 0.75b_0$.

The research by [58] also found that reinforcing the open chord end with a rigid cap plate (Figure 4.1c) effectively restrains the connection deformation and allows it to develop connection static strength comparable to regular connections (Figure 4.1a). Therefore, for cap plate-reinforced connections, the e_{min} requirement does not apply.

Research on the effects of end distance and boundary conditions on CHS-to-CHS connections has also been performed, by [10,11]. CHS T- and X-connections covering a wide range of non-dimensional parameters (β, 2γ and τ) and chord length parameters ($\alpha = 2l_o/d_o$, where l_o = chord length) under branch axial loading were modelled. The effect of rigid chord end cap plate was also studied numerically. To prevent a significant strength reduction, the research proposed simple limits of $\alpha \geq 20$ (for chords with $2\gamma > 25$) and $\alpha \geq 12$ (for chords with $2\gamma \leq 25$). These limits were later confirmed for transverse branch plate-to-CHS T- and X-connections [14,15].

The FE parametric study by [10,11] showed that the minimum end distance requirement can be waived with the addition of a chord end cap plate, as – similar to connections with RHS chords – it largely restrained chord ovalization. In response to this research, an amendment was made to EN 1993-1-8 [71] (via prEN1993-1-8 Clause 9.1.2(10) [63]) which stipulates that:

"for joints with a chord end not connected to other members, the chord end shall be at a distance of at least $(2\gamma/10)d_0$ from the heel or toe of the closest branch, with a minimum of $2.5d_0$. For RHS chords, substitute d_0 by the largest of b_0 or h_0".

When the end-distance requirement cannot be met, the amendment suggests that the chord end shall be "welded to a cap plate with a thickness of at least $1.5t_0$, at a minimum distance of $0.5d_0(1 - \beta)$ or $0.5b_0(1 - \beta)$" from the branch toe or heel of the joint to prevent the strength reduction.

It should be noted that the minimum end distance requirement in prEN1993-1-8 Clause 9.1.2(10) [63] was developed based on research on CHS-to-CHS connections only. In this amendment to EN 1993-1-8 [71], the same requirement was transcribed to cover RHS-to-RHS connections, by replacing the CHS external diameter (d_0) with the RHS external width (b_0). However, no research evidence was available to support this transcription at the time.

Clearly, there is quite a disparity between the minimum end distance requirements in AISC 360-16 [71] and prEN1993-1-8 [73], mainly because the research by [10,11] focused on connections that were symmetrical about the branch member, while the research by [14,15] catered to end connections with reduced chord length on only one side of the connection. Nonetheless, all the above research and recent updates to design standards on connection static strength acknowledge the addition of chord-end cap plate as a solution allowing waiver of the end-distance requirement.

While research has been performed to develop design rules for HSS-(or plate-)to-HSS end connections under static loading, only limited research has been conducted on fatigue design of end connections. Recently, [18,19] performed a series of experimental and FE study to determine SCFs for directly welded RHS-to-RHS and CHS-to-CHS axially loaded X-connections at 90° near an open chord end. It was found that the existing formulae in CIDECT DG8 [21] (for regular connections) led to inaccurate SCF predictions. SCF correction factors (ψ), and parametric formulae to estimate ψ based on chord end distance and member cross-sectional dimensions (i.e. β, 2γ, τ and e/b_0) were hence derived [18,19], allowing SCFs in end connections near open chord ends to be predicted by multiplying ψ by the SCF values calculated using the existing CIDECT DG8 formulae [21].

Since it has been confirmed by [10-15] already that a chord-end cap plate can largely restrain chord deformation, and influence connection behaviour, it was deemed necessary to extend the work by [18,19] to investigate SCFs chord-end RHS-to-RHS X-connections with cap plates.

4.3. Finite Element Model Validation

4.3.1. Connection modelling

Commercial software programs (ANSYS and ABAQUS) [20,21] were used to conduct FE modelling and analyses of the RHS-to-RHS connections considered herein (see Section 4.1). The modelling approaches were previously validated by comparing the responses of the FE models with the experimental data of identical connections [18,19]. All modelling parameters were varied in sensitivity studies to ensure that FE models were not excessively large (computationally), but still provided convergence. The recommendations in CIDECT DG8 were followed throughout the modelling and analyses, including element selection, mesh refinement, weld details, boundary conditions and extrapolation of hot spot stress. Detailed discussions can be found in [18,19].

Four layers of eight-noded solid elements through the branch and chord wall thicknesses were used, with the approach used by [10,11,16] adopted to model the rigid chord end plates [by adding a row of stiff ($E = 2\times10^9$ MPa) linear-elastic solid elements to the short chord end (Figure 4.4b and Figure 4.4d)]. A half of

each connection was modelled, by taking advantage of the symmetries of geometry, loading and boundary conditions, to save computational time. Symmetry boundary conditions were applied along the cut face.

A literature survey was performed on previous research involving modelling of welds in HSS connections [22-36], and the weld modelling approach(es) was found to be consistent. A similar approach was adopted herein.

Linear elastic material properties, including Young's modulus (E) = 200 GPa, and Poisson's ratio (ν) = 0.3, were applied to both the steel and weld materials in the FE models. Figure 4.4 shows the geometry, mesh layout and boundary conditions of typical models. For each model, an axial compression force was applied in the upper branch with nodes on the end of the lower branch restrained from transition.

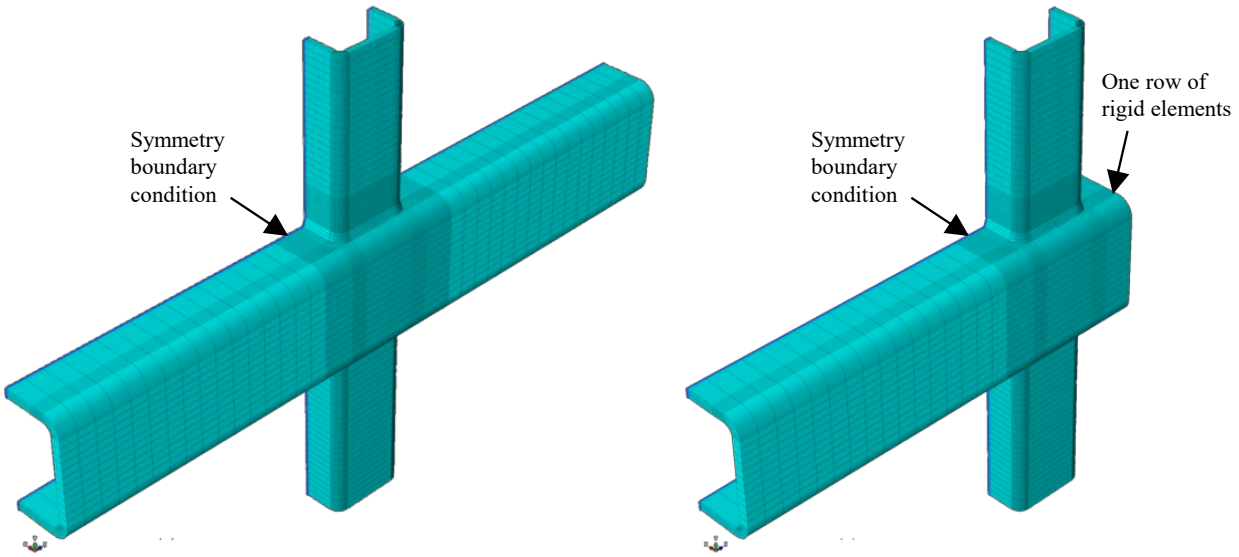

(a) Regular RHS connection (b) RHS connection with rigid chord end

Figure 4.4. Typical connection model geometry, mesh layout, and boundary conditions

In accordance with the CIDECT DG8 [21] recommendations, the welded joint location was partitioned and meshed, carefully, to allow accurate calculation of hot spot stresses within the extrapolation zones. The extrapolation zones at the critical locations are shown in

Table 4.1. For all FE models in this study, the hot spot stresses were calculated by using the extrapolation approach [21]. The branch nominal stress was hence calculated by dividing the applied force by the branch cross-sectional area. The SCF-values at the critical locations were then calculated by dividing the hot spot stresses by the branch nominal stress.

Table 4.1. Boundaries of extrapolation region for RHS-to-RHS connections

Distance from weld toe	Locations B, C and D	Locations A and E
$L_{r,min}$ *	$0.4t_0$	$0.4t_1$
$L_{r,max}$	$L_{r,min} + t_0$	$L_{r,min} + t_1$

* Minimum value for $L_{r,min}$ is 4 mm.

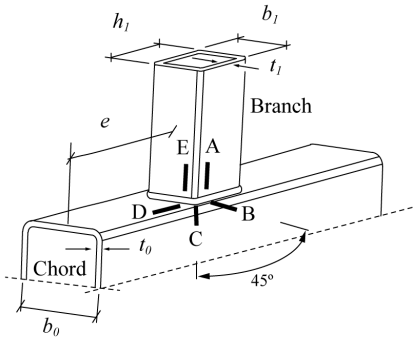

4.4. Chord-End RHS-to-RHS X-Connections with Cap Plates

In CIDECT DG8 [21], connection fatigue life is determined by using hot spot stress vs. fatigue life (S-N) curves. The hot spot stresses are calculated by multiplying the member nominal stresses by the SCFs at the critical locations. In this section, the SCF data from the parametric study for RHS-to-RHS connections are compared to the predicted values calculated using the existing SCF formulae in CIDECT DG8 [21]. The relationships among the SCF-values, the member cross-sectional dimensions, and the chord end distances are explored. Revised formulae are developed for calculation of SCFs in chord-end RHS-to-RHS X-connections with cap plates.

4.4.1. CIDECT Design Guide 8 Formulae

For RHS connections, CIDECT DG8 [21] considers five hot spot stress locations (locations A to E in

Table 4.1). The CIDECT DG8 SCF formulae for regular RHS-to-RHS axially loaded T- and X-connections at these locations are as follows:

- For the chord:

$$SCF_B = \left(0.143 - 0.204\beta + 0.064\beta^2\right)\left(2\gamma\right)^{\left(1.377+1.715\beta-1.103\beta^2\right)}\tau^{0.75} \quad \text{Equation 4.2}$$

$$SCF_C = \left(0.077 - 0.129\beta + 0.061\beta^2 - 0.0006\gamma\right)\left(2\gamma\right)^{\left(1.565+1.874\beta-1.028\beta^2\right)}\tau^{0.75} \quad \text{Equation 4.3}$$

$$SCF_D = \left(0.208 - 0.387\beta + 0.209\beta^2\right)\left(2\gamma\right)^{\left(0.925+2.389\beta-1.881\beta^2\right)}\tau^{0.75} \quad \text{Equation 4.4}$$

where SCF_B, SCF_C, and SCF_D = chord SCFs at hot spot B, C, and D, respectively.

- For the branch(es):

$$SCF_A = SCF_E = \left(0.013 + 0.693\beta - 0.278\beta^2\right)(2\gamma)^{\left(0.790+1.898\beta-2.109\beta^2\right)} \quad \text{Equation 4.5}$$

where $SCF_A = SCF_E$ = branch SCF at hot spots A and E, respectively.

Equation 4.2-Equation 4.5 are valid within the following range of validity: $0.35 \le \beta \le 1.0$, $12.5 \le 2\gamma \le 25$, $0.25 \le \tau \le 1.0$.

For connections with fillet welds, SCF_A and SCF_E are multiplied by 1.4, and for X-connections with β = 1.0, SCF_C is multiplied by 0.65 and SCF_D is multiplied by 0.50. A minimum SCF-value of 2.0 is recommended by CIDECT DG8 [21] at all locations.

4.4.2. Parametric Study

The FE parametric study for RHS-to-RHS X-connections consisted of 64 regular connection models and 192 cap plate-reinforced end connection models. A constant RHS chord member external width and height ($b_0 = h_0$) of 200 mm, and a wide ranges of non-dimensional parameters (β = 0.35, 0.5, 0.65, and 0.8; 2γ = 12.5, 16, 20 and 25; and τ = 0.25, 0.5, 0.75, and 1.0) were applied. The chord thickness (t_0) and branch cross-sectional dimensions ($b_1 = h_1$ and t_1) were hence determined based on the selected non-dimensional parameters. The end distance (e) was varied between $0.1b_0$, $0.5b_0$, $1.0b_0$ and $3.0b_0$, with $3.0b_0$ representing a conservative upper, beyond which "end effects" can be safely ignored [10-16]. The 64 "control models", with $e = 3b_0$ on both sides, served as the basis for the parametric study. For the control models, the SCF formulae in CIDECT DG8 [21] [i.e. Equation 4.2-Equation 4.5] are valid, in theory.

For the control models, the numerically obtained SCF-values on the two sides of the connections are the same due to symmetry. For the end connection models (i.e. those with $e < 3.0b_0$), the SCFs were obtained at the critical locations (Locations A to E, in

Table 4.1) on both the long chord side and the cap plate-reinforced (short) chord side of the connection (see Figure 4.2a). The values on the two sides were then compared – to identify the governing side. Representative data is shown in Figure 4.5. According to the comparison using <u>all</u> parametric study results, it was found, for RHS-to-RHS end connections, that the long chord side is always the governing side.

As shown by the representative data in Figure 4.5 (on the following page), the cap plate-reinforced short chord side has smaller SCFs values at all hot-spot locations. It is pointed out in CIDECT DG8 [21] that, for regular RHS-to-RHS X-connections under branch axial loading, the lower the 2γ ratio, the lower is the SCF, where $2\gamma = b_0 / t_0$ is an indicator of connection flexibility. In other words, for regular RHS-to-RHS connections, the SCFs at all hot-spot locations increase as the connection flexibility increases. This is consistent with the trend shown in Figure 4.5. For the cap plate-reinforced short chord side, the connection deformation is largely restrained by the cap plate (i.e. the long chord side is more flexible). In the following discussion, only the SCF-values from the governing sides are used for formulae development.

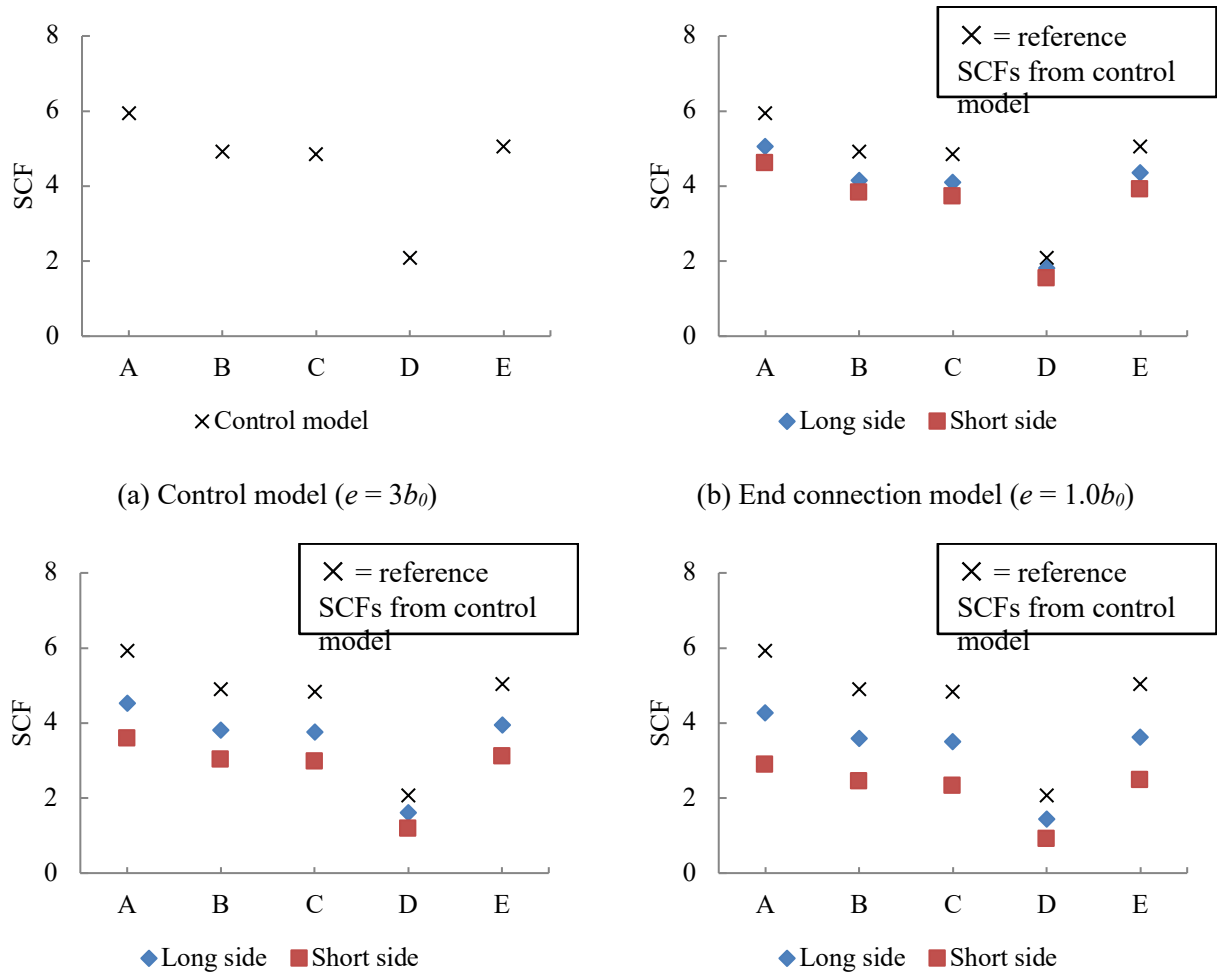

(a) Control model ($e = 3b_0$)

(b) End connection model ($e = 1.0b_0$)

(c) End connection model ($e = 0.5b_0$)

(d) End connection model ($e = 0.1b_0$)

Figure 4.5. SCFs for RHS-to-RHS connection models with $\beta = 0.65$, $2\gamma = 12.5$ and $\tau = 0.5$

The SCF-values from the end connection models (with different end distances) were also compared to the predictions using the existing CIDECT DG8 [21] formulae for regular connections [i.e. Equation 4.2-Equation 4.5]. According to the representative comparisons shown in Figure 4.6, the application of existing formulae can be excessively conservative. Therefore, modified formulae catering specifically to chord-end RHS-to-RHS X-connections with cap plates are deemed necessary.

The relationships among the SCF-values, the connection nondimensional parameters, the chord end distance and chord end cap plate were further explored using the parametric study results by calculating ψ equal to the ratios of SCFs in the cap plate-reinforced end-connection models ($SCF_{end\ connection}$) to those in the corresponding control models ($SCF_{control\ model}$). Representative plots of ψ (= $SCF_{end\ connection}$/ $SCF_{control\ model}$) vs. e/d_0 at the five hot-spot locations (identified in

Table 4.1) are shown in Figure 4.7-Figure 4.9. The following observations can be made (for all hot-spot locations):

i) ψ in general decreases as e/d_0 decreases.

ii) For different e/d_0, ψ increases as β decreases, or as 2γ increases.

iii) ψ does not change significantly for different τ.

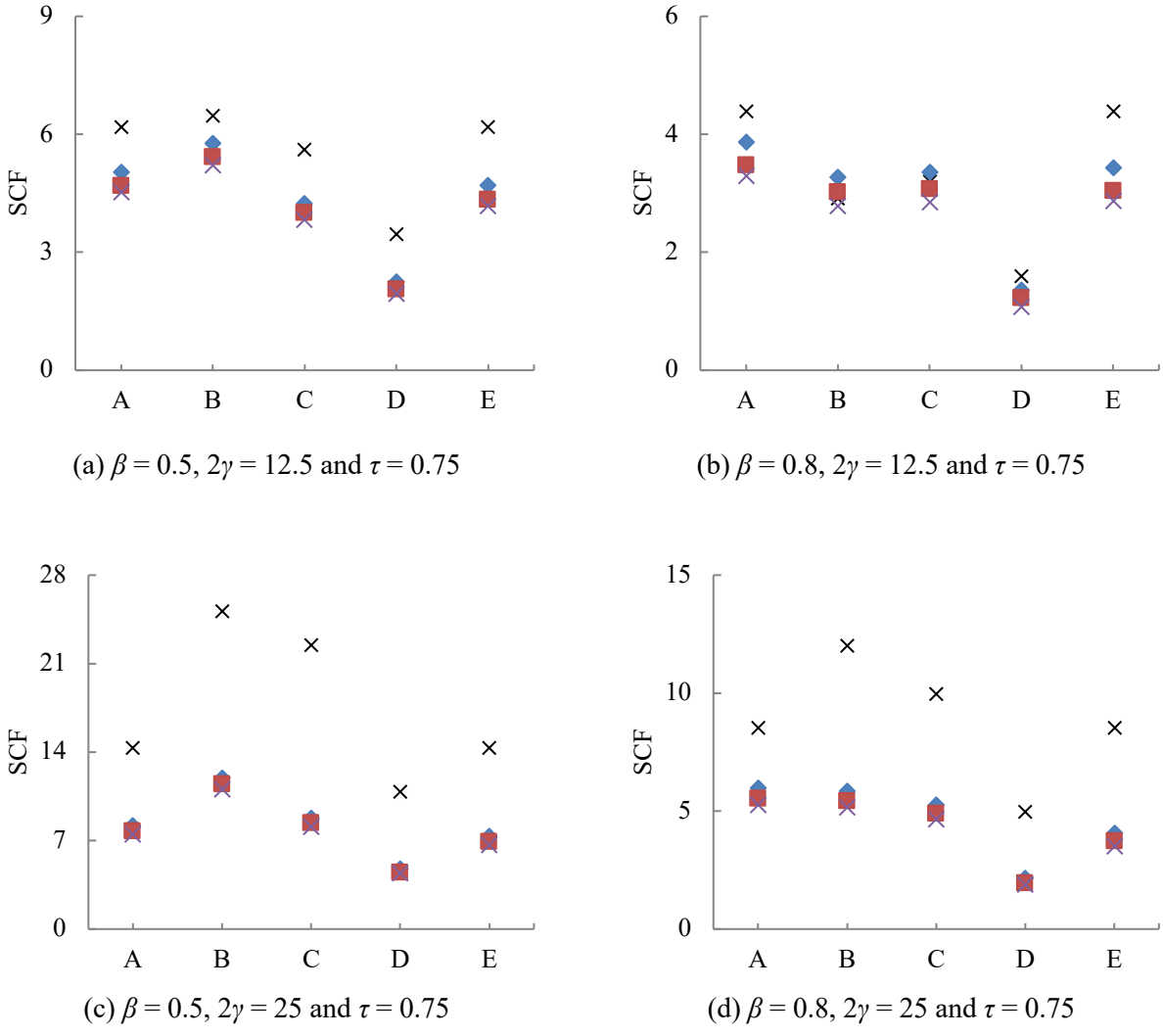

Figure 4.6. Comparison of FE results for RHS-to-RHS end connections with predictions by CIDECT DG8 [21]

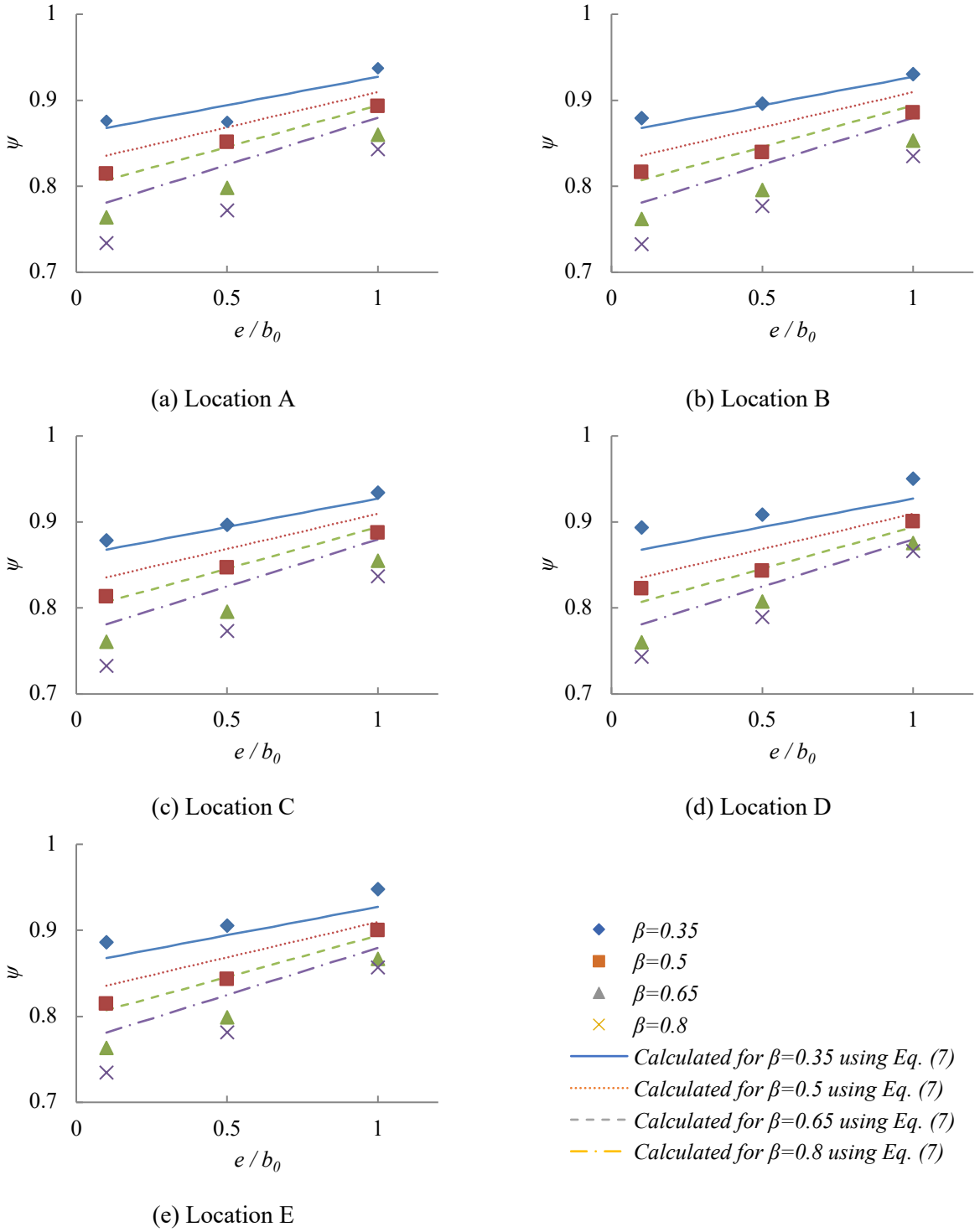

Figure 4.7. Effects of e/b_0 and β on SCFs in RHS-to-RHS end connections (2γ=20 and τ=0.75)

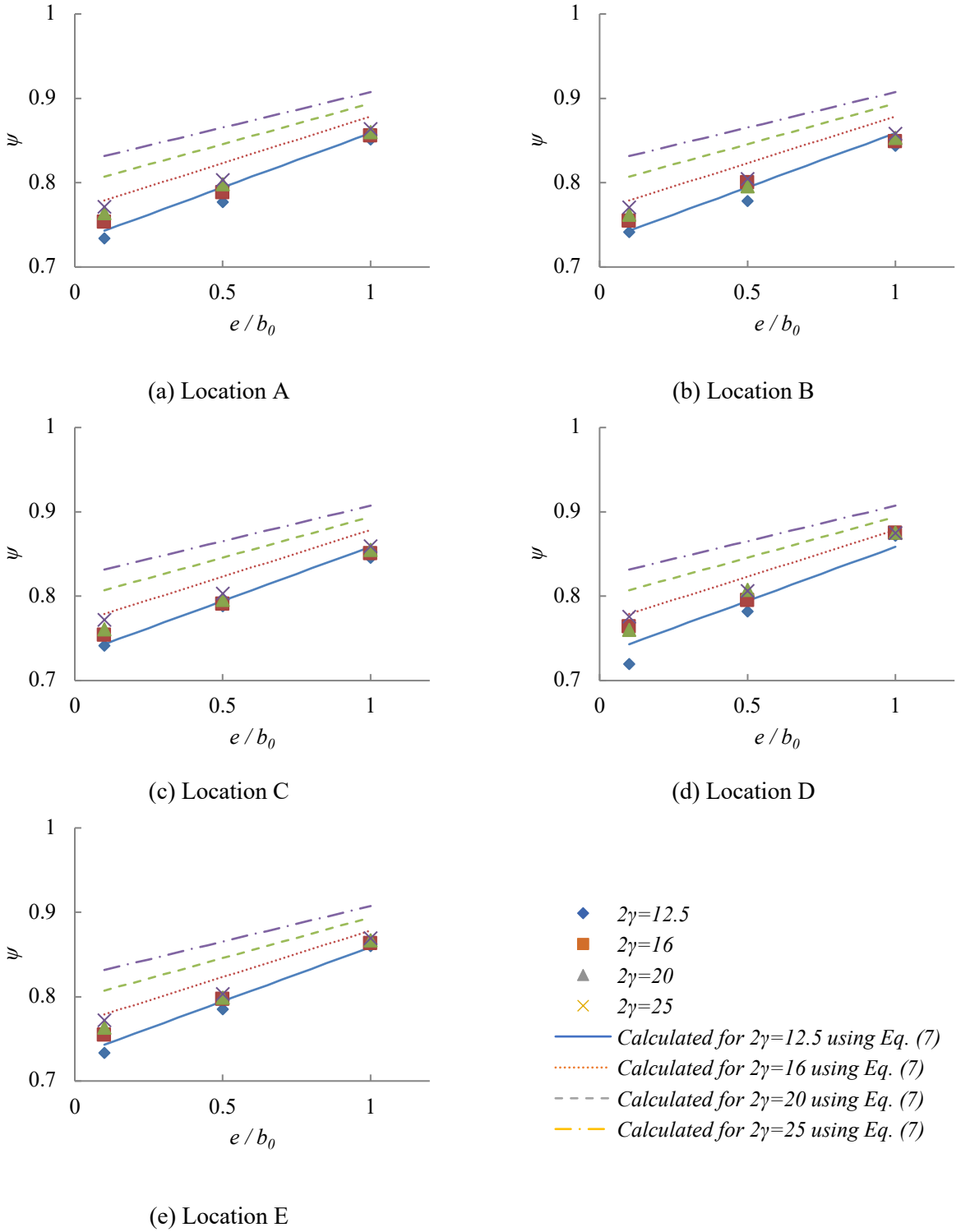

Figure 4.8. Effects of e/b_0 and 2γ on SCFs in RHS-to-RHS end connections (β=0.65 and τ=0.75)

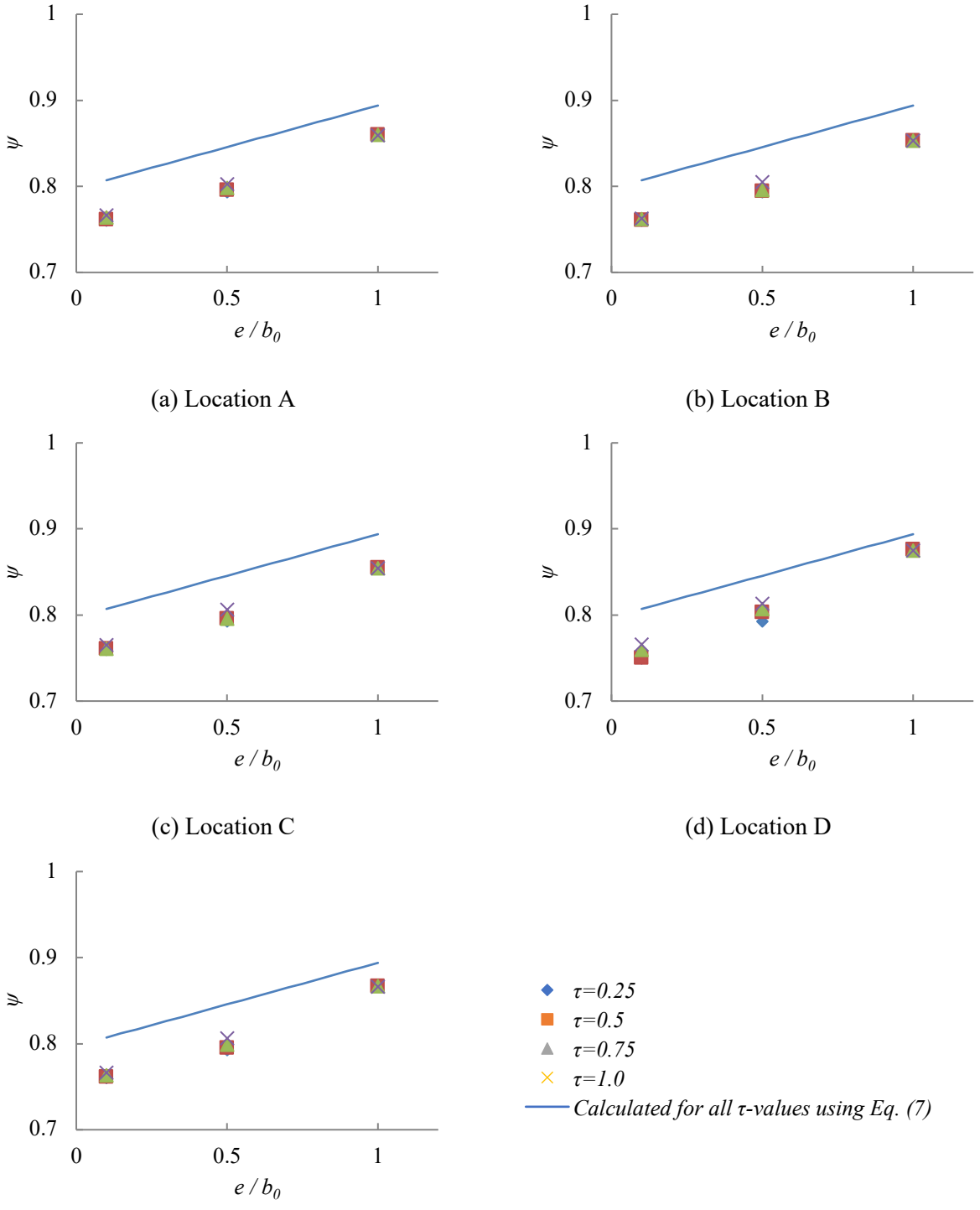

Figure 4.9. Effects of e/b_0 and τ on SCFs in RHS-to-RHS end connections (β=0.65 and 2γ=20)

4.4.3. Proposed Formulae

According to the parametric study, the SCFs in regular RHS X-connections and chord-end RHS X-connections with cap plates can differ considerably. For the latter, predictions using the existing CIDECT DG 8 [21] SCF formulae are inaccurate [because the change of chord end distance and boundary conditions (i.e. effects of chord end distance and cap plate) were not considered in their development].

As shown by Equation 4.6, the ψ-factors presented above can be used in conjunction with existing CIDECT DG8 SCF formulae [i.e. by multiplying the result of Equation 4.2-Equation 4.5 by ψ] to determine the SCFs in axially loaded chord-end RHS X-connections with cap plates; i.e.:

$$SCF_{end,i} = SCF_i \cdot \psi \qquad \text{Equation 4.6}$$

where SCF_i = SCF at hot spot i in a regular HSS-to-HSS X-connection [calculated using Equation 4.2-Equation 4.5]; ψ = correction factor; $SCF_{end,i}$ = SCF at hot spot i in a chord-end HSS-to-HSS X-connection with cap plate.

As discussed in Section 4.4.2, in the parametric study, SCFs were obtained from the cap plate-reinforced end connection models (with $e = 0.1b_0$, $0.5b_0$, $1.0b_0$), and from the control connections (with $e = 3b_0$). The correction factors (ψ) were obtained by dividing the former by the latter.

The parametric study shows that, for each chord-end RHS X-connection with cap plate, the ψ-values for hot spot locations A-E are nearly constant – since all locations are adjacent to the branch corner at the welded joint. It was then deemed appropriate to use a single formula to estimate the maximum of the five ψ-values (from locations A-E) in a chord-end RHS X-connection with cap plate for determination of SCFs according to Equation 4.6.

As discussed in Section 4.2, for all hot spot locations, ψ changes as e/d_0, β and 2γ change. ψ does not vary significantly for different τ. An extensive evaluation of different types of formulae was conducted, followed by a non-linear least-squares regression analysis. The resulting approximate "best-fit" equation is given by Equation 4.7:

$$\psi = 1 - 0.78\left(2.10 - e/b_0\right)\Big/\left(2\gamma/\beta\right)^{0.61} \qquad \text{Equation 4.7}$$

Figure 4.7-Figure 4.9 show sample comparisons between: (i) ψ-values calculated using Equation 4.7 and (ii) ψ-values obtained by dividing $SCF_{end\ connection}$ by $SCF_{control\ model}$ (based on the parametric study results). Table 4.2 includes the key statistics from comparisons based on the complete parametric study (i.e. 64 regular connection models and 192 end connection models). As shown in Figure 4.7-Figure 4.9 and Table 4.2, Equation 4.7 is reasonably accurate over the range of parameters considered. For consistency with CIDECT DG 8 [21], a minimum SCF-value of 2.0 is still recommended.

Table 4.2. Mean values and COVs of FE-to-predicted ψ based on Equation 4.7 for 192 RHS-to-RHS cap plate-reinforced end X-connection models

Location	Mean	COV
A	0.98	0.03
B	0.98	0.03
C	0.98	0.03
D	0.98	0.04
E	0.98	0.03

4.5. Conclusions

To establish definitive design provisions for chord-end RHS-to-RHS X-connections with cap plates, a total of 256 FE models were developed and analysed in the parametric study presented in this section. Based on the results, SCF correction factors (ψ), and parametric formulae to estimate ψ based on chord end distance-to-width (e/b_0), branch-to-chord width (β), branch-to-chord thickness (τ), and chord slenderness (2γ) ratios, were derived. The ψ formulae developed in this study can be used in conjunction with the existing SCF formulae in CIDECT Design Guide 8 (or other design guides) for calculation of SCFs in cap plate-reinforced RHS-to-RHS end connections.

Chapter 5

5. Bird-Beak SHS X-Connections near an Open Chord End: Stress Concentration Factors

5.1. Introduction

The formulae in current standards and guidelines [1-7] for welded hollow structural section (HSS) connections in general assume a chord member with sufficient continuity on both sides of the connection (hereafter referred to as "regular connection"). The chord-continuity assumption is inevitably violated for HSS connections situated near a truss/girder end (hereafter referred to as "end connections"). Research on the behaviour and design of end connections (Figure 5.1) has become increasingly sought after.

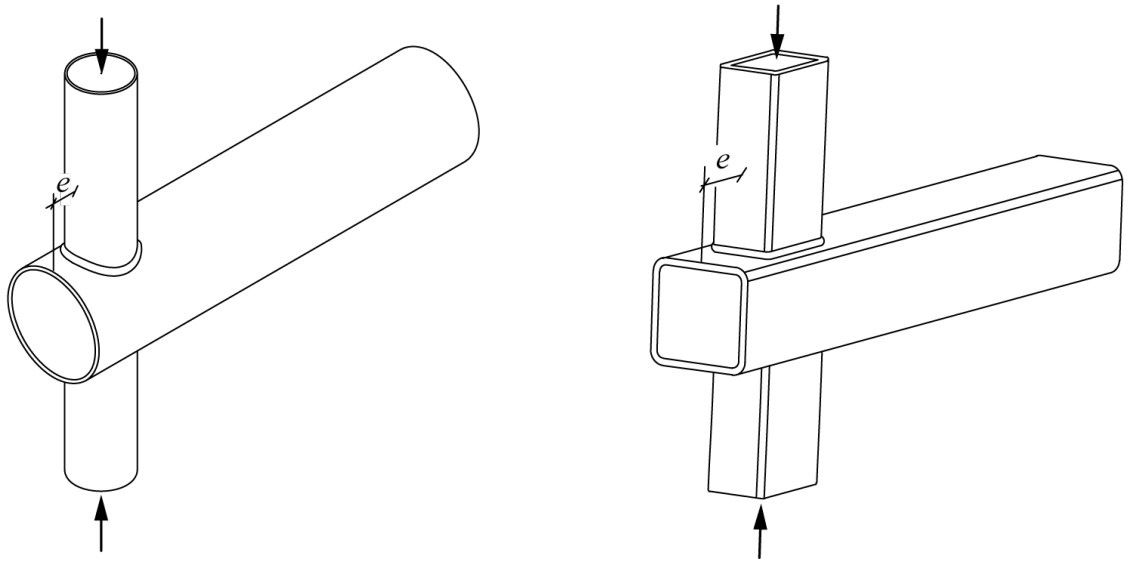

(a) CHS-to-CHS chord-end X-connection (b) RHS-to-RHS chord-end X-connection

Figure 5.1. HSS-to-HSS X-type end connections

Research on the chord end distance effect on circular hollow section (CHS)-to-CHS connections has been performed by [8,9] who found that the connection static strength decreases as the chord end distance (e in Figure 5.1) decreases. In response to this research, an amendment was made to EN 1993-1-8 [57] (via prEN1993-1-8 Clause 9.1.2(10) [63]) for truss/girder-end CHS-to-CHS connections under static loading. This amendment includes a requirement for the minimum value of e to ensure the full (predicted) connection strength according to EN 1993-1-8 [57] can be developed. The requirement was speculatively transcribed to cover rectangular hollow section (RHS)-to-RHS connections (by replacing the CHS external diameter with the RHS external width).

In AISC 360-16 [55], minimum chord end distance requirements for HSS connections are included in Chapter K. These requirements, which differ from those in EN 1993-1-8 [57], are supported by experimental and numerical research on both RHS-to-RHS and CHS-to-CHS connections [11-15], as discussed in [16-18].

For fatigue loading, HSS design standards and guidelines [19,20] lack clear coverage of end connections. To address this, research [16-18] has been performed on the effects of chord end distance and cap plates (the most common reinforcement solution for HSS end connections) on the stress concentration factors (SCFs) in RHS-to-RHS and CHS-to-CHS connections. This research aimed to derive SCF correction factors (ψ), and parametric formulae to estimate ψ [based on chord end distance-to-width (or diameter) (e/b_0 or e/d_0), branch-to-chord width (β), branch-to-chord thickness (τ), and chord slenderness (2γ) ratios] to account for the so-called "end effect".

With square hollow section (SHS)-to-SHS connections, chord and/or branch members can be rotated by 45° to create so-called square bird-beak (SBB) or diamond bird-beak (DBB) connections (Figure 5.2 and Figure 5.3, respectively). While CIDECT Design Guide 3 (DG3) [51] contains static design formulae for DBB connections, CIDECT Design Guide 8 (DG8) [21] is silent regarding formulae for SBB and DBB connections under fatigue.

Research on regular SBB and DBB connections under fatigue loading has recently been performed by [21-30] who found that, in general, they have better fatigue performance than their counterpart connections with conventional branch and chord member orientations. This is mainly due to them having less severe stress concentrations (i.e. lower SCFs) at the welded joint hot spots. The research in this chapter presents a study on the chord end distance effect on SCFs in SBB and DBB X-connections near an open chord end.

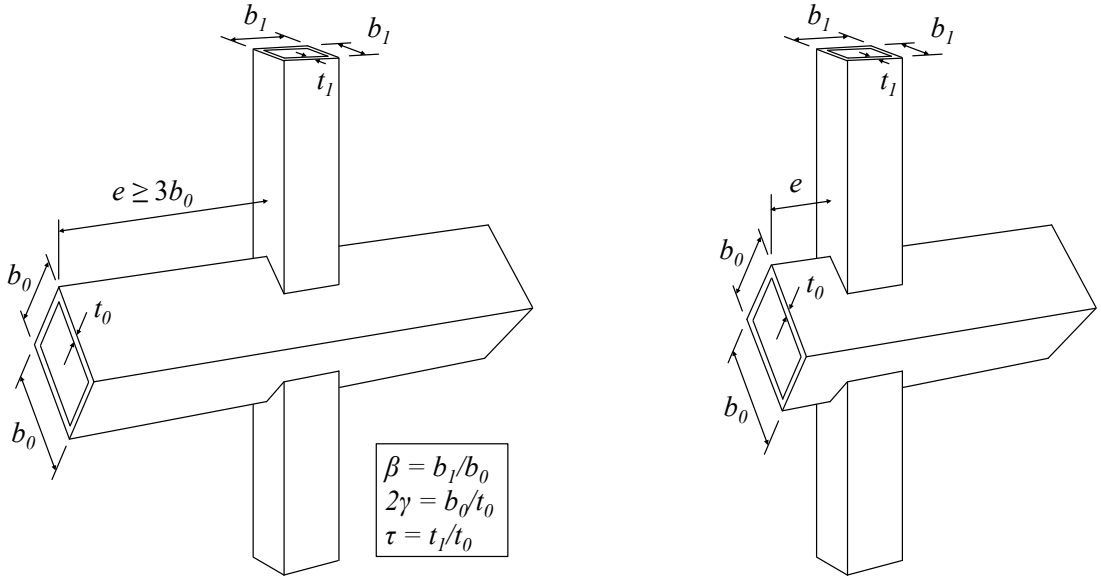

(a) Regular SBB X-connection (b) Chord-end SBB X-connection

Figure 5.2. SBB X-connections

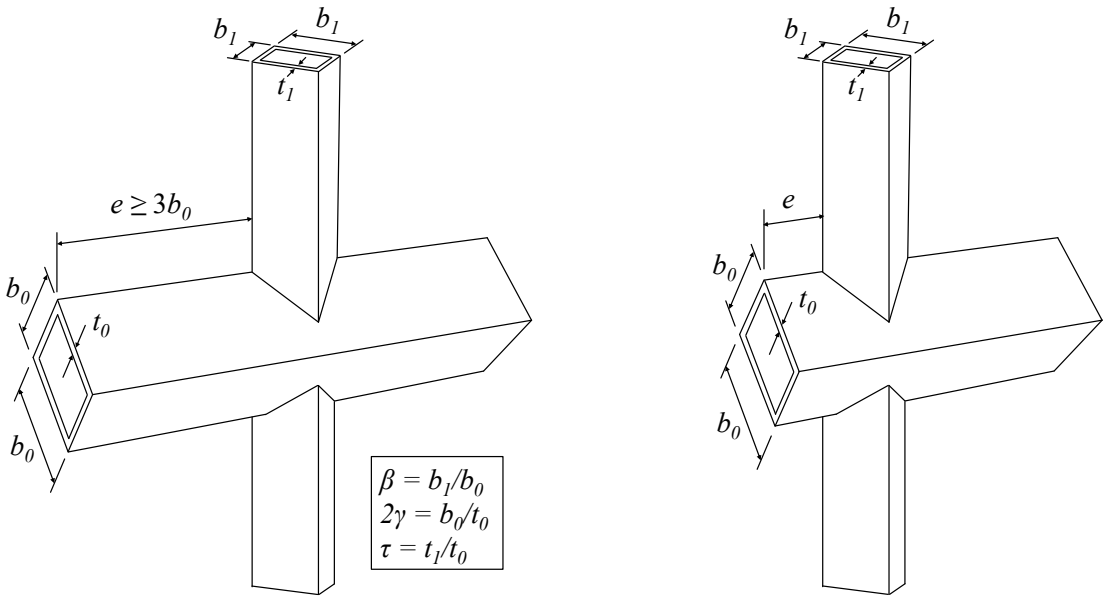

(a) Regular DBB X-connection (b) Chord-end DBB X-connection

Figure 5.3. DBB X-connections

5.2. SCF formulae for regular SBB and DBB connections

Hot spot stress locations for regular SBB and DBB connections under branch axial loading have been identified by [89] (Figure 5.4). [89] also developed SCF formulae for these locations [Equation 5.1-Equation 5.14]. The research presented in this paper aims to extend this work, by developing accurate formulae for correction factors (ψ) to be used in conjunction with Equation 5.1-Equation 5.14 to calculate SCFs in SBB and DBB connections near an open chord end.

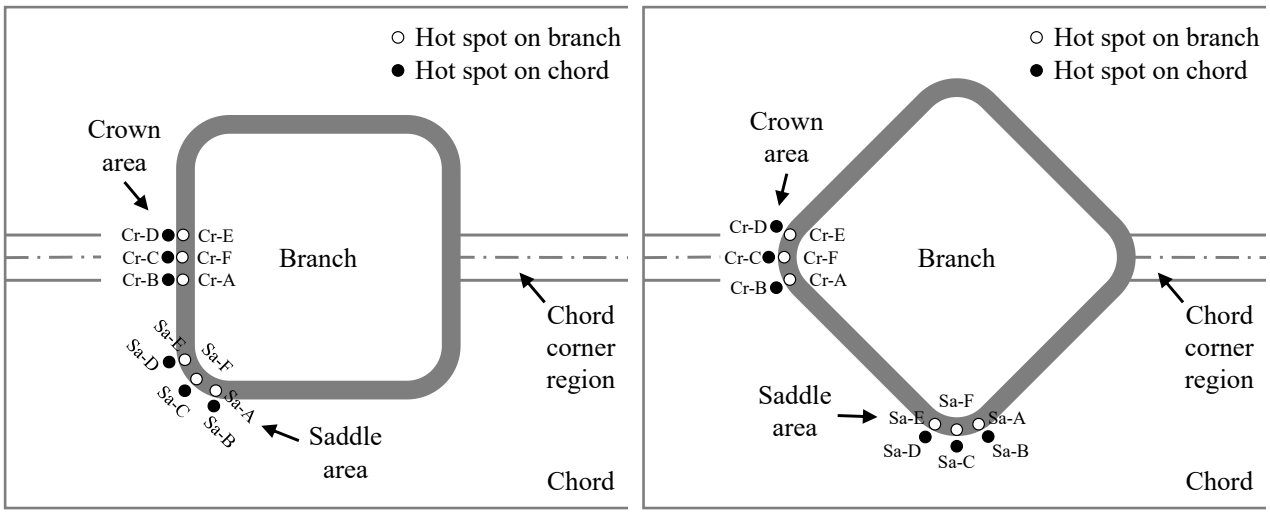

Figure 5.4. Hot spot stress locations in SBB and DBB connections based on [89]

SCF formulae for <u>SBB connections</u>:

$$SCF_{Cr\text{-}A} = SCF_{Cr\text{-}E} = SCF_{Cr\text{-}F} = (\tau^2 - 1.609\,.\,\tau - 1.309)\,.\,(-0.155\,.\,\beta^2 + 0.381\,.\,\beta - 0.223).\,2\gamma^{(-0.560\,.\,\beta^2 + 1.269\,.\,\beta + 0.305)} \quad \text{Equation 5.1}$$

$$SCF_{Cr\text{-}B} = SCF_{Cr\text{-}C} = SCF_{Cr\text{-}D} = (\tau^2 + 1.130\,.\,\tau + 0.279)\,.\,(0.159\,.\,\beta^2 - 0.693\,.\,\beta + 0.604).\,2\gamma^{(-0.993\,.\,\beta^2 + 1.400\,.\,\beta + 0.129)} \quad \text{Equation 5.2}$$

$$SCF_{Sa\text{-}A} = SCF_{Sa\text{-}E} = SCF_{Sa\text{-}F} = (\tau^2 - 1.625\,.\,\tau - 0.177)\,.\,(-0.011\,.\,\beta^2 + 0.295\,.\,\beta - 0.425).\,2\gamma^{(-1.157\,.\,\beta^2 + 2.337\,.\,\beta + 0.253)} \quad \text{Equation 5.3}$$

$$SCF_{Sa\text{-}B} = (\tau^2 - 4.851\,.\,\tau + 0.188)\,.\,(-0.153\,.\,\beta^2 + 0.380\,.\,\beta - 0.239).\,2\gamma^{(-0.552\,.\,\beta^2 + 2.013\,.\,\beta + 0.384)} \quad \text{Equation 5.4}$$

$$SCF_{Sa\text{-}C} = (\tau^2 - 3.450\,.\,\tau + 0.154)\,.\,(-0.178\,.\,\beta^2 + 0.444\,.\,\beta - 0.281).\,2\gamma^{(-0.639\,.\,\beta^2 + 2.081\,.\,\beta + 0.427)} \quad \text{Equation 5.5}$$

$$SCF_{Sa\text{-}D} = (\tau^2 - 2.479\,.\,\tau + 0.110)\,.\,(-0.165\,.\,\beta^2 + 0.421\,.\,\beta - 0.274).\,2\gamma^{(-0.679\,.\,\beta^2 + 2.059\,.\,\beta + 0.498)} \quad \text{Equation 5.6}$$

Equation 5.1-Equation 5.6were developed based on the parametric study in [89] covering the following ranges of non-dimensional parameters:

$0.3 \leq \beta \leq 1.1 \qquad 12.5 \leq 2\gamma \leq 25 \qquad 0.25 \leq \tau \leq 1.0$

SCF formulae for DBB connections:

$SCF_{Cr\text{-}A} = SCF_{Cr\text{-}E} = (\tau^2 - 2.407\,.\,\tau - 0.141)$ Equation 5.7
$.(-6.512\,.\,\beta^2 + 11.150\,.\,\beta - 5.350 - 0.120\,.\,2\gamma).\,2\gamma^{(-0.994\,.\,\beta^2 + 1.468\,.\,\beta - 0.813)}$

$SCF_{Cr\text{-}B} = SCF_{Cr\text{-}D} = (\tau^2 + 3.677\,.\,\tau + 0.388)$ Equation 5.8
$.(1.174\,.\,\beta^2 - 1.889\,.\,\beta + 1.099 + 0.041\,.\,2\gamma).\,2\gamma^{(-1.531\,.\,\beta^2 + 1.729\,.\,\beta - 0.591)}$

$SCF_{Cr\text{-}C} = (\tau^2 - 6.869\,.\,\tau - 0.106)$ Equation 5.9
$.(-0.331\,.\,\beta^2 + 0.177\,.\,\beta + 0.293 - 0.119\,.\,2\gamma).\,2\gamma^{(-1.624\,.\,\beta^2 + 1.758\,.\,\beta - 0.744)}$

$SCF_{Cr\text{-}F} = (\tau^2 - 1.588\,.\,\tau - 0.301)$ Equation 5.10
$.(-2.535\,.\,\beta^2 + 2.180\,.\,\beta - 0.934 - 0.017\,.\,2\gamma).\,2\gamma^{(-2.172\,.\,\beta^2 + 2.260\,.\,\beta - 0.180)}$

$SCF_{Sa\text{-}A} = SCF_{Sa\text{-}E} = (\tau^2 - 1.550\,.\,\tau - 0.191)$ Equation 5.11
$.(-5.192\,.\,\beta^2 + 5.794\,.\,\beta - 2.009 - 0.064\,.\,2\gamma).\,2\gamma^{(-2.314\,.\,\beta^2 + 3.303\,.\,\beta - 0.465)}$

$SCF_{Sa\text{-}B} = SCF_{Sa\text{-}D} = (\tau^2 - 2.859\,.\,\tau + 0.153)$ Equation 5.12
$.(-0.315\,.\,\beta^2 + 1.716\,.\,\beta - 0.768 - 0.094\,.\,2\gamma).\,2\gamma^{(-1.529\,.\,\beta^2 + 2.458\,.\,\beta - 0.373)}$

$SCF_{Sa\text{-}C} = (\tau^2 - 6.810\,.\,\tau - 0.398)$ Equation 5.13
$.(0.483\,.\,\beta^2 + 0.214\,.\,\beta - 0.042 - 0.160\,.\,2\gamma).\,2\gamma^{(-1.353\,.\,\beta^2 + 2.277\,.\,\beta - 0.365)}$

$SCF_{Sa\text{-}F} = (\tau^2 - 1.903\,.\,\tau - 0.029)$ Equation 5.14
$.(-5.540\,.\,\beta^2 + 6.628\,.\,\beta - 2.404 - 0.112\,.\,2\gamma).\,2\gamma^{(-2.006\,.\,\beta^2 + 2.962\,.\,\beta - 0.436)}$

Equation 5.7-Equation 5.14were developed based on the parametric study in [89] covering the following ranges of non-dimensional parameters:

$0.3 \le \beta \le 0.7 \qquad 12.5 \le 2\gamma \le 25 \qquad 0.25 \le \tau \le 1.0$

5.3. Finite Element Model Validation

A detailed FE modelling approach for SBB and DBB connections was developed by [88], which is adopted in this study. Experimental data from [89] is then used to validate the approach.

[89] tested a total of four regular connection specimens (two SBB X-connections and two DBB-X connections, as shown in Table 5.1) under branch axial tensile forces. The magnitudes of the forces were determied based on pre-testing finite element (FE) analysis to ensure that the maximum hot spot stress was lower than 25% of the nominal yield strength of the steel material used (345 MPa). Chain strain gauges were used by [89] to record the elastic strains within the extrapolation region shown in Figure 5.5. The upper and lower bounds of the extrapolation region ($L_{r,max}$ and $L_{r,min}$) were determined based on the wall thicknesses of the branch and chord members following the requirements in CIDECT DG8 [21]. $L_{r,min}$ was taken as the greater value between 0.4 times the SHS branch or chord member wall thickness (t_0 or t_1) and 4 mm, and $L_{r,max}$ was taken as $L_{r,min}$ plus the SHS branch or chord member wall thickness. Using the recorded elastic strains within the extrapolation zones, the quadratic extroplation approach (Figure 5.5) recommeded by CIDECT [21] was used to calculate the hot spot strains at the cricital locaions. The nominal strain under branch axial loading was measured using the linear strain gauges installed on the branch member. The calculated hot spot strains were then devided by the branch nominal strain to determine the strain concentration factors (SNCFs) at the critical locations. For each regular X-connection specimen in Table 5.1, [89] installed two sets of chain strain gauges on the upper and lower sides of the connection (i.e. one set for each welded joint). The experimentally obtained SNCFs on the upper and lower sides of the connections at the hot spot locations are shown in Table 5.2.

Table 5.1. Nominal geometrical properties of test specimens [89]

Specimen ID	Chord ($b_0 \times b_0 \times t_0$) (mm×mm×mm)	Branch ($b_1 \times b_1 \times t_1$) (mm×mm×mm)	Total chord length (mm)	$\beta = b_1/b_0$	$2\gamma = b_0/t_0$	$\tau = t_1/t_0$
SBB-X1	200×200×11.5	90×90×7.6	1200	0.45	17.39	0.661
SBB-X2	200×200×9.5	120×120×4.5	1200	0.60	21.05	0.474
DBB-X1	200×200×11.5	90×90×7.6	1200	0.45	17.39	0.661
DBB-X2	200×200×9.5	120×120×4.5	1200	0.60	21.05	0.474

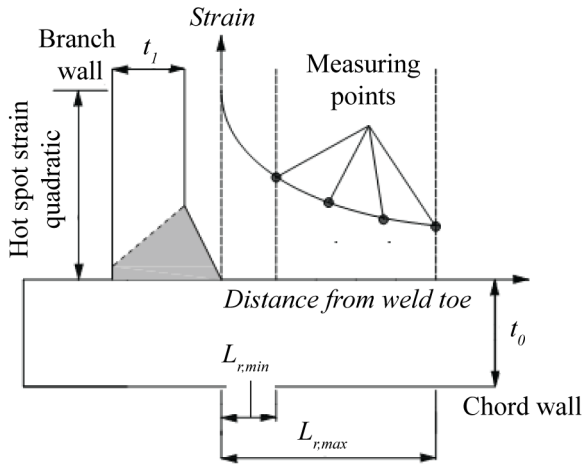

Figure 5.5. CIDECT DG8 approach [21] for calculation of hot spot strain

Table 5.2. SNCFs from previous connection tests [89]

		SNCF at crown area				SNCF at saddle area					
Specimen	Location	Cr-C	Cr-B	Cr-F	Cr-A	Sa-D	Sa-C	Sa-B	Sa-E	Sa-F	Sa-A
SBB-X1	Upper side	2.39	2.08	1.46	N/A	4.20	5.44	5.79	2.43	3.08	3.76
	Lower side	2.09	2.39	1.62	1.24	4.05	5.52	6.40	2.42	2.91	3.55
SBB-X2	Upper side	1.68	1.43	N/A	N/A	4.20	5.79	6.45	4.04	4.76	5.23
	Lower side	1.67	1.49	N/A	N/A	4.05	5.78	6.40	3.86	4.81	5.14
DBB-X1	Upper side	2.93	2.27	1.46	1.17	5.39	5.96	6.15	4.48	7.68	N/A
	Lower side	3.16	1.84	1.71	1.25	5.72	6.43	4.84	4.47	7.14	4.72
DBB-X2	Upper side	2.60	1.88	2.10	1.22	5.83	7.04	6.96	5.82	6.99	6.08
	Lower side	2.27	2.00	2.43	N/A	6.45	7.09	6.36	6.16	6.64	6.24

For validation of the FE modelling approach used in the current study, four FE connection models (replicating those in Table 5.1) were developed in ABAQUS [23]. Linear elastic material properties [Young's modulus (E) = 200 GPa and Poisson's ratio = 0.3] were applied to the SHS member and weld materials, and the outer corner radii of the SHS members were taken as two times the nominal wall

thickness. The approach suggested by [88], as noted above, was used to model the welds – where the shape and size of the welds were determined based on AWS D1.1/D1.1M:2020 [56].

Four layers of through-thickness solid elements (C3D20R in ABAQUS) were used in modelling the branch and chord members, following the recommendations from CIDECT [21]. A “one-half model” with symmetry boundary conditions (which was permissible due to symmetry in geometry, loading and boundary conditions along the “cut face”), was used (Figure 5.6). A fixed end condition was applied to the bottom of the lower branch, while all nodes at the top of the upper branch were set free, and a tensile force was applied to the top of the upper branch, axially. The FE models were carefully partitioned and meshed at the welded joint locations to allow accurate calculation of the SNCFs at the hot spot locations. Figure 5.7 shows the region partition and meshing at the welded joint locations.

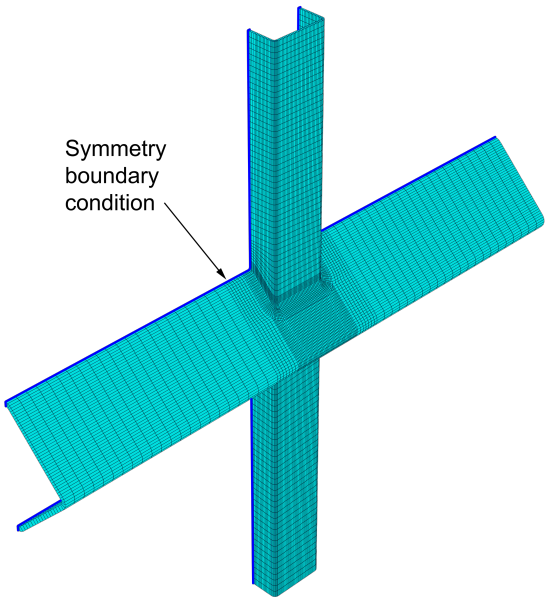

(a) Regular SBB X-connection

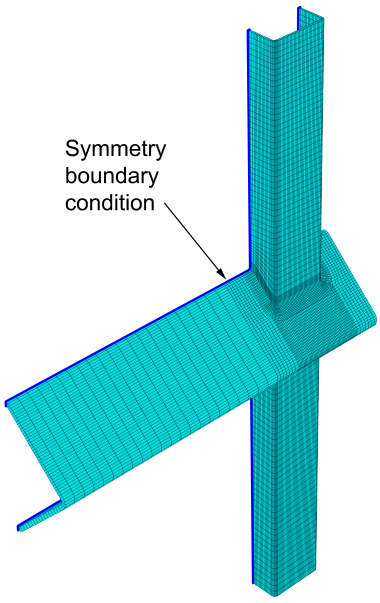

(b) chord-end SBB X-connection

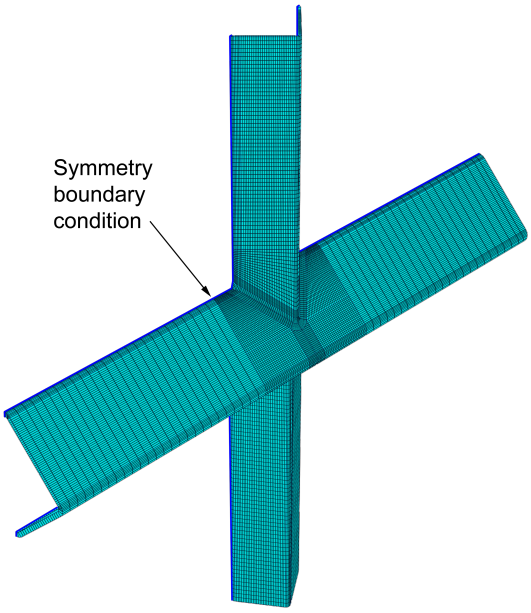

(c) Regular DBB connection

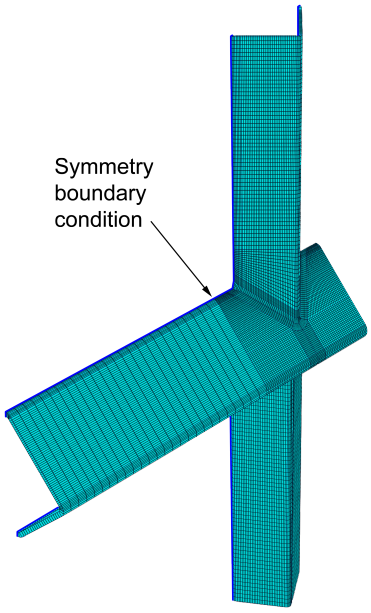

(d) chord-end DBB X-connection

Figure 5.6. Typical connection model geometry, mesh layout, and boundary conditions

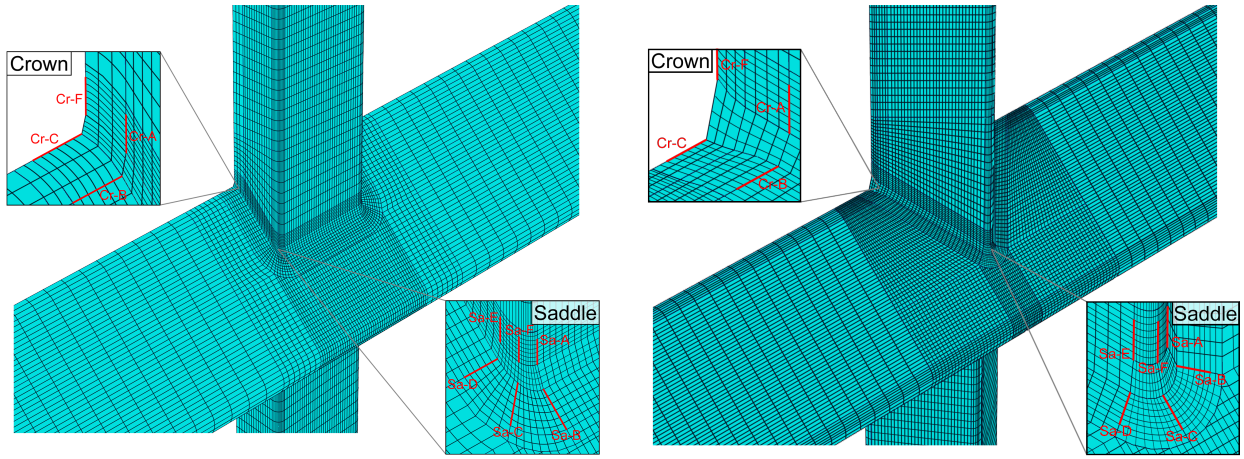

(a) Chord-end SBB X-connection (b) Chord-end DBB X-connection

Figure 5.7. Region partition and meshing at welded joint location

Using the quadratic extrapolation approach recommended by CIDECT [21], the SNCFs at the hot spot locations from the four FE connection models were determined and listed in Table 5.3. Since only half of each connection was modelled, SNCFs at locations Cr-D and Cr-E (Figure 5.4) are not included in the table; however, these would be the same as those at locations Cr-A and Cr-B due to symmetry (see Figure 5.6).

Table 5.3. SNCFs from finite element simulation

	SNCF at crown area				SNCF at saddle area					
Specimen	Cr-C	Cr-B	Cr-F	Cr-A	Sa-D	Sa-C	Sa-B	Sa-E	Sa-F	Sa-A
SBB-X1	2.41	2.09	1.46	1.23	4.17	5.45	5.76	2.40	3.11	3.81
SBB-X2	1.69	1.41	1.36	1.15	4.31	5.74	6.2	3.97	4.81	5.45
DBB-X1	3.17	2.54	1.64	1.32	5.39	5.72	6.20	4.49	7.82	3.78
DBB-X2	2.71	2.08	2.09	1.32	6.05	6.06	7.10	5.91	7.19	6.10

For comparison and validation, the experimentally obtained SNCFs in Table 5.3 were divided by the FE results in Table 5.2. The test-to-FE ratios are listed in Table 5.4. For each of the four connections, the mean and coefficient of variation (COV) of the test-to-FE SNCF ratios at all critical locations were calculated. These values are also listed in Table 5.4. As shown by the statistics, the FE results agree well with the experiments, which gives credence to the accuracy of the FE modelling approach for use in the subsequent parametric studies.

Table 5.4. Test-to-FE SNCF ratios

		SNCF at crown area				SNCF at saddle area					
Specimen	Location	Cr-C	Cr-B	Cr-F	Cr-A	Sa-D	Sa-C	Sa-B	Sa-E	Sa-F	Sa-A
SBB-X1	Upper side	0.99	1.00	1.00	N/A	1.01	1.00	1.01	1.01	0.99	0.99
	Lower side	0.87	1.14	1.11	1.01	0.97	1.01	1.11	1.01	0.94	0.93
		Mean:	*1.00*	*COV:*	*0.063*						
SBB-X2	Upper side	0.99	1.01	N/A	N/A	0.97	1.01	1.04	1.02	0.99	0.96
	Lower side	0.99	1.06	N/A	N/A	0.94	1.01	1.03	0.97	1.00	0.94
		Mean:	*1.00*	*COV:*	*0.033*						
DBB-X1	Upper side	0.92	0.89	0.89	0.89	1.00	1.04	0.99	1.00	0.98	N/A
	Lower side	1.00	0.72	1.04	0.95	1.06	1.12	0.78	1.00	0.91	1.25
		Mean:	*0.97*	*COV:*	*0.120*						
DBB-X2	Upper side	0.96	0.90	1.00	0.92	0.96	1.16	0.98	0.98	0.97	1.00
	Lower side	0.84	0.96	1.16	N/A	1.07	1.17	0.90	1.04	0.92	1.02
		Mean:	*1.00*	*COV:*	*0.092*						

5.4. Square bird beak X-Connections near an open chord end

5.4.1. Parametric Study

A total of 64 regular SBB connection models (with sufficient chord continuities on both sides of the connections) were first developed to serve as "control models" and provide the basis for investigation of "end effects". All 64 regular connection models had a total chord length of $6b_0 + b_1$ (i.e. $e = 3b_0$ on both

sides of the connection). As discussed in [16-18], and acknowledged by CIDECT [21], $3.0b_0$ represents a conservative limit beyond which "end effects" can be safely ignored.

A constant SHS chord member external width (b_0) of 200 mm was used for all the regular connection models, with variations in the branch cross-sectional dimensions (b_1 and t_1) and the chord thickness (t_0), to cover a wide range of non-dimensional parameters (β = 0.35, 0.5, 0.65, and 0.8; 2γ = 12.5, 16, 20 and 25; and τ = 0.25, 0.5, 0.75, and 1.0). It should be noted that Equation 5.1-Equation 5.6 were developed based on experimental and numerical research on regular connections such as these [89].

By changing the chord length on one side of the regular SBB connection models, another three sets of SBB connection models near an open chord end (with e = $0.1b_0$, $0.5b_0$, $1.0b_0$ on one side of the connection) were created. Each set had a total of 64 models covering the same ranges of non-dimensional parameters (β = 0.35, 0.5, 0.65, and 0.8; 2γ = 12.5, 16, 20 and 25; and τ = 0.25, 0.5, 0.75, and 1.0).

With the careful region partition and meshing at welded joint location (Figure 5.7(a)), it was possible to monitor, around the entire perimeter of the welded joint of each FE connection model, the stress distribution within the extrapolation zone recommended by CIDECT [21]. After a rigorous evaluation of the stress distributions in all models, it was confirmed that the hot spot locations for SBB connections near an open chord end are the same as those for regular SBB connections (Figure 5.4(a)).

For each FE connection model, nominal stress was calculated by dividing the branch axial force by the branch cross-sectional area. For each hot spot location, four readings of stresses perpendicular to the weld within the extrapolation zone recommended by CIDECT [21] were obtained and used to calculate the hot spot stress by quadratic extrapolation. By dividing the hot spot stress by the nominal stress, the SCFs at the critical locations were determined.

Like Section 5.3, in the parametric study, only half of each connection was modelled. Therefore, SCFs at locations Cr-D and Cr-E (Figure 5.4) are not included as they are the same as those at locations Cr-A and Cr-B, as previously noted.

For the control models (with e = $3b_0$ on both sides), the SCF-values on the two sides of the FE connections are the same due to symmetry (about a plane containing the branch longitudinal axis and perpendicular to the chord longitudinal axis). For the end connection models (with e = $0.1b_0$, $0.5b_0$, $1.0b_0$), the SCFs were obtained at the critical locations (Figure 5.4(a)) on both the long chord side and the short chord side (Figure 5.6(b)). The values on the two sides were then compared – to identify the governing side. Representative data is shown in Figure 5.8, where the SCFs values from the control models are also shown for comparison. Based on the overall results, the following observations can be made:

(1) The SCFs in SBB end connections are smaller than those in the regular SBB connection counterparts.
(2) SCFs decrease as e/b_0 decreases. This is consistent with the findings in [16,18]. As pointed out by [72], for regular connections, the chord deformation resulting from the branch axial loading decays as the distance from the welded joint increases. On the other hand, for connections near an open chord end, such decay is interrupted by the short chord length on one side of the connections, which in turn affects the geometric stresses (i.e. hot spot stresses) around the perimeter of the welded joint.

(3) As shown in Figure 5.8, for typical SBB end connections, the SCFs on the short chord side are slightly larger than those on the long chord side. In fact, according to the comparison using all parametric study results, it was found, for SBB end connections, that the short chord side SCFs always governed. In the following discussion, only the SCF-values from the governing sides are used for the analysis and formulae development.

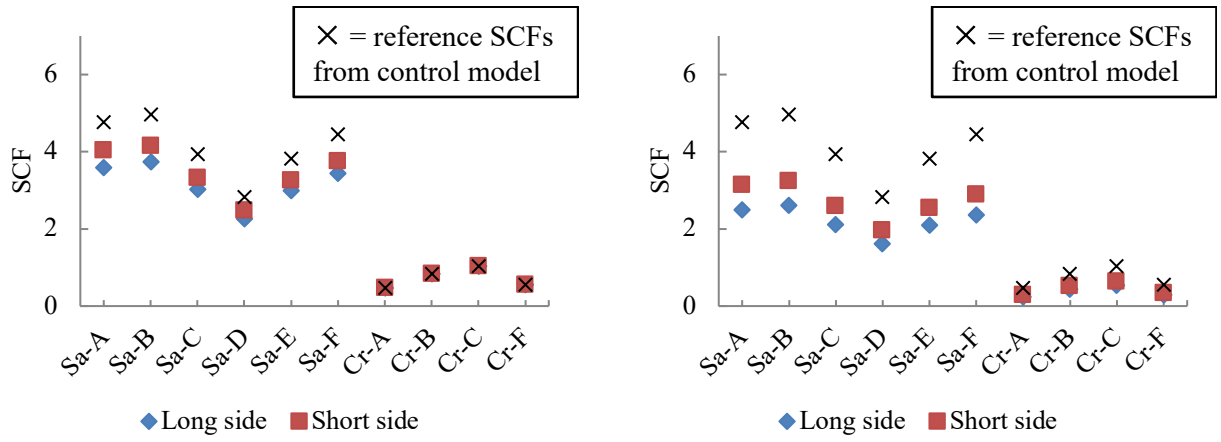

(a) End connection model ($e = 1b_0$)

(b) End connection model ($e = 0.5b_0$)

Figure 5.8. SCFs in regular and chord-end SBB X-connections with $\beta = 0.8$, $2\gamma = 16$ and $\tau = 0.5$

For the crown locations in all regular SBB connection models ($e = 3b_0$), the SCFs at Cr-A and Cr-F are shown in Figure 5.9(a). As shown, the SCFs at the two locations are very similar. This is consistent with Equation 5.1. Similarly, the SCFs at Cr-B and Cr-C in regular SBB connections ($e = 3b_0$) are similar in Figure 5.9(c). This is consistent with Equation 5.2. For the saddle locations in regular SBB connections ($e = 3b_0$), the SCFs at Sa-A, Sa-E and Sa-F are close in Figure 5.9(e), which is consistent with Equation 5.3, giving further credence to the FE modelling herein. The same phenomena were observed for all end connections ($e = 0.1b_0$, $0.5b_0$, $1.0b_0$). SCFs in typical end connections ($e = 0.5b_0$) are shown in Figs. 9(b), (d) and (f). Therefore, for calculation of SCFs in SBB end connections, it was deemed feasible to use Equation 5.1-Equation 5.6 multiplied by correction factors considering different chord end distances.

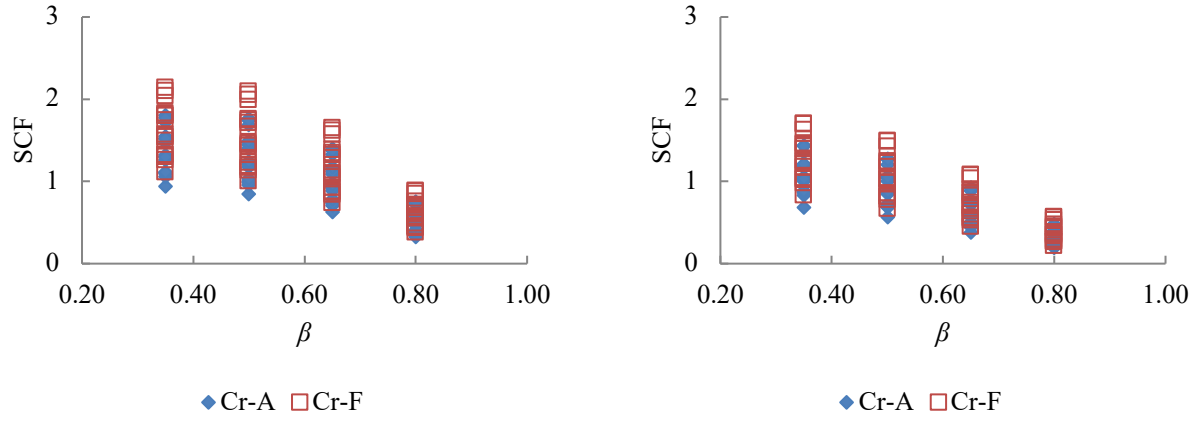

(a) Cr-A and Cr-F ($e = 3b_0$)

(b) Cr-A and Cr-F ($e = 0.5b_0$)

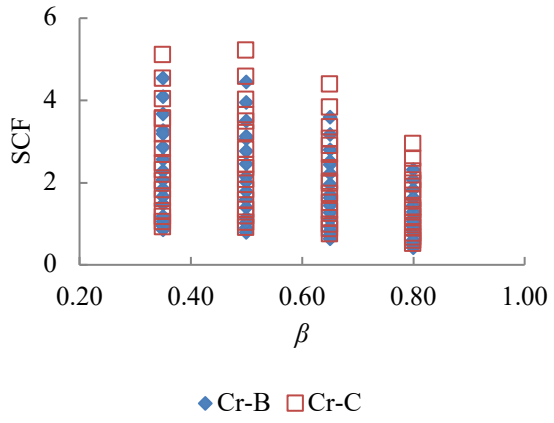

(c) Cr-B and Cr-C ($e = 3b_0$)

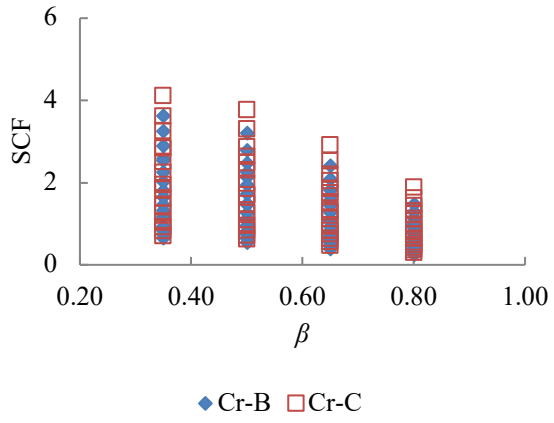

(d) Cr-B and Cr-C ($e = 0.5b_0$)

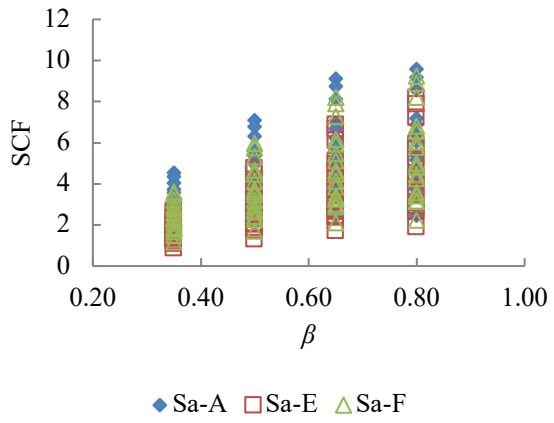

(e) Sa-A, Sa-E and Sa-F ($e = 3b_0$)

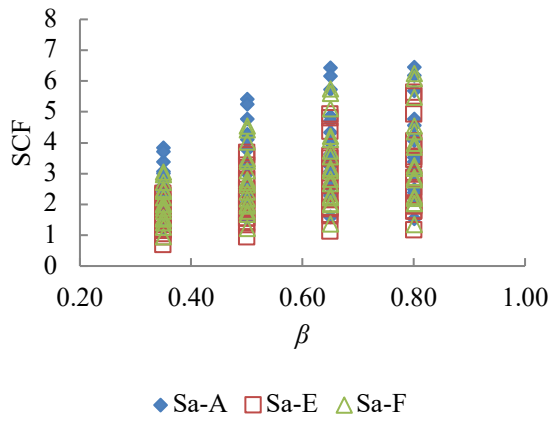

(f) Sa-A, Sa-E and Sa-F ($e = 0.5b_0$)

Figure 5.9. SCFs in regular and typical chord-end SBB X-connections

The relationships among SCFs in connections with different non-dimensional parameters and chord end distance (on one side) are further investigated using the parametric study results by calculating ψ equal to the ratios of SCFs in the SBB end-connection models ($SCF_{end\ connection}$) to those in the

corresponding control models ($SCF_{control\ model}$). Representative plots of ψ (= $SCF_{end\ connection}$/ $SCF_{control\ model}$) vs. e/b_0 at the hot spot locations (Figure 5.4(a)) are shown in Figure 5.10-Figure 5.12. The following observations can be made:

a) For Cr-A, Cr-B, Cr-C and Cr-F, ψ decreases as e/b_0 decreases. Based on all parametric study results, considering geometric symmetry (Cr-A = Cr-E, and Cr-B = Cr-D in Fig. 4(a)), it was deemed possible to use a single formula for prediction of ψ-values at all crown hot spot locations, since the values are close and show similar trends. The single ψ-formulae is to be used in conjunction with Equation 5.1 and Equation 5.2 for calculation of SCFs at the crown hot spots in SBB end connections.
b) For Sa-A, Sa-B, Sa-C, Sa-D, Sa-E and Sa-F, nonlinear relationships between ψ and e/b_0 were observed. Similar to the previous observation, it was deemed possible, based on all parametric study results, to use a single formula for prediction of ψ-values at all saddle hot spot locations, since the values are close and show similar trends. The single ψ-formulae is to be used in conjunction with Equation 5.3-Equation 5.6 for calculation of SCFs at the saddle hot spots in SBB end connections.
c) For different e/b_0, ψ increases as β decreases. On the other hand, ψ does not change significantly for different 2γ *and* τ.

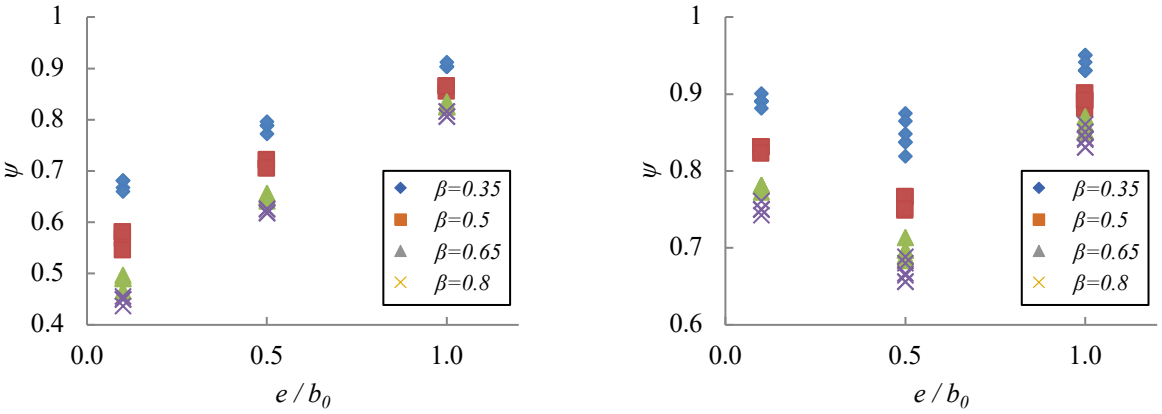

(a) Cr-A, Cr-B, Cr-C and Cr-F

(b) Sa-A, Sa-B, Sa-C, Sa-D, Sa-E and Sa-F

Figure 5.10. Effects of e/b0 and β on SCFs in chord-end SBB X-connections (2γ=20 and τ=0.75)

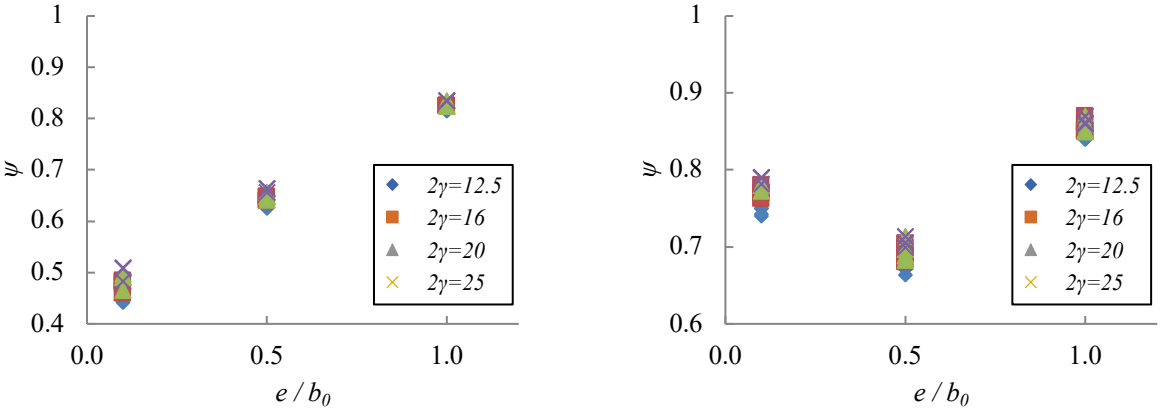

(a) Cr-A Cr-B, Cr-C and Cr-F

(b) Sa-A, Sa-B, Sa-C, Sa-D, Sa-E and Sa-F

Figure 5.11. Effects of e/b_0 and 2γ on SCFs in chord-end SBB X-connections (β=0.65 and τ=0.75)

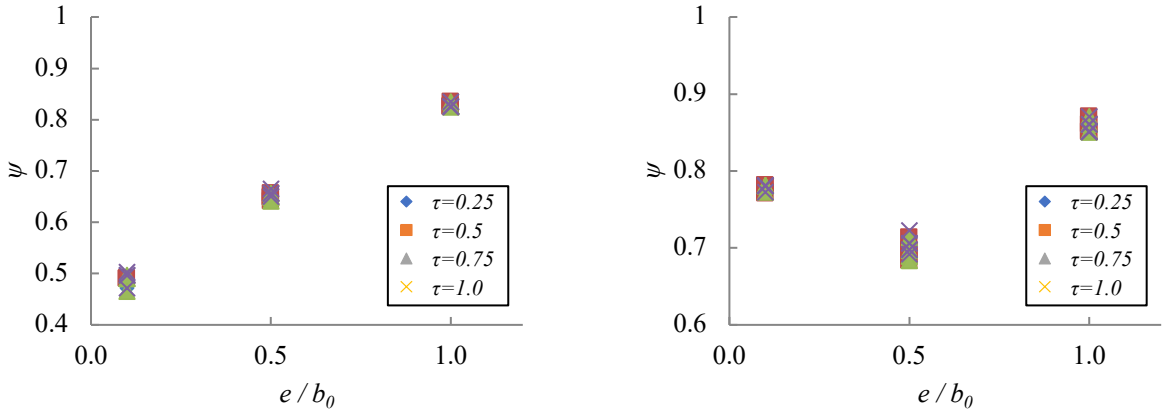

(a) Cr-A Cr-B, Cr-C and Cr-F

(b) Sa-A, Sa-B, Sa-C, Sa-D, Sa-E and Sa-F

Figure 5.12. Effects of e/b_0 and τ on SCFs in chord-end SBB X-connections (β=0.65 and 2γ=20)

5.4.2. Proposed Formulae

Using the parametric study results discussed in Section 5.4.1, the SCF correction factors (ψ), and parametric formulae to estimate ψ based on chord end distance-to-width (e/b_0), branch-to-chord width (β), branch-to-chord thickness (τ), and chord slenderness (2γ) ratios, are derived in this section.

According to the parametric study, the SCFs in regular and chord-end SBB X-connections can differ considerably. For the latter, predictions using the existing SCF formulae from [89] (reproduced as Equation 5.1-Equation 5.6) are inaccurate. As shown by Equation 5.15, the ψ-factors presented in Section 5.4.1 can be used in conjunction with Equation 5.1-Equation 5.6to determine the SCFs in axially loaded chord-end SBB X-connections, i.e.:

$$SCF_{end,i} = SCF_i \cdot \psi \qquad \text{Equation 5.15}$$

where SCF_i = SCF at hot spot i in a regular X-connection [calculated using Equation 5.1-Equation 5.6]; ψ = correction factor; $SCF_{end,i}$ = SCF at hot spot i in a chord-end X-connection.

As discussed in Section 5.4.1, in the parametric study, SCFs were obtained from end connection models (with $e = 0.1b_0$, $0.5b_0$, $1.0b_0$), and from the control connections (with $e = 3b_0$). The correction factors (ψ) were obtained by dividing the former by the latter. By analyzing the numerically obtained ψ-values, it was deemed possible to use a single formula for prediction of ψ at all crown hot spot locations (Cr-A = Cr-E, Cr-B = Cr-D, Cr-C and Cr-F) since the values are close and show similar trends. Thus, for each FE connection model the maximum ψ-value of all crown hot spot locations was used to develop the ψ-formula. As discussed in Section 5.4.1, for all hot spot locations, ψ changes as e/d_0 and β change. ψ does not vary significantly for different 2γ and τ. An extensive evaluation of different types of formulae was performed, followed by a non-linear least-squares regression analysis. The resulting approximate "best-fit" equation is given by Equation 5.16. Similarly, as discussed in Section 5.4.1, it was deemed possible to use a single formula for prediction of ψ at all saddle hot spot locations (Sa-A = Sa-E = Sa-F, Sa-B, Sa-C,

and Sa-D). Thus, for each FE connection model the maximum ψ-value of all saddle hot spot locations was used to develop the ψ-formula. The resulting approximate "best-fit" equation is given by Equation 5.17. Thus:

For all crown hot spot locations:

$$\psi = 1.00 + 0.134\left(e/b_0\right) + 0.51\beta^2 + 0.359\left(\beta\right)\left(e/b_0\right) - 1.15\beta \qquad \text{Equation 5.16}$$

For all saddle hot spot locations:

$$\psi = 1.00 + 0.465\left(e/b_0\right)^2 - 0.288\beta - 0.419\left(e/b_0\right) \qquad \text{Equation 5.17}$$

To evaluate the accuracy of proposed ψ-formulae, comparisons were made between: (i) ψ-values obtained by dividing $SCF_{end\ connection}$ by $SCF_{control\ model}$ (based on the parametric study results), and (ii) ψ-values calculated using Equation 5.16 and Equation 5.17. Table 5.5 includes the key statistics from comparisons based on 192 end connection models. As shown in the table, Equation 5.16 and Equation 5.17 are reasonably accurate over the range of parameters considered. For consistency with CIDECT DG 8 [21], a minimum SCF-value of 2.0 is still recommended.

Table 5.5. Mean values and COVs of FE-to-predicted ψ based on Equation 5.16-Equation 5.17 for 192 SBB chord-end X-connection models

Location	Eq.	Mean	COV
Cr-A & Cr-E	(5.16)	0.99	0.03
Cr-B & Cr-D	(5.16)	0.98	0.03
Cr-C	(5.16)	0.98	0.03
Cr-F	(5.16)	0.97	0.04
Sa-A, Sa-E & Sa-F	(5.17)	1.00	0.03
Sa-B	(5.17)	0.99	0.03
Sa-C	(5.17)	1.00	0.03
Sa-D	(5.17)	1.01	0.05

5.5. Diamond bird beak X-Connections near an open chord end

5.5.1. Parametric Study

Similar to the parametric study on SBB connections (Section 5.4.1), for DBB connections a total of 64 regular connection models (with $e = 3b_0$ on both sides of the connection) were first developed and served as the "control models". A constant 200 mm SHS member width (b_0) was used for all regular connection models. By varying the branch cross-sectional dimensions (b_1 and t_1) and the chord thickness (t_0), the parametric study covers wide ranges of non-dimensional parameters (β = 0.35, 0.5, 0.65, and 0.8; 2γ = 12.5, 16, 20 and 25; and τ = 0.25, 0.5, 0.75, and 1.0). It should be noted that Equation 5.7-Equation 5.14 were developed based on experimental and numerical research on regular connections [89]. By modifying the chord length on one side, another three sets of end connections were developed (with $e = 0.1b_0$, $0.5b_0$, $1.0b_0$ on one side of the connection). Each set has 64 models, covering the same ranges of non-dimensional parameters as the control models. All models were carefully partitioned and meshed (Figure 5.7(b)). By evaluating the stress distribution within the extrapolation zone recommended by CIDECT DG8 [21] for all end connection models, it was found that the hot spot locations for DBB connections near an open chord end are the same as those for regular DBB connections (Figure 5.4(b)).

Like Section 5.4.1, for the end connection models, the SCFs at the long chord side and short chord side are compared, to identify the governing side. Representative data is shown in Figure 5.13, where the SCFs values from the control models are also shown for comparison. Like SBB connections, the SCFs in DBB end connections are smaller than those in the regular connection counterparts. SCFs decrease as e/b_0 decreases. Based on the complete parametric study, by comparing the SCFs at the crown hot spots on the two sides of the connections, it was found, for DBB end connections, that the crown spots on the short

chord side always govern. In the following discussion, only the crown SCFs from the governing sides are used for the analysis and formulae development. For the saddle area, all hot spots in Figure 5.4(b) remain critical.

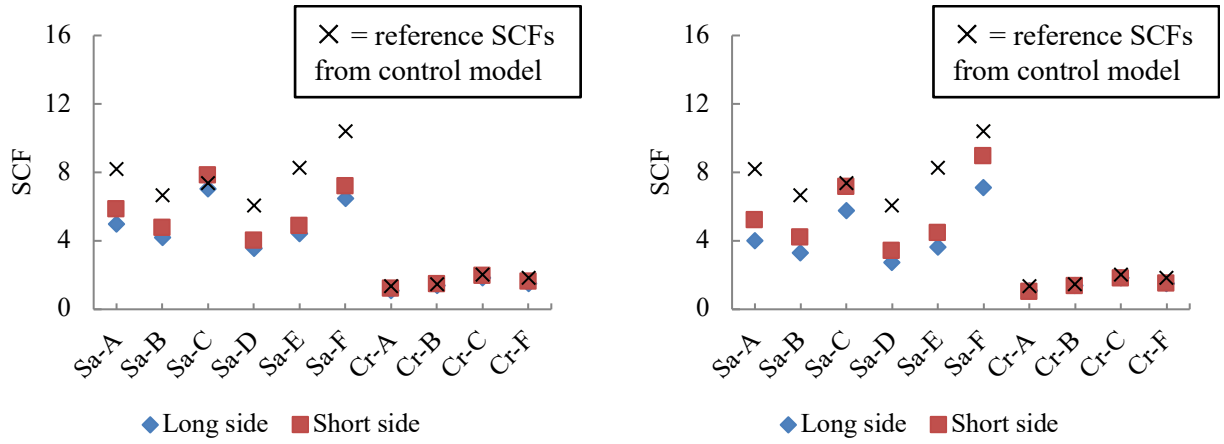

(a) End connection model ($e = 1b_0$) (b) End connection model ($e = 0.5b_0$)

Figure 5.13. SCFs in regular and chord-end DBB X-connections with $\beta = 0.8$, $2\gamma = 16$ and $\tau = 0.5$

In Section 5.4.1, it was proven by the parametric study (Figure 5.9) that for regular SBB connections, the SCFs at certain hot spot locations are quite close (not due to symmetry) and can be grouped together to simplify the calculation. This is consistent with Equation 5.1-Equation 5.6. The same phenomena were observed for SBB end connections (see Figure 5.9 for representative results). Therefore, for calculation of SCFs in end SBB connections, it was deemed feasible to use Equation 5.1-Equation 5.6 multiplied by correction factors considering different chord end distances. However, for regular DBB connections, the SCFs at the unsymmetrical locations were different. Therefore, a total of eight formulae (Equation 5.7-Equation 5.14 were developed in [89] to calculate the SCFs at the hot spot locations shown in Figure 5.4(b). The same phenomena were observed in the parametric study in this section on regular and end DBB connections. Therefore, for calculation of SCFs in DBB end connections, it was deemed necessary to use Equation 5.7-Equation 5.14 multiplied by correction factors considering different chord end distances.

The relationships among SCFs in connections with different non-dimensional parameters and chord end distance (on one side) are further investigated using the parametric study results by calculating ψ equal to the ratios of SCFs in the DBB end-connection models ($SCF_{end\ connection}$) to those in the corresponding control models ($SCF_{control\ model}$). Representative plots of ψ (= $SCF_{end\ connection}$/ $SCF_{control\ model}$) vs. e/b_0 at the hot-spot locations (Figure 5.4(b)) are shown in Figs. Figure 5.14-Figure 5.19.

For the crown hot spot locations, the following observations can be made:

a) For Cr-A, Cr-B, Cr-C and Cr-F (Figure 5.14-Figure 5.16), ψ in general decreases as e/b_0 decreases. Unlike SBB connections (Figure 5.10-Figure 5.12), the magnitudes and trends of ψ for

different crown hot spot locations in DBB connections are different. Therefore, considering geometric symmetry (Cr-A = Cr-E, and Cr-B = Cr-D in Figure 5.4(b)), it was deemed necessary to develop four ψ-formulae for the crown hot spot locations, for use in conjunction with Equation 5.7-Equation 5.10.

b) For Cr-A, Cr-B, Cr-C and Cr-F (Figs. 16-18), approximately linear relationships between ψ and e/b_0 were observed.
c) Overall, comparing to 2γ *and* τ, ψ is more sensitive to the variation of β over the investigated range of e/b_0.

For the saddle hot spot locations, the following observations can be made:

d) For Sa-A, Sa-B, Sa-C, Sa-D, Sa-E, and Sa-F (Figure 5.10Figure 5.12), both linear and nonlinear relationships between ψ and e/b_0 were observed. Unlike SBB connections (Figure 5.10Figure 5.12), the magnitudes and trends of ψ for the saddle hot spot locations are different for DBB connections.
e) Overall, comparing to 2γ *and* τ, ψ is more sensitive to the variation of β over the investigated range of e/b_0.

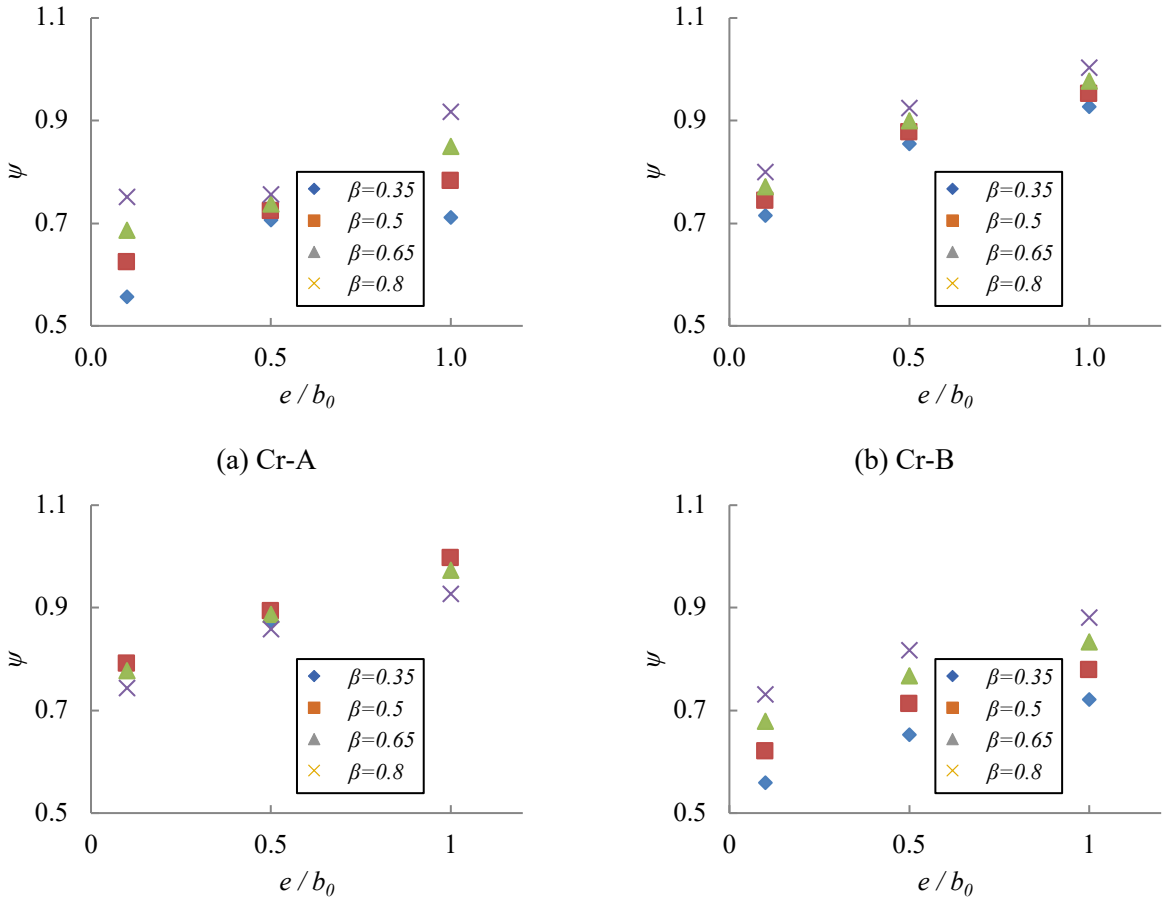

Figure 5.14. Effects of e/b_0 and β on SCFs at crown area in chord-end DBB X-connections (2γ=20 and τ=0.75)

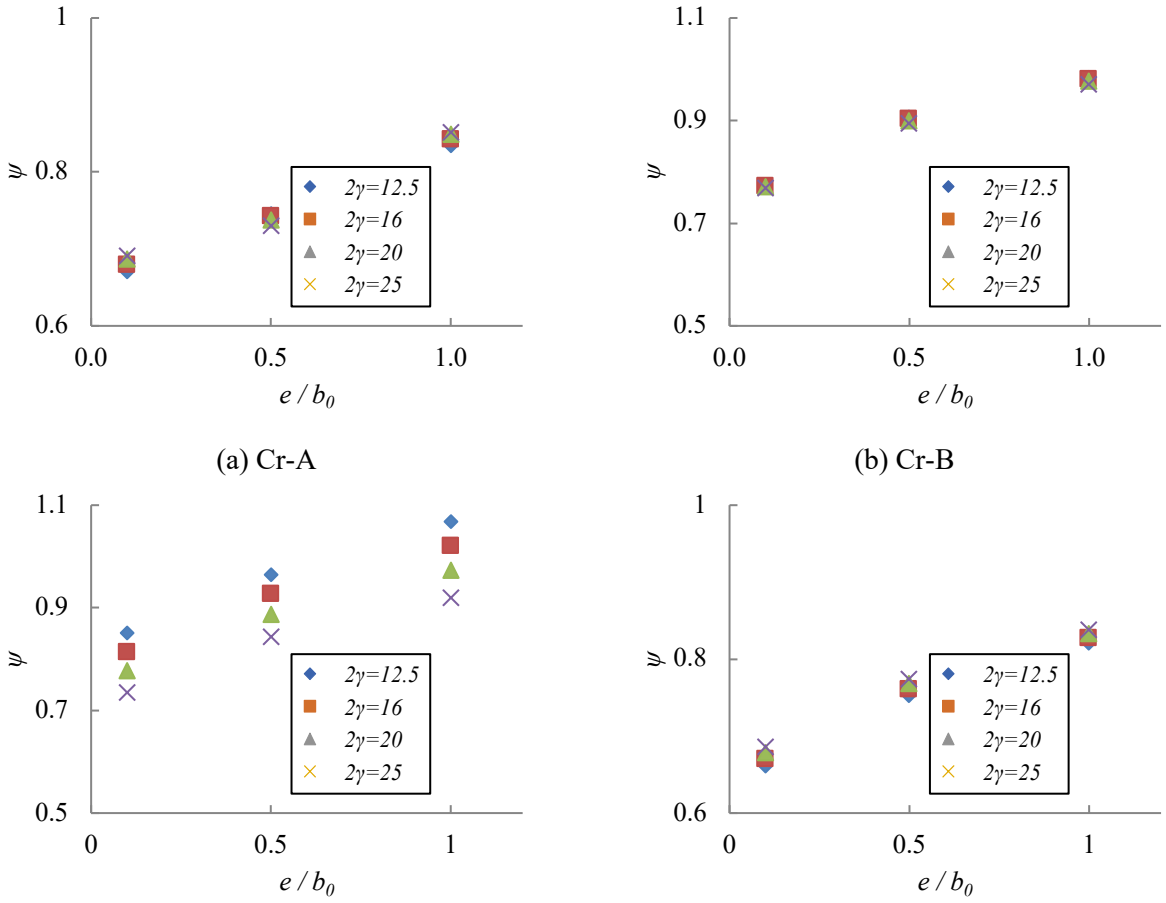

(a) Cr-A (b) Cr-B

(c) Cr-C (d) Cr-F

Figure 5.15. Effects of e/b_0 and 2γ on SCFs at crown area in chord-end DBB X-connections (2γ=20 and τ=0.75)

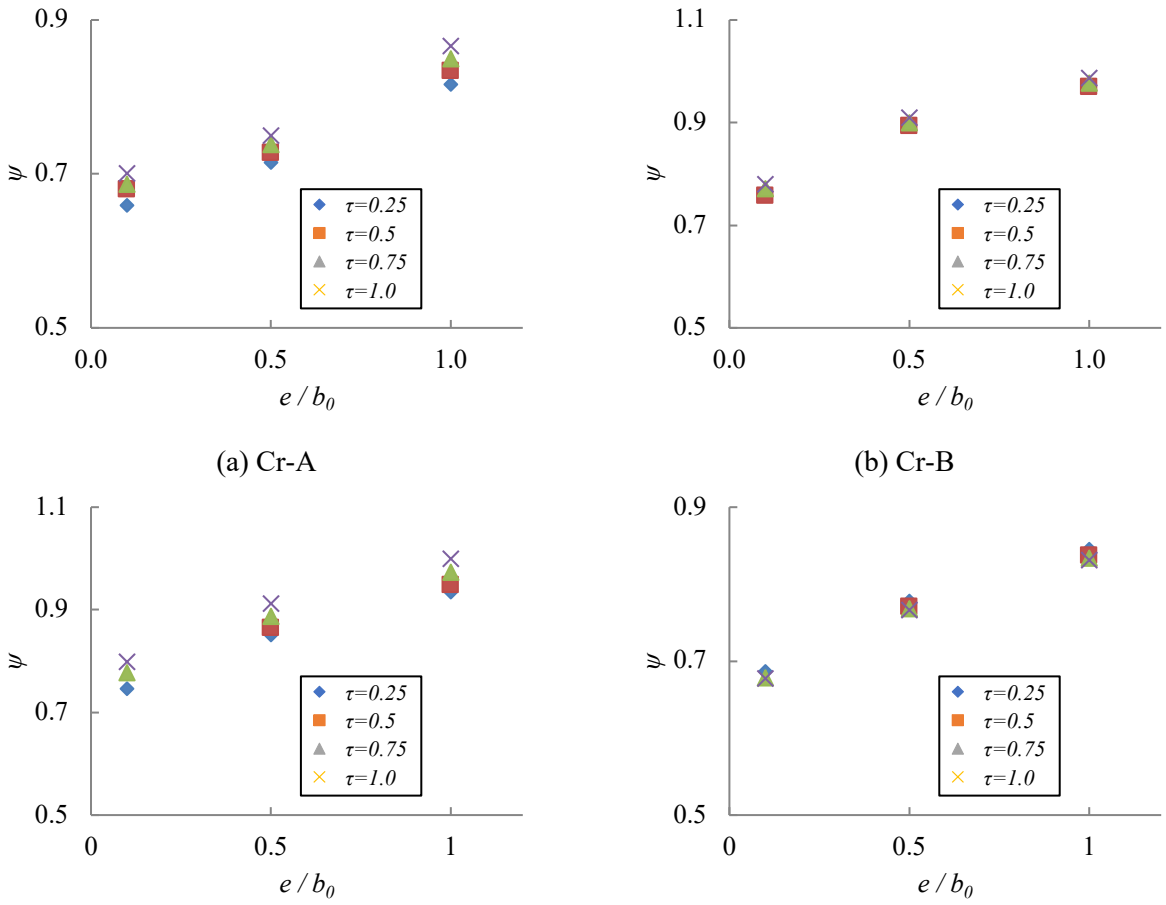

Figure 5.16. Effects of e/b_0 and τ on SCFs at crown area in chord-end DBB X-connections (2γ=20 and τ=0.75)

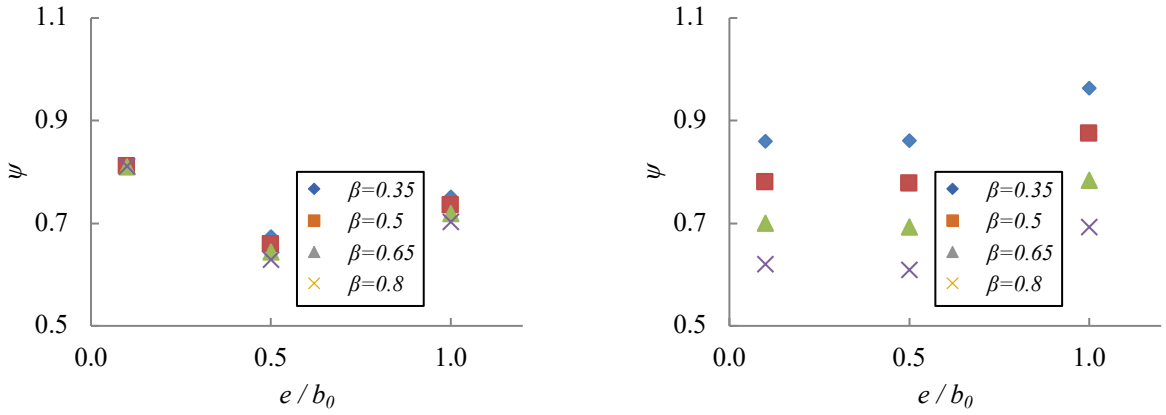

(a) Sa-A

(b) Sa-B

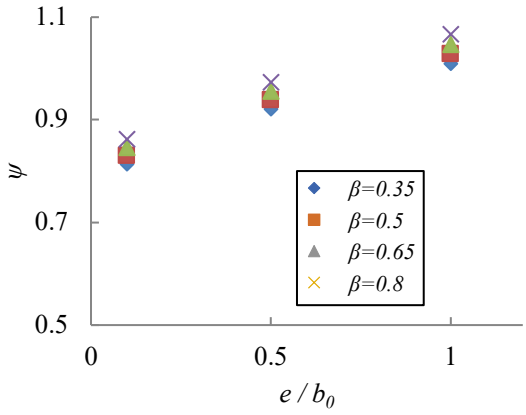

(c) Sa-C

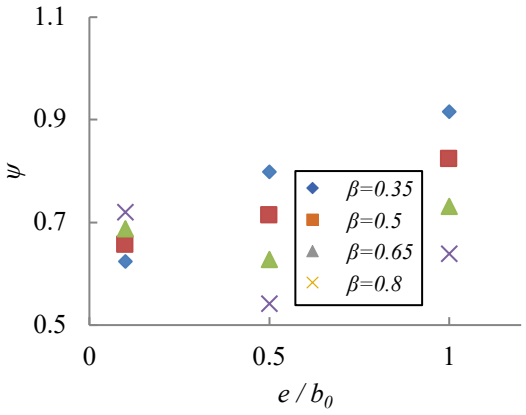

(d) Sa-D

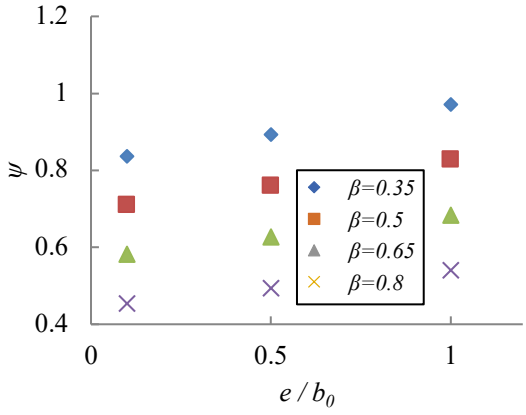

(e) Sa-E

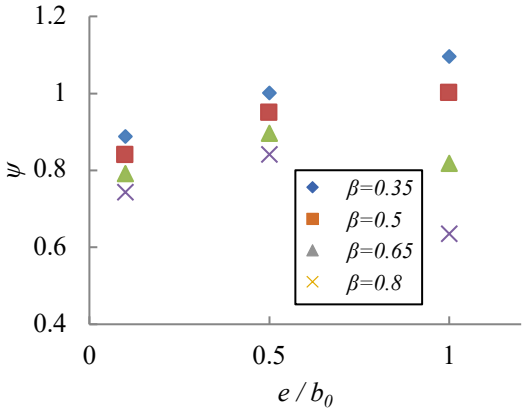

(f) Sa-F

Figure 5.17. Effects of e/b_0 and β on SCFs at saddle area in chord-end DBB X-connections (2γ=20 and τ=0.75)

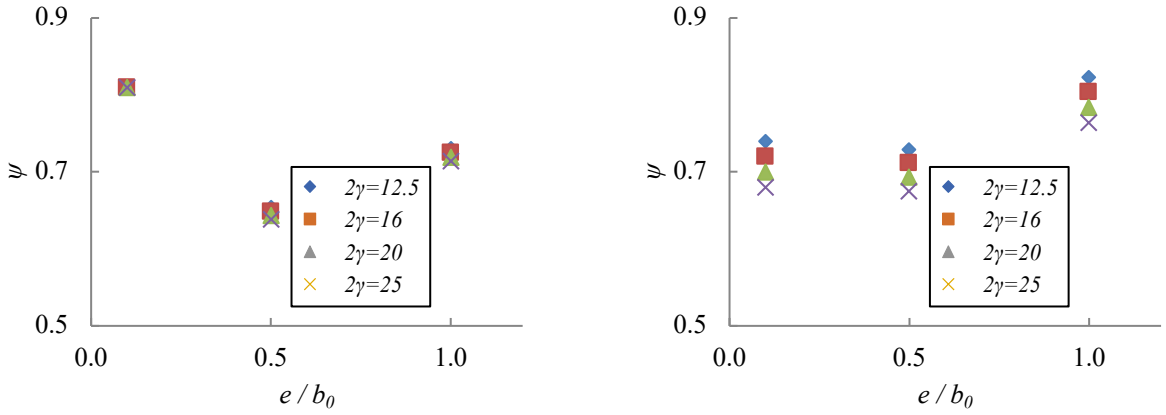

(a) Sa-A

(b) Sa-B

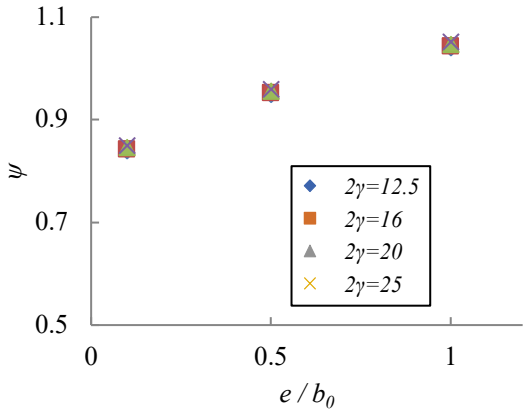

(c) Sa-C

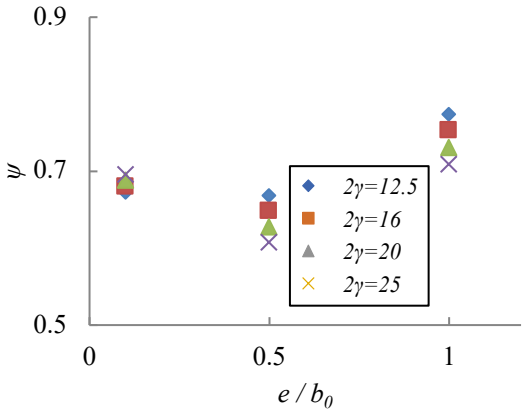

(d) Sa-D

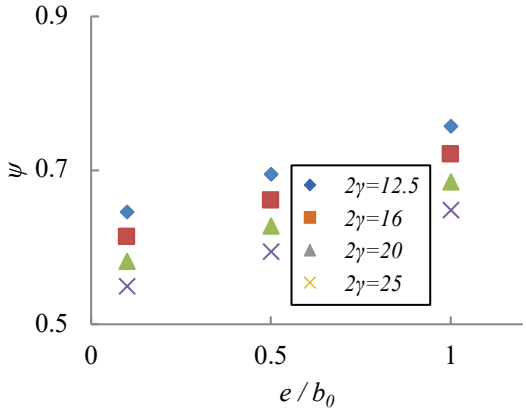

(e) Sa-E

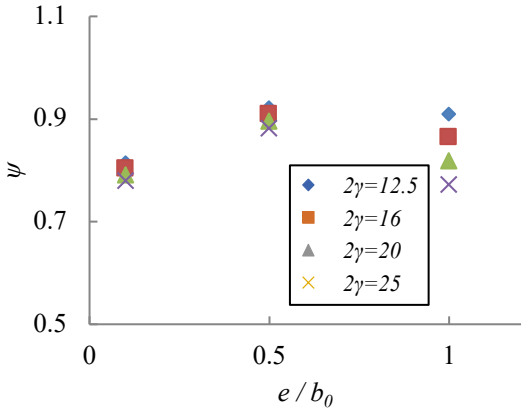

(f) Sa-F

Figure 5.18. Effects of e/b_0 and 2γ on SCFs at saddle area in chord-end DBB X-connections (2γ=20 and τ=0.75)

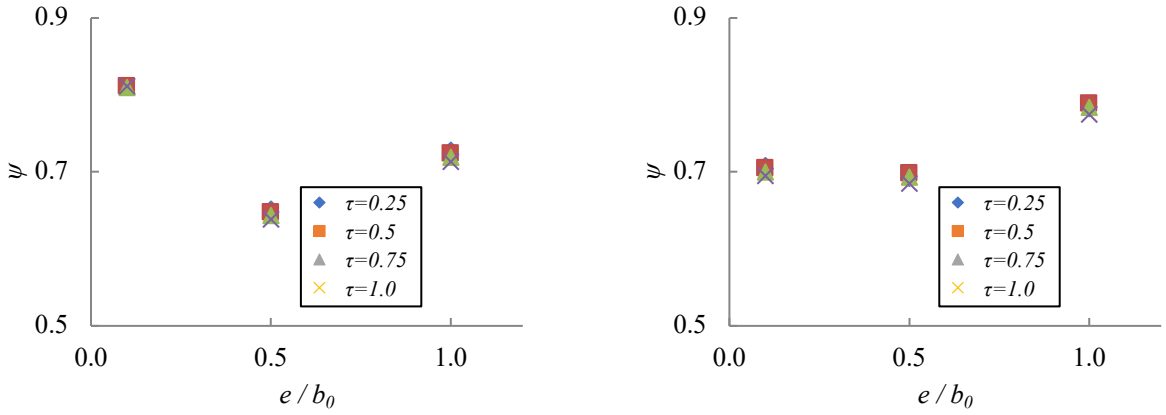

(a) Sa-A

(b) Sa-B

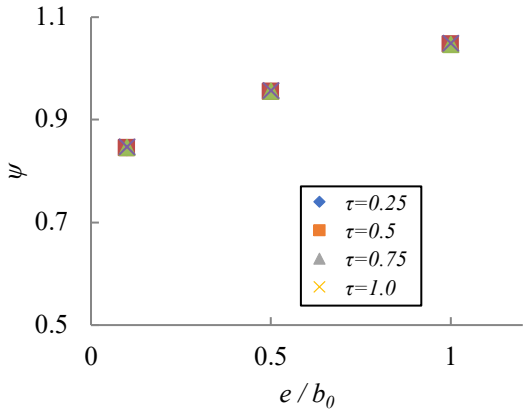

(c) Sa-C

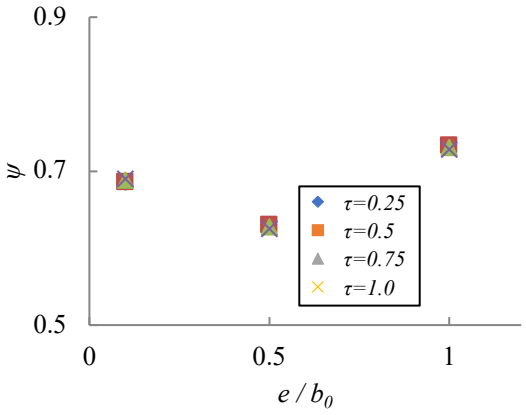

(d) Sa-D

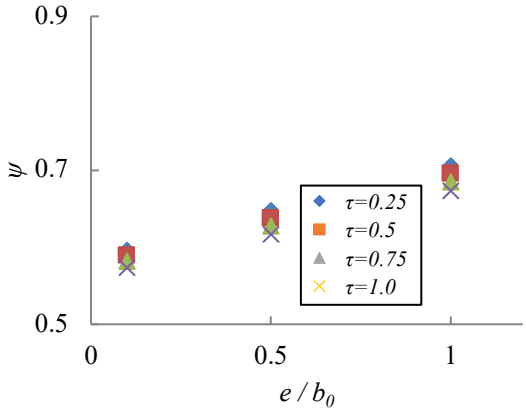

(e) Sa-E

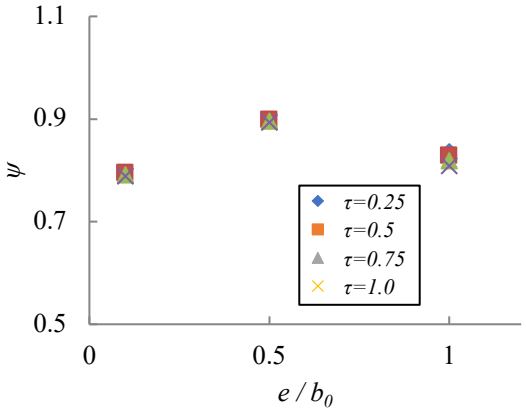

(f) Sa-F

Figure 5.19. Effects of e/b_0 and τ on SCFs at saddle area in chord-end DBB X-connections (2γ=20 and τ=0.75)

5.5.2. Proposed Formulae

According to the parametric study in Section 5.5.1, the SCFs in regular and chord-end DBB X-connections can differ considerably. For the latter, predictions using the existing SCF formulae from [89] (reproduced as Equation 5.7-Equation 5.14) are inaccurate. This section presents the development of parametric formulae to estimate ψ for chord-end DBB X-connections, based on the results of the parametric study. As discussed in Section 5.5.1, comparing to 2γ *and* τ, ψ is more sensitive to the variation of β over the investigated range of e/b_0. Using Equation 5.15 and the method discussed in Section 5.4.2, for each of the hot spot locations in Fig. 4(b), an extensive evaluation of different types of formulae was performed, followed by a non-linear least-squares regression analysis. The resulting approximate "best-fit" equations are given by Equation 5.18-Equation 5.27.

For all crown hot spot locations:

Cr-A = Cr-E
$$\psi = 0.238 + 4.48\beta + 1.28(e/b_0) + 0.048\tau - (e/b_0)^2 - 1.96\beta(e/b_0) - 3.86\beta\cos(e/b_0) \quad \text{Equation 5.18}$$

Cr-B = Cr-D
$$\psi = 0.606 + 0.457(e/b_0) + 0.185\beta - 0.205(e/b_0)^2 \quad \text{Equation 5.19}$$

Cr-C
$$\psi = 0.64 + 0.419\beta + 0.231(e/b_0) + 0.112(\beta)(\tau) - 0.0241(\beta)^2(2\gamma) \quad \text{Equation 5.20}$$

Cr-F
$$\psi = 0.354 + 0.398\beta + 0.178(e/b_0) + 0.00245(2\gamma) \quad \text{Equation 5.21}$$

For all saddle hot spot locations:

Sa-A
$$\psi = 0.88 + 0.601(e/b_0)^2 - 0.674(e/b_0) - 0.134(\beta)(e/b_0) \quad \text{Equation 5.22}$$

Sa-B
$$\psi = 1.16 + 0.0964(e/b_0)^3 - 0.00466(2\gamma) - 0.586(\beta) \quad \text{Equation 5.23}$$

Sa-C
$$\psi = 0.738 + 0.338(e/b_0) + 0.111(\beta) - 0.105(e/b_0)^2 \quad \text{Equation 5.24}$$

Sa-D
$$\psi = 0.927 + 0.145(e/b_0) + \frac{1.96}{2\gamma} - \frac{0.0359}{(e/b_0)} - \frac{0.252}{2\gamma(e/b_0)} + \frac{0.00818\beta}{(e/b_0)^2} - 0.611\beta \quad \text{Equation 5.25}$$

Sa-E
$$\psi = 1.31 + 0.126(e/b_0) - 0.00816(2\gamma) - 0.891(\beta) \quad \text{Equation 5.26}$$

Sa-F
$$\psi = 1.00 + 0.282(e/b_0) - 0.00254(2\gamma) - 0.313(\beta) - 0.0392(\beta)^3(2\gamma)(e/b_0)^4 \quad \text{Equation 5.27}$$

To evaluate the accuracy of proposed ψ-formulae, comparisons were made between: (i) ψ-values obtained by dividing $SCF_{end\ connection}$ by $SCF_{control\ model}$ (based on the parametric study results), and (ii) ψ-values calculated using Equation 5.1-Equation 5.6. Table 5.6 includes the key statistics from comparisons based

on the complete parametric study on 192 end connection models. As shown in the table, Equation 5.1-Equation 5.6 are reasonably accurate over the range of parameters considered. For consistency with CIDECT DG 8 [21], a minimum SCF-value of 2.0 is still recommended.

Table 5.6. Mean values and COVs of FE-to-predicted ψ based on Equation 5.18-Equation 5.27for 192 DBB chord-end X-connection models

Location	Eq.	Mean	COV
Cr-A & Cr-E	(5.18)	1.00	0.02
Cr-B & Cr-D	(5.19)	1.00	0.01
Cr-C	(5.20)	1.00	0.02
Cr-F	(5.21)	1.01	0.02
Sa-A	(5.22)	1.00	0.07
Sa-B	(5.23)	1.00	0.08
Sa-C	(5.24)	1.00	0.07
Sa-D	(5.25)	1.00	0.01
Sa-E	(5.26)	1.00	0.02
Sa-F	(5.27)	1.00	0.04

5.6. Conclusions

To establish approaches for calculation of stress concentration factors (SCFs) in truss/girder-end square and diamond bird-beak X-connections under branch axial loading, a total of 512 FE models were developed and analysed in the parametric study presented in this chapter. Based on the results, SCF correction factors (ψ), and parametric formulae to estimate ψ based on chord end distance-to-width (e/b_0), branch-to-chord width (β), branch-to-chord thickness (τ), and chord slenderness (2γ) ratios, were derived. The ψ formulae developed in this study can be used in conjunction with the existing SCF formulae in [89] for calculation of SCFs in truss/girder-end square and diamond bird-beak X-connections (with $e/b_0 < 3$) under branch axial loading.

Chapter 6

6. Future Work

For fatigue design of welded hollow structural sections connections, the “hot spot stress method” in CIDECT Design Guide 8 is widely used and forms the basis of various national and international design standards. However, the existing approaches cannot be directly applied to the following practical cases:

(1) RHS-to-RHS X- and T-connections with vent/drain holes (under branch axial force and in-plane bending)

(2) RHS-to-RHS X-connections situated at the end of a truss/girder (under branch axial force)

(3) Square and diamond bird-beak X-connections situated at the end of a truss/girder (under branch axial force)

In this thesis, modified approaches were developed for calculation of stress concentration factors in the above connection types. In the future, the research can be extended to cover the other connection types, such as circular hollow section (CHS)-to-CHS connections.

Bibliography

[1] AGA, Hot-dip galvanized steel bridges: a practical design guide, American Galvanizer's Association, Centennial, CO, 2017.

[2] G. Shi, J. Xue, W. Zhou, Y. Zhang, Experimental study on overall buckling behavior of Q420 high strength welded galvanized tubes under axial compression. Journal of Harbin Institute of Technology 45(10) (2013) 75-80.

[3] G. Shi, J. Xue, W. Zhou, T.M. Chan, Y. Zhang, Experimental investigation and modeling on residual stress of welded steel circular tubes. International Journal of Steel Structures 13(3) (2013) 495-508.

[4] M. Sun, J.A. Packer, Hot-dip galvanizing of cold-formed steel hollow sections: a state-of-the-art review. Frontiers of Structural and Civil Engineering 13(1) (2019) 49-65.

[5] M. Sun, Z. Ma, Effects of heat-treatment and hot-dip galvanizing on mechanical properties of RHS. Journal of Constructional Steel Research 153 (2019) 603-617.

[6] J.A. Packer, S.P. Chiew, R. Tremblay, G. Martinez-Saucedo, Effect of material properties on hollow section performance. Structures and Buildings 163(SB6) (2010) 375-390.

[7] A. Stem, N. Richman, C. Pool, C. Rios, T. Anderson, K. Frank, Fatigue life of steel base plate to pole connection for traffic structures. Texas Department of Transportation Report FHWA/TX-11/9-1526-1. Austin, USA: Center for Transportation Research, University of Texas at Austin, 2011.

[8] R. Goyal, H.B. Dhonde, M. Dawood, Fatigue failure and cracking in high mast poles. Texas Department of Transportation Report No. FHWA/TX-12/0-6650-1. Houston, USA: Department of Civil and Environmental Engineering, University of Houston, 2012.

[9] C.M. Foley, J.A. Diekfuss, B. Wan, Fatigue risks in the connections of sign supporting structures. Wisconsin Department of Transportation Report No. WHRP 0092-09-07. Milwaukee, USA: Department of Civil and Environmental Engineering, Marquette University, 2013.

[10] J.M. Ocel, Fatigue testing of galvanized and ungalvanized socket connections. Federal Highway Administration Report No. FHWA-HRT-14-066. McLean, USA: Federal Highway Administration, 2014.

[11] C. DiGiovanni, L. Li, R. Driver, L. Callele, Cracking in welded steel platform structures during hot-dip galvanization. Engineering Failure Analysis 79 (2017) 1031-1042.

[12] M. Feldmann, T. Pinger, D. Schafer, R. Pope, W. Smith, G. Sedlacek, Hot-dip-zinc-coating of prefabricated structural steel components. JRC Scientific and Technical Research Report No. 56810. Luxembourg: European Commission Joint Research Centre, 2010.

[13] F. Berto, F. Mutignani, L. Pittarello, Effect of hot-dip galvanization on the fatigue behaviour of welded structural steel. Procedia Structural Integrity 2 (2016) 1813-1820.

[14] F. Berto, O. Fergani, Fatigue behaviour of welded structural steel subjected to hot-dip galvanization process. International Journal of Fatigue 101(2) (2017) 439-447.

[15] Y. Zhou, M. Dawood, B. Gencturk, High-cycle fatigue performance of high-mast illumination pole bases with pre-existing cracks. Journal of Constructional Steel Research 138 (2017) 463-472.

[16] K. Nguyen, R. Nasouri, C. Bennett, A. Matamoros, J. Li, and A. Montoya, Thermomechanical modeling of welding and galvanizing a steel beam connection detail to examine susceptibility to cracking. Materials Performance and Characterization 7(2) (2018) 165-190.

[17] R. Nasouri, K. Nguyen, A. Montoya, A. Matamoros, C. Bennett, J. Li, Thermally-induced demands due to hot dip galvanization of high mast illumination poles. Part I: finite element model development. Journal of Constructional Steel Research 162 (2019a) 105705.

[18] R. Nasouri, K. Nguyen, A. Montoya, A. Matamoros, C. Bennett, J. Li, Simulating the hot dip galvanizing process of high mast illumination poles. Part II: effects of geometrical properties and galvanizing practices. Journal of Constructional Steel Research 159 (2019b) 584-597.

[19] ASTM, Standard practice for providing high-quality zinc coating (hot-dip), ASTM A385/A385M-15. American Society for Testing and Materials, West Conshohocken, USA, 2015.

[20] J.A. Packer, D.R. Sherman, M. Lecce, Design guide 24: hollow structural section connections. American Institute of Steel Construction, Chicago, USA, 2010.

[21] X.L. Zhao, S. Herion, J.A. Packer, R.S. Puthli, G. Sedlacek, J. Wardenier, K. Weynand, A.M. van Wingerde, N.F. Yeomans, Design guide for circular and rectangular hollow section welded joints under fatigue loading, CIDECT Design Guide No. 8, CIDECT and Verlag TÜV Rheinland GmbH, Köln, Germany, 2001.

[22] Dassault Systèmes, ABAQUS Version 6.14 [Computer software]. Dassault Systèmes, Providence, USA, 2014.

[23] L.W. Tong, G.W. Xu, Y.Q. Liu, D.Q. Yan, X.L. Zhao, Finite element analysis and formulae for stress concentration factors of diamond bird-beak SHS T-joints. Thin-Walled Structures 86 (2015) 108-120.

[24] L.W. Tong, G.W. Xu, D.L. Yang, F.R. Mashiri, X.L. Zhao, Stress concentration factors in CHS-CFSHS T-joints: experiments, FE analysis and formulae. Engineering Structures 151 (2017) 406-421.

[25] CSA, General requirements for rolled or welded structural quality steel/structural quality steel, CAN/CSA-G40.20-13/G40.21-13. Canadian Standards Association, Toronto, Canada, 2013.

[26] R. Feng, B. Young, Stress concentration factors of cold-formed stainless steel tubular X-joints. Journal of Constructional Steel Research 91 (2013) 26-41.

[27] CSA, Welded steel construction, W59-18. Canadian Standards Association, Toronto, Canada, 2018.

[28] J.A. Packer, C.E. Cassidy, Effective weld length for HSS T, Y, and X connections, Journal of Structural Engineering 121(10) (1995) 1402-1408.

[29] M.R. McFadden, J.A. Packer, Effective weld properties for hollow structural section T-connections under branch in-plane bending, Eng. J. AISC 51(4) (2014) 247-266.

[30] Y.J. Fan, J.A. Packer, RHS-to-RHS axially loaded X-connections near an open chord end, Canadian Journal of Civil Engineering 44 (2017) 881-892.

[31] ASTM, Standard practice for providing high-quality zinc coating (hot-dip), ASTM A385/A385M-17. American Society for Testing and Materials, West Conshohocken, USA, 2017.

[32] API, Planning, designing, and constructing fixed offshore platforms - load and resistance factor design, API RP 2A-LRFD:2019. American Petroleum Institute, USA, Washington, 2019.

[33] AWS, Structural welding code – steel, ANSI/AWS D1.1/D1.1M:2010. American Welding Society, Miami, USA, 2010.

[34] DNV, Fatigue design of offshore steel structures, DNVGL-RP-C203. DET NORSKE VERITAS, Høvik, Norway, 2011.

[35] ISO, Fatigue – Design procedure for welded hollow-section joints – Recommendations, ISO 14347:2008. International Organization for Standardization, Geneva, Switzerland, 2008.

[36] IIW, Recommended fatigue design procedure for hollow section joints. Part 1 – hot spot stress method for nodal joints. International Institute of Welding Subcommission XV-E, IIW Doc. XV-582-85, IIW Assembly, Strasbourg, France, 1985.

[37] AASHTO, LRFD guide specifications for design of pedestrian bridges, 2nd Edition. American Association of State Highway and Transportation Officials, Washington, USA, 2009.

[38] S. Daneshvar, M. Sun, Galvanized RHS X-Connections. I: Effects of Holes on SCFs under Branch Axial Loading, Journal of Constructional Steel Research (2019) (accepted for publication).

[39] CSA, General requirements for rolled or welded structural quality steel/structural quality steel, CAN/CSA-G40.20-13/G40.21-13. Canadian Standards Association, Toronto, Canada, 2013.

[40] CSA, Welded steel construction, CSA W59-18. Canadian Standards Association, Toronto, Canada, 2018.

[41] J. Jiang, C.K. Lee, S.P. Chiew, Residual stress and stress concentration effect of high strength steel built-up box T-joints. Journal of Constructional Steel Research 105 (2015) 164-173.

[42] A.M. van Wingerde, The fatigue behaviour of T- and X-joint made of square hollow section. HERON 37(2) (1992) 1-180.

[43] B. Cheng, Q. Qian, X.L. Zhao, Numerical investigation on stress concentration factors of square bird-beak SHS T-joints subject to axial forces. Thin-Walled Structures 94 (2015) 435-445.

[44] Y.S. Choo, X.D. Qian, J. Wardenier, Effects of boundary conditions and chord stresses on static strength of thick-walled CHS K-joints, Journal of Constructional Steel Research 62 (2006) 316-328.

[45] G.J. van der Vegte, Y. Makino, Further research on chord length and boundary conditions of CHS T- and X-joints, Advanced Steel Construction 6(3) (2010) 879-890.

[46] M. Yaghoubshahi, M. Sun, K. Tousignant, Design of fillet welds in RHS-to-RHS moment T-connections under branch in-plane bending. Journal of Constructional Steel Research 159 (2019) 122-133.

[47] K. Tousignant, J.A. Packer, Fillet weld effective lengths in CHS X connections. II: Finite element modeling, parametric study and design. J. Constr. Steel Res. 141 (2018) 77-90.

[48] A.M. van Wingerde, J.A. Packer, J. Wardenier, SCF formulae for fatigue design of K-connections between square hollow sections. Journal of Constructional Steel Research 43 (1997) 87-118.

[49] J.A. Packer, J.E. Henderson, Hollow Structural Section Connections and Trusses – a Design Guide, 2nd ed. Canadian Institute of Steel Construction, Toronto, Canada, 1997.

[50] J. Wardenier, Y. Kurobane, J.A. Packer, A. van der Vegte, X.L. Zhao, Design Guide for Circular Hollow Section (CHS) Joints under Predominantly Static Loading, CIDECT Design Guide No. 1, 2nd ed. CIDECT, Geneva, Switzerland, 2008.

[51] J.A. Packer, J. Wardenier, X.L. Zhao, G.J. van der Vegte, Y. Kurobane, Design Guide for Rectangular Hollow Section (RHS) Joints under Predominantly Static Loading, CIDECT Design Guide No. 3, 2nd ed. CIDECT, Geneva, Switzerland, 2009.

[52] ISO (International Organization for Standardization), ISO 14346:2013, Static Design Procedure for Welded Hollow Section Joints – Recommendations, Geneva, Switzerland, 2013.

[53] ISO (International Organization for Standardization), ISO 14347:2008, Fatigue – Design Procedure for Welded Hollow-Section Joints – Recommendations, Geneva, Switzerland, 2008.

[54] CSA (Canadian Standard Association), CSA S16-19, Design of Steel Structures, Toronto, Canada, 2019.

[55] AISC (American Institute of Steel Construction), ANSI/AISC 360-16, Specification for Structural Steel Buildings. Chicago, IL, USA, 2016.

[56] AWS (American Welding Society), AWS D1.1/D1.1M:2020, Structural Welding Code – Steel, Miami, FL, USA, 2020.

[57] CEN (European Committee for Standardization), EN 1993-1-8:2010, Eurocode 3: Design of Steel Structures – Part 1–8: Design of Joints, Brussels, Belgium, 2010.

[58] X.D. Bu, J.A. Packer. Chord end distance effect on RHS connections. Journal of Constructional Steel Research, 168 (2020) 105992.

[59] Y.J. Fan, J.A. Packer, RHS-to-RHS axially loaded X-connections near an open chord end. Canadian Journal of Civil Engineering 44 (2017) 881-892.

[60] G.J. van der Vegte, Y. Makino, Further research on chord length and boundary conditions of CHS T- and X-joints. Advanced Steel Construction 6(3) (2010) 879-890.

[61] A.P. Voth, J.A. Packer, Branch plate-to-circular hollow section connections. II: X-type parametric numerical study and design. Journal of Structural Engineering, American Society of Civil Engineers, 138(8) (2012) 1007–1018.

[62] A.P. Voth, J.A. Packer, Numerical study and design of T-type branch plate-to-circular hollow section connections. Engineering Structures 41 (2012) 477–489.

[63] CEN (European Committee for Standardization), Eurocode 3: Design of steel structures – Part 1–8: Design of joints. prEN 1993-1-8:2018, Brussels, Belgium, 2018.

[64] K. Tousignant, Effect of chord length and boundary conditions on welds in CHS X-joints. Proceedings of the 17th International Symposium on Tubular Structures, Singapore (2019) 63-70.

[65] L.M. Connelly & N. Zettlemoyer. Frame behaviour effects on tubular joint capacity. Proceedings of the 3rd International Symposium on Tubular Structures, Lappeenranta, Finland. 1989. pp. 91-89.

[66] H.M. Bolt, H. Seyed-Kebari & J.K. Ward. The influence of chord length and boundary conditions on K-joint capacity. Proceedings of the 2nd International offshore and polar engineering conference, San Fransico, USA, 1992, Vol. IV, pp. 347-354.

[67] Y.S. Choo, X.D. Qian, J. Wardenier, Effects of boundary conditions and chord stresses on static strength of thick-walled CHS K-joints. Journal of Constructional Steel Research 62 (2006) 316-328.

[68] G.J. van der Vegte, Y. Makino, Ultimate strength formulation for axially loaded CHS uniplanar T-joints, International Journal of Offshore and Polar Engineering (2006) 16(4) 305-312.

[69] M. Efthymiou, S. Durkin, Stress concentration in T/Y and gap/overlap K-joints, Proceedings of the 4th International Conference on Behaviour of Offshore Structures, Amsterdam, The Netherlands (1985) 429–440.

[70] CSA (Canadian Standards Association), CAN/CSA-G40.20-13/G40.21-13, General requirements for rolled or welded structural quality steel/structural quality steel. Toronto, Canada, 2013.

[71] CEN (European Committee for Standardization), EN 1993-1-8:2010, Eurocode 3: Design of Steel Structures – Part 1–8: Design of Joints, Brussels, Belgium, 2010.

[72] S. Daneshvar, M. Sun, K. Tousignant, Stress concentration factors for RHS-to-RHS X-connections near an open chord end. Journal of Constructional Steel Research 175 (2020) 106352.

[73] A. Ziaei Nejad, M. Sun, K. Tousignant, Circular hollow section X-connections near an open chord end: stress concentration factors. Journal of Constructional Steel Research (2020) (under review).

[74] S. Daneshvar, M. Sun, Stress concentration factors of RHS T-connections with galvanizing holes under in-plane bending. Journal of Constructional Steel Research 169 (2020) 106039.

[75] K. Tousignant, J.A. Packer, Fillet weld effective lengths in CHS X-connections. I: Experimentation. Journal of Constructional Steel Research 128 (2017) 420-431.

[76] K. Tousignant, J.A. Packer, Numerical investigation of fillet welds in HSS-to-rigid end-plate connections. Journal of Structural Engineering, ASCE 143(12) (2017) 04017165:1-04017165-16.

[77] K. Tousignant, J.A. Packer, Weld effective lengths for round HSS cross-connections under branch axial loading. Engineering Journal, AISC 56(3) (2019) 173-186.

[78] K. Tousignant, J.A. Packer, Fillet welds around circular hollow sections. Welding in the World, IIW 63 (2019) 421-433.

[79] H. Ahmadi, A. Ziaei Nejad, Local joint flexibility of two-planar tubular DK-joints in OWTs subjected to axial loading: parametric study of geometrical effects and design formulation. Ocean Engineering 136(5) (2017) 1-10.

[80] H. Ahmadi, A. Ziaei Nejad, A study on the local joint flexibility (LJF) of two-planar tubular DK-joints in jacket structures under in-plane bending loads. Applied Ocean Research 64(3) (2017) 1-14.

[81] H. Ahmadi, A. Ziaei Nejad, (2017). Geometrical effects on the local joint flexibility of two-planar tubular DK-joints in jacket substructure of offshore wind turbines under OPB loading. Thin-Walled Structures 114(5) (2017) 122-133.

[82] H. Ahmadi, A. Ziaei Nejad, Stress concentration factors in uniplanar tubular KT-joints of jacket structures subjected to in-plane bending loads. International Journal of Maritime Technology 5(2) (2016) 27-39.

[83] M. Sun, K. Tousignant, A. Ziaei Nejad, S. Daneshvar, Chord-end RHS-to-RHS and CHS-to-CHS X-connections with cap plates: stress concentration factors. Journal of Constructional Steel Research (2020) (under review).

[84] L.W. Tong, Y.G. Fu, Y.Q. Liu, X.L. Zhao, Stress concentration factors of diamond bird-beak SHS T-joints under branch loading, Thin-Walled Struct. 74 (2014) 201–212.

[85] L.W. Tong, G.W. Xu, D.Q. Yan, X.L. Zhao, Fatigue tests and design of diamond bird-beak SHS T-joints under axial loading in branch, J. Constr. Steel Res. 118 (2016) 49–59.

[86] B. Cheng, Q. Qian, X.L. Zhao, Tests to determine stress concentration factors for square Bird-Beak SHS joints under chord and branch axial forces, J. Struct. Eng. 140 (11) (2014) (04014088.

[87] B. Cheng, Q. Qian, X.L. Zhao, Stress concentration factors and fatigue behavior of square bird-beak SHS T-joints under out-of-plane bending, Eng. Struct. 99 (2015) 677–684.

[88] B. Cheng, C. Li, Y. Lou, X.L. Zhao, Parametric FE modeling to predict hot spot stress concentrations of bird-beak SHS joints in offshore structures, Ocean Eng. 160 (2018) 54–67.

[89] C. Li, F. Huang, Y. Lou, B. Cheng, Stress concentration factors of bird-beak SHS X-joints under branch axial forces, J. Constr. Steel Res. 150 (2018) 87–98.

[90] F.H. Huang, B. Cheng, C. Li, X.L. Zhao, Fatigue behavior of bird-beak SHS X-joints under cyclic branch axial forces, J. Constr. Steel Res. 169 (2020) 106021.

[91] B. Cheng, F.H. Huang, C. Li, Y.H. Duan, X.L. Zhao, Hot spot stress and fatigue behavior of bird-beak SHS X-joints subjected to branch in-plane bending, Thin-Walled Struct. 150 (2020) 106701.